Mechanisms of Sterile Inflammation in the Testis

Lena Walenta

Dissertation der Fakultät für Biologie der
Ludwig-Maximilians-Universität München

München, 2018

Diese Dissertation wurde angefertigt
unter der Leitung von Prof. Dr. Artur Mayerhofer
im Bereich Zellbiologie – Anatomie III
des Biomedizinischen Centrums München
der Ludwig-Maximilians-Universität München

Erstgutachter: PD Dr. Lars Kunz

Zweitgutachterin: Prof. Dr. Gisela Grupe

Tag der Abgabe: 24.04.2018

Tag der mündlichen Prüfung: 17.07.2018

Eidesstattliche Erklärung

Ich versichere hiermit an Eides statt, dass meine Dissertation selbständig und ohne unerlaubte Hilfsmittel angefertigt worden ist.
Die vorliegende Dissertation wurde weder ganz, noch teilweise bei einer anderen Prüfungskommission vorgelegt.
Ich habe noch zu keinem früheren Zeitpunkt versucht, eine Dissertation einzureichen oder an einer Doktorprüfung teilzunehmen.

München, den 24.04.2018

Lena Walenta

TABLE OF CONTENTS

ABSTRACT

Causes of human male infertility are only partially known. In the numerous idiopathic cases, the underlying causes remain unknown. Sterile inflammation of the testis, which frequently proceeds asymptomatically and therefore stays undetected, may be involved. This scenario has often been associated with increased numbers of immune cells infiltrating the testis and fibrotic remodeling of the seminiferous tubular wall. The peritubular cells forming the tubular wall together with extracellular matrix are thus hypothesized to participate in these pro-inflammatory processes.

Peritubular cells produce the small leucine-rich repeat proteoglycan and extracellular matrix molecule biglycan. Once secreted, it is usually found sequestered in the extracellular matrix serving a structural purpose, but in its soluble form it has been shown to act as inducer of (pro-)inflammatory signaling in immune cells by activating toll-like receptors 2 and 4. To recapitulate these findings, a systemic mouse model of male infertility and sterile inflammation was examined. Biglycan and associated receptor levels were increased in the mouse model. However, a biglycan knock-out in this mouse failed to rescue the inflammatory testicular phenotype.

Besides activating toll-like receptors 2 and 4, which are expressed by peritubular cells, biglycan can also act via purinergic receptors P2RX4 and 7. Expression of P2RX4 and 7 in human peritubular cells could be confirmed and a functional assessment through calcium imaging pointed to P2RX4 as predominantly acting ion channel in these cells. Treatment of human peritubular cells with the physiological purinergic ligand ATP revealed an induction of cytokine production and secretion, whereas synthesis of characteristic peritubular features like smooth muscle cell markers and extracellular matrix molecules declined. Thus, ATP can act as a danger molecule via purinergic signaling in peritubular cells, thereby contributing to testicular inflammation.

One possible signaling mechanism integrating purinergic activation and release of cytokines is represented by activation of the NLRP3 inflammasome. This macromolecular complex consisting of the sensor NLRP3, the adapter ASC and the effector caspase1 assembles in response to cellular damage and induces inflammation and pyroptotic cell death. Expression of the NLRP3 molecule was confirmed in human and mouse Sertoli cells as well as human peritubular cells. In both species, NLRP3 was additionally linked to subfertile pathologies. Together, these findings argue for an involvement of NLRP3 in inflammatory as well as non-inflammatory mechanisms in the testis.

In summary, biglycan deficiency could not attenuate testicular inflammation in a mouse model, but ATP-induced signaling by purinergic receptors was identified as a pathway to promote sterile testicular inflammation via cytokine production and putative activation of the NLRP3 inflammasome in a human cellular model.

ZUSAMMENFASSUNG

Ursachen der männlichen Unfruchtbarkeit sind nur teilweise bekannt, in den zahlreichen idiopathischen Fällen bleiben sie unbekannt. Die sterile Entzündung des Hodens, die häufig asymptomatisch und dadurch unentdeckt verläuft, könnte eine mögliche Ursache sein. Oftmals wird dabei ein Anstieg der Anzahl an einwandernden Immunzellen im Hoden sowie die fibrotische Verdickung der Wand der Hodenkanälchen beobachtet. Die peritubulären Zellen, die diese Wand zusammen mit extrazellulärer Matrix bilden, tragen daher vermutlich zu entzündungsförderlichen Prozessen bei.

Peritubuläre Zellen stellen das kleine Leucine-rich Repeat Proteoglykan und Extrazellulär-Matrixmolekül Biglycan her. In sezernierter Form wird es meist zu strukturellen Zwecken in der extrazellulären Matrix eingelagert, aber in seiner löslichen Form kann es durch Aktivierung von Toll-like Rezeptoren 2 und 4 proinflammatorische Signalkaskaden in Gang setzen. Um diese Erkenntnisse zu überprüfen, wurde ein systemisches Mausmodell für männliche Unfruchtbarkeit und sterile Entzündung untersucht. Die Menge an Biglycan und die Anzahl der damit verknüpften Rezeptoren waren in diesem Mausmodell erhöht. Jedoch konnte der infammatorische Phänotyp nicht durch einen zusätzlichen Biglycan-Knockout gerettet werden.

Neben der Aktivierung der Toll-like Rezeptoren 2 und 4, die in peritubulären Zellen exprimiert werden, kann Biglycan auch mittels der purinergen Rezeptoren P2RX4 und 7 wirken. Die Expression von P2RX4 und 7 konnte in humanen peritubulären Zellen nachgewiesen werden und eine funktionelle Bewertung mittels Calcium Imaging deutete auf P2RX4 als vorwiegend aktiven Ionenkanal in diesen Zellen hin. Die Behandlung von peritubulären Zellen mit dem physiologischen purinergen Liganden ATP führte zu einem Anstieg in der Cytokinproduktion und -ausschüttung, während sich die Expression charakteristischer peritubulärer Merkmale wie Glattmuskelzellmarker und Extrazellulär-Matrixmoleküle verminderte. ATP kann daher über purinerge Signalwege als Gefahren-molekül in peritubulären Zellen wirken und so zur Entzündung des Hodens beitragen.

Ein möglicher Signalweg der Umsetzung purinerger Aktionen bis zur Freisetzung von Cytokinen ist die Aktivierung des NLRP3 Inflammasoms. Dieser makromolekulare Komplex bestehend aus dem Sensor NLRP3, dem Adapter ASC und dem Effektor Caspase1 fügt sich aufgrund von Beschädigung der Zelle zusammen und vermittelt Entzündung und pyroptotischen Zelltod. Die Expression von NLRP3 konnte in humanen und murinen Sertoli-Zellen sowie in humanen peritubulären Zellen gezeigt werden. In beiden Spezies konnte NLRP3 zusätzlich mit subfertilen Pathologien verknüpft werden. Zusammen sprechen diese Erkenntnisse für eine Beteiligung von NLRP3 an entzündlichen wie nicht-entzündlichen Mechanismen im Hoden.

Insgesamt konnte das Fehlen von Biglycan die sterile Entzündung des Hodens in einem Mausmodell nicht abschwächen. In einem humanen, zellulären Modell konnte jedoch ATP-vermitteltes Signaling über purinerge Rezeptoren als Signalweg, der die sterile Entzündung des Hodens durch Cytokinproduktion und vermeintliche Aktivierung des NLRP3 Inflammasoms begünstigt, identifiziert werden.

1 INTRODUCTION

1.1 The human testis and male infertility

1.1.1 Testicular organization and spermatogenesis

The testis is the central male reproductive organ composed of the tubular and the interstitial compartment encapsulated in a layer of connective tissue, the tunica albuginea. Its main purpose is the generation of sperm in the tubular compartment and the production of steroid hormones in the interstitial compartment, thereby ensuring male fertility.

The tubular compartment consists of coiled seminiferous tubules organized in lobules, which take up the majority of the testicular volume. The interior of the seminiferous tubules is lined by the tubular epithelium, formed by Sertoli cells, which enclose the developing germ cells (Figure 1.1). Seminiferous tubules are encompassed by the tubular wall, which is built from a basement membrane surrounded by concentric layers of peritubular cells and extracellular matrix (ECM). In the interstitial compartment, Leydig cells, blood and lymphatic vessels as well as nerve fibers and resident immune cells like macrophages are embedded in loose connective tissue[1].

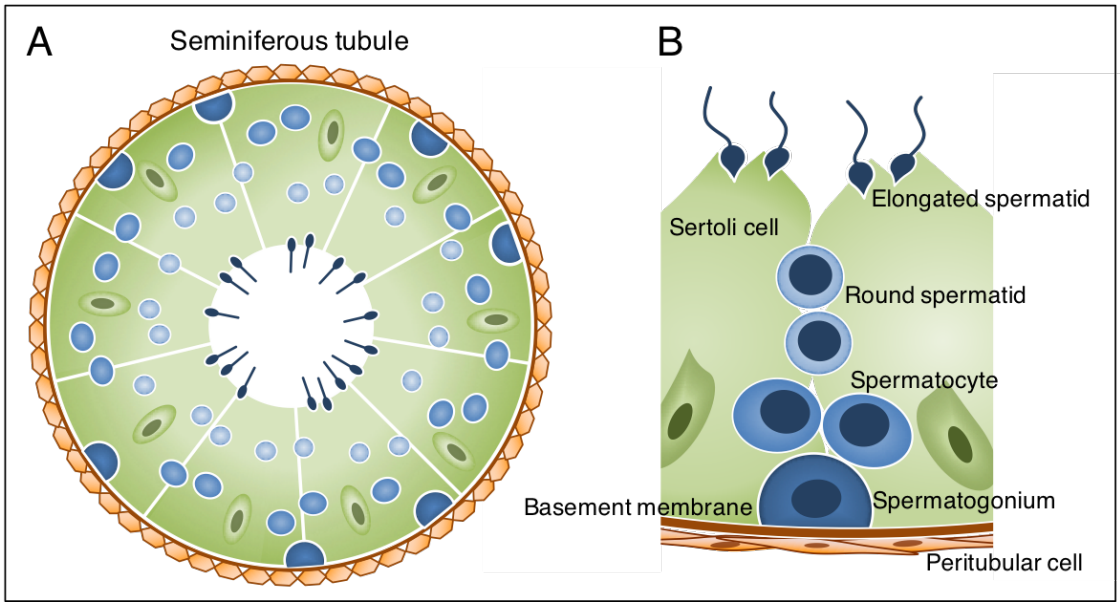

Figure 1.1 Organization of the seminiferous tubule.

A. Schematic cross section of a seminiferous tubule. Peritubular cells (orange) and the basement membrane (brown) form the wall surrounding the tubule. The tubular epithelium consisting of Sertoli cells (green), which line the tubular wall, embeds germ cells at different stages of their developmental process (blue) migrating from the basement membrane towards the tubular lumen (white). **B.** Schematic detail of a tubular cross section. Two Sertoli cells sitting on the tubular wall composed of basement membrane and peritubular cells enclose spermatogonium and resultant spermatocytes and spermatids. Elongated spermatids are found at the apical end of the Sertoli cells before their release into the tubular lumen. Modified on the basis of [2].

Spermatogenesis is the developmental process of generating spermatozoa from spermatogonia via mitotic and meiotic division (Figure 1.2). It takes place in the

seminiferous tubule epithelium, where spermatogonia reside at the basement membrane. Spermatogonia are distinguished into A dark (A_d), A pale (A_p) and B spermatogonia[3,4]. The original classification was based on appearance, but it correlates with mitotic activity. Type A_d spermatogonia are the quiescent reserve, while type A_p spermatogonia either are self-renewing or give rise to type B spermatogonia, thus type A spermatogonia represent the spermatogonial stem cell (SSC) population[5-7]. Type B spermatogonia divide mitotically into primary spermatocytes, which start to undergo meiotic division. Hence, diploid primary spermatocytes can be distinguished according to their prophase1 stage of meiosis (preleptotene, leptotene, zygotene and pachytene). After the first meiotic division, the resulting haploid intermediates have been termed secondary spermatocytes, which become round spermatids upon completion of the second meiotic division[3,4]. During the process of spermiogenesis, round spermatids mature through chromatin compaction and formation of acrosome and sperm tail. Emanating elongated spermatids or spermatozoa are subjected to spermiation, meaning detachment from the Sertoli cell and thus, release into the testicular lumen[8,9]. Subsequently, spermatozoa are transported through the seminiferous tubules via the rete testis into the epididymis for further maturation and storage[10,11].

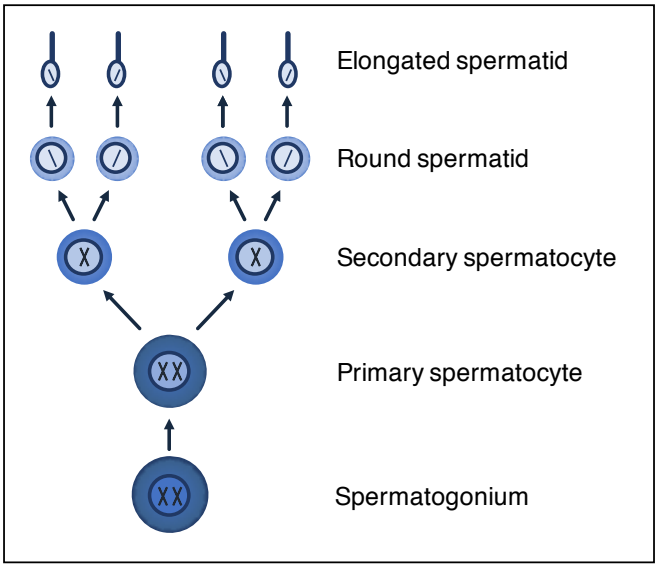

Figure 1.2 Sequence of spermatogenesis.

Schematic illustration of spermatogenic development from spermatogonium to elongated spermatid via mitotic and meiotic division. The spermatogonium divides asymmetrically resulting in a primary spermatocyte. Diploid primary spermatocytes undergo meiosis, thereby giving rise to haploid secondary spermatocytes, which further complete meiosis and become round spermatids. During spermiogenesis round spermatids are subjected to extensive remodeling to become elongated spermatids, which are released into to tubular lumen.

The testis is an immune-privileged organ due to the blood-testis barrier[12-14], which is comprised of anatomical, physiological and immunological barriers formed and maintained by different somatic cells of the testis[15]. Its primary physical components are tight junctions between adjacent Sertoli cells that divide the tubular epithelium in a basal and an adluminal compartment[16,17]. The blood-testis barrier serves three essential functional purposes. It shields developing germ cells from the immune system, limits the passage of molecules and provides a special environment for the completion of meiosis and spermiogenesis[18,19]. Thus,

primary spermatocytes are the first to cross the blood-testis barrier before entering their second meiotic phase.
Steroid hormone production is the second substantial function of the testis, primarily accomplished by Leydig cells in the interstitial compartment. Leydig cells predominantly synthesize testosterone dependent on stimulation with luteinizing hormone, but also further androgens and estradiol via testosterone conversion by the enzyme aromatase. Testosterone is critical to spermatogenesis and the development and maintenance of male phenotypic characteristics[1,20-22].

1.1.2 Testicular alterations and male infertility

While there are many prerequisites for male fertility, testicular integrity is a crucial one. If disturbed, spermatogenesis is bound to fail resulting in non-obstructive azoospermia, meaning the absence of sperm in the semen without obstruction of the ductal system. Underlying causes can be genetic aberrations, disturbance in the hypothalamic-pituitary axis or varicocele, for instance, but the majority of cases is idiopathic, i.e. the reasons remain unknown[23]. Resulting hormonal imbalances or failure of somatic cells, Sertoli cells in particular, to support spermatogenic development manifest in testicular alterations characteristic to subfertile or infertile patients.
Inflammation of the testis, although rarely reported due to its often asymptomatic course, is a well-established cause of male infertility evoked either by infection or sterile stimuli[24]. Sterile triggers include mechanical trauma, autoimmune reaction or pre-existing disorders that are accompanied by inflammatory processes[24,25]. This scenario is not very well investigated, but thereby released cytokines and chemokines from somatic cells and resident immune cells can serve as initial attractants for immune cell infiltration[26]. Inflammatory cytokines like interleukin 1 (IL1) or tumor necrosis factor α (TNFα) inhibit steroidogenesis and thus, reduce intra-testicular testosterone levels contributing to spermatogenic failure. In parallel, the cytokines increase the formation of reactive oxygen species (ROS), which may negatively impact sperm integrity[24,27]. Cytokines can furthermore act on components of the blood-testis barrier and by that overcome this barrier and enter the tubular lumen to induce germ cell apoptosis[28-30]. Eventually, cytokine signaling leads to production and deposition of ECM molecules and hence, fibrosis[31,32]. All these processes can substantially contribute to the overall picture of testicular pathologies.
Typical testicular phenotypes include mixed atrophy (MA), germ cell arrest or Sertoli cell only (SCO) syndrome. In mixed atrophy patients, seminiferous tubules with intact spermatogenesis are located next to tubules with different extent of impaired spermatogenic function. These tubules are characterized by disorganized structure of the germinal epithelium as well as fibrotic tubular walls[33]. Germ cell or maturation arrest can appear at various stages of spermatogenesis resulting in tubules with incomplete spermatogenic development[34,35]. In SCO syndrome, germ cells are either completely absent or present in rare foci that do not develop further than spermatogonial stage[5,36].
Fibrosis is a classical hallmark of infertility-related pathophysiology[37-39]. It is defined as a process of extensive tissue remodeling in response to stress or injury characterized by excess

ECM production and deposition[40]. In the testis, the tubular wall typically undergoes fibrotic remodeling under pathophysiologic conditions as documented by increased wall thickness. Collagen fibers become overabundant and irregularly arranged between peritubular cell layers often accompanied by thickening of the basement membrane, thereby contributing to disorganization and fibrosing of the tubular wall[38,41]. In addition, peritubular cell morphology becomes altered including loss of cell polarity and hypertrophy[42,43], which indicate impaired cellular function and signaling activity.

A second characteristic trait of subfertile and infertile pathologies is the accumulation of immune cells, which occurs particularly in the tubular wall[44-47]. Mast cells and macrophages define the immune cell population of the human testis, complemented by few lymphocytes[44,48,49]. It is generally accepted, that resident testicular immune cells exert regulatory functions and thus, maintain the immune privilege of the testis. However, if immunoregulation is disturbed, circulating immune cells are able to infiltrate the testis and participate in inflammatory processes[50].

In the healthy human testis, mast cells are primarily located in the interstitial tissue, but can also be found intermingling with peritubular cells in the wall of the seminiferous tubules[51,52]. Both, increases in mast cell abundance and their more frequent localization in the tubular wall have been linked to infertile pathologies such as MA, germ cell arrest or SCO syndrome[44,47,53-55]. In particular, elevated mast cell presence coincides with fibrotically thickened tubular walls[46,47]. Further, the mast cell subpopulation expressing chymase in addition to tryptase is numerically enhanced[56], particularly in the tubular wall[57]. Mast cell-secreted tryptase promotes proliferation of fibroblasts[58,59] as well as collagen[58,60,61] and proteoglycan synthesis[62]. Tryptase is an activator of the protease activated receptor 2 (PAR2), which mediates not only proliferative actions[59,63], but induces pro-inflammatory actions via factors like cyclooxygenase 2 (COX2) and thereby prostaglandins or monocyte chemoattractant C-C motif chemokine ligand 2 (CCL2)[59,64-66]. PAR2 expression and function have been described in peritubular cells[67], germ cells[65,68,69] and macrophages[46] of the testis. Mast cell-derived chymase cleaves angiotensin I to angiotensin II resulting in pro-inflammatory interleukin 6 (IL6) production in peritubular cells[57]. Thus, mast cell products exert pro-fibrotic and pro-inflammatory effects in the testis, which are enhanced in infertile patients due to augmented mast cell abundance[70,71].

Macrophages in the human testis mainly reside in the interstitial tissue, but also in the tubular wall and even the lumen of the seminiferous tubules[44,45,48]. Similar to mast cells, a numerical increase of macrophages correlates with testicular pathologies, where macrophage localization shifts in favor of tubular wall and lumen[44,45]. Generation of pro-inflammatory molecules such as IL1 or TNFα by testicular macrophages[45,72] implicates a contribution to testicular inflammation.

The scarce testicular lymphocyte population mainly consists of interstitial T cells[48,73]. Albeit under inflammatory conditions, lymphocytes infiltrate interstitial and peritubular sites coinciding with tubular fibrosis and disturbed germinal epithelium[50,74,75].

1.1.3 The peritubular compartment of the testis

The tubular wall is primarily created by two components at the basement membrane, peritubular cells and extracellular matrix. In human, the elongated spindle-like shaped peritubular cells are arranged in five to seven concentric layers separated by ECM and connective tissue, whereas there is merely one layer of peritubular cells in rodents[76,77]. Peritubular cells and adjacent Sertoli cells collaborate in synthesizing these ECM components, prevalently collagens, fibronectin, laminin and proteoglycans[78-80], thereby forming and stabilizing the tubular wall. Apart from ECM production and deposition, smooth muscle cell-like contractile abilities are the second prime characteristic of peritubular cells, therefore also termed peritubular myoid cells. Smooth muscle cell-like features of mature peritubular cells are articulated by expression of smooth muscle actin[67,81,82], myosin heavy chain 11 and calponin[43,83] as well as the intermediate filament-forming desmin[84,85]. The smooth muscle cell properties allow peritubular cells to contract and thus, transport the yet immotile spermatozoa from the lumen of the seminiferous tubules to the epididymis[10,86,87]. However, smooth muscle cell function can only be attributed to the inner layers of peritubular cells, whereas the outer layers display a fibroblast phenotype[88].
Due to the localization next to the basement membrane, in the immediate proximity to spermatogonial stem cells, Sertoli and Leydig cells as well as blood and lymph vessels or immune cells like mast cells or macrophages, peritubular cells are downright predestined to interact with their surroundings. Hence, substantial paracrine signaling activity by peritubular cells e.g. via growth factors has been identified. Peritubular cells modulate Sertoli cells function via secreted factors[89,90] as well as Leydig cell differentiation and function in an androgen-dependent manner[91]. In turn, the peritubular phenotype is maintained by Sertoli cells[92]. In addition, peritubular cells anatomically contribute to the blood-testis barrier by forming a semi-permeable barrier to exclude large molecules from the tubular lumen[16,17], although this function seems less pronounced in primates[93].

1.1.4 Human testicular peritubular cells (HTPCs) as a cellular model

Peritubular cells of the seminiferous tubules are characterized by their smooth muscle cell functions that are of utmost relevance for sperm transport and their ability to produce and secrete ECM molecules to build and stabilize the tubular wall. Human Testicular Peritubular Cells (HTPCs) have been established as an *in vitro* and therefore cell culture model of the peritubular cells. These cells are derived from individual testicular tissue samples using an explant culture method[67]. To date, HTPCs are the sole available cell culture model of human somatic testicular cells that can be cultivated and subcultivated for a longer period of time. Hence, they provide an ideal model for mechanistic studies[94].
Characterization of cultured HTPCs revealed their ability to synthesize and release pro-inflammatory molecules such as the cytokines IL6, the monocyte chemoattractant CCL2 or the soluble pattern recognition receptor (PRR) pentraxin 3 (PTX3)[95,96]. HTPCs harbor a functional Toll-like receptor (TLR) 2 inducing IL6, CCL2 as well as PTX3 expression and release by activation through its natural ligand, but alternatively through the proteoglycan

and ECM molecule biglycan[95]. Hence, HTPCs could participate in infectious and sterile testicular inflammation via cytokine secretion.
In addition, release of IL6 and CCL2 attests a close interaction of HTPCs with testicular immune cells, since mast cell products TNFα and chymase modulate expression of these factors via their corresponding receptors on HTPCs[57,96]. TLR2 expression in HTPCs is also positively correlated with TNFα[95]. Further TNFα increases the expression of nerve growth factor by HTPCs[96] whose proliferative actions are regulated via cleavage by another mast cell product, tryptase[97]. TNFα and tryptase both induce synthesis of the proteoglycan decorin[62,98]. As a result, secreted decorin restricts growth factor signaling[62] and its abundant deposition is associated with impaired spermatogenesis[62,98].
Alterations of testicular morphology are also related to the production of prostaglandins and metabolites. Prostaglandins are synthesized by constitutively present COX1 and e.g. by TNFα inducible COX2 in HTPCs[96,99]. Prostaglandins and metabolites cause a partial loss of contractility markers such as calponin or SMA in peritubular cells as it has been observed in subfertile pathologies[43,99,100]. Hence, prostaglandin effects are able to disturb testicular function by reducing contractile abilities of HTPCs and thus, sperm transport.
A proteomic approach[101] confirmed secretory properties for ECM molecules, especially proteoglycans, and cytokines and brought closer insight into HTPC signaling functions. Together with *in vitro* and *in vivo* assessment of peritubular cells, it allowed for the identification of factors that imply a direct contribution to the stem cell niche. Stem cell niche regulatory factors Glial cell line-derived neurotrophic factor (GDNF) and C-X-C motif chemokine ligand 12 (CXCL12) are produced and secreted by HTPCs[101,102]. Both factors are synthesized by Sertoli cells as well[103-105], yet a peritubular-specific knock-out confirmed that peritubular-derived GDNF, which is e.g. induced by prostaglandins[99], is crucial in SSC maintenance[106,107]. Another factor identified in the HTPC secretome is pigment epithelium-derived factor, which could promote tubular avascularity and thus, provides further evidence for a contribution of HTPCs to the blood-testis barrier[108].
Moreover, studies of HTPCs have attributed them steroidogenic capacity[109] and implicated regulation of their functions via androgen and estrogen receptors[94,110].
Altogether, mechanistic studies on cultured HTPCs complemented by different approaches revealed capabilities in contributing to inflammatory processes, communicating with testicular immune cells and influencing testicular microenvironments.

1.1.5 The *AROM*$^+$ mouse as a systemic model of sterile inflammation

The *AROM*$^+$ transgenic mouse line has been established as valid model of sterile inflammation and male infertility[111]. The *AROM*$^+$ mouse was created by introducing human P450 aromatase (*CYP19A1*) under control of a universal promoter[112,113]. Excess expression of aromatase was achieved in the testis as well as in extragonadal tissues[112]. Due to the systemic aromatase overexpression, the balance between testosterone and estradiol shifts gravely in favor of estradiol as aromatase is the rate-limiting enzyme for the conversion of androgens to estrogens[114]. The phenotype is characterized by malformation of endocrine organs such as adrenal glands, impairment of the urogenital tract and retarded bone

development. Male offspring suffer from disturbed development of reproductive organs, especially the testis as testosterone-sensitive organ is critically affected. Males exhibit cryptorchidism and reduced testis size. Testicular structure is dramatically altered in regard to seminiferous tubular architecture, collagen deposition, abundance and size of Leydig cells and number of macrophages and mast cells paralleled by spermatogenic arrest. Thus, males are collectively infertile, while female mice remain largely unaffected[111-113]. The severity of these phenotypic changes aggravates with increasing age. While at four months of age, Leydig cell hypertrophy and hyperplasia can already be observed, spermatogenesis is still ongoing. At nine months of age, merely few germ cells can be detected in the seminiferous tubules and at 15 months, tubules are almost completely devoid of germ cells, illustrating spermatogenic failure with age. Concomitantly, macrophages in the interstitial tissue become immensely more abundant and form giant multinucleated cells engulfing Leydig cells from nine months onward. Macrophages were identified as the source of the inflammatory cytokine TNFα in the testicular interstitium. TNFα levels, hence, increase with age of the *AROM*$^+$ mice as well[111]. However, mast cells in the interstitial tissue, which also represent a putative origin of TNFα[115], were not found before 15 months of age. Collagen deposition can hardly be observed at four months of age, albeit from nine months onward fibrosing through accumulation of collagen fibers is markedly enhanced[111].
Thus, inflammation-related changes such as the number of immune cell progress with age, accompanied by augmented TNFα levels and accumulating fibrosis in the tubular walls and the interstitial tissue. These findings provide evidence for severe chronic inflammation of the *AROM*$^+$ testes, that is evoked by a sterile, therefore non-infectious cause, namely aromatase overexpression. In the human, similar phenotypic alterations have been reported in the testes of infertile patients. For instance, numbers of macrophages expressing TNFα are elevated in the testes in infertile men[44,45] and fibrotic remodeling occurs in these patients[46,47]. Consequently, the sterile inflammatory situation observed in the *AROM*$^+$ mouse can be employed as a model mimicking the human phenotype i.e. for systemic investigation of inflammation-associated male infertility[45,47,111].

1.2 The extracellular matrix molecule biglycan

1.2.1 Structure and function of biglycan

Small leucine-rich proteoglycans (SLRPs) are a subgroup of the family of proteoglycans that are characterized by a central domain of leucine-rich repeats (LRRs) flanked by two conserved cysteine-rich regions[116]. SLRPs have been classified according to their structural homology and functional similarity. The SLRP biglycan (BGN) belongs to the canonical class I, which distinctively displays two disulfide bonds in the N-terminal flanking cysteine cluster[117,118]. The biglycan gene contains eight exons and is located on the X chromosome in both, humans and mice[119-121]. Biglycan is a 42 kDa modularly arranged protein (Figure 1.3) with a core unit of twelve leucine-rich repeats, the last one exhibiting a so-called “ear repeat”[116,122-124]. Its N-terminus is modified by attachment of one or two glycosaminoglycan (GAG) side chains consisting of chondroitin or dermatan sulfate depending on the tissue[125-

[127]. Biglycan is ubiquitously expressed and was discovered in the human testis, originating from the peritubular compartment in particular, over two decades ago[128,129]. After synthesis, the biglycan precursor protein is secreted into pericellular space, where the N-terminus is removed by cleavage through bone morphogenetic protein 1 (BMP1) to gain the mature protein[130].

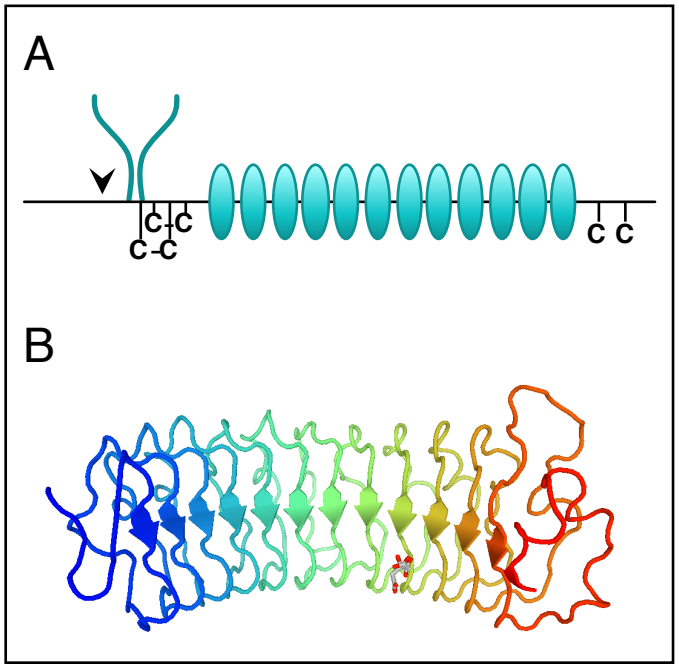

Figure 1.3 Structure of the small leucine-rich proteoglycan biglycan.

A. The modular protein structure of biglycan consists of twelve leucine-rich repeats. The repeat core is flanked by two cysteine (C)-rich regions including two disulfide bonds between cysteine residues in the N-terminal cluster. Two GAG chains are covalently linked at the N-terminus. For maturation, N-terminal cleavage is necessary (arrowhead; modified on the basis of [116,131]). **B.** Putative three-dimensional biglycan structure (SWISS-MODEL) based on the crystalline dimer[123] shows the tandem LRRs in a concave assembly with the "ear repeat" at the last LRR.

Secreted biglycan interacts with a variety of ECM structural molecules, e.g. different types of collagens, via its core sequence or the GAG chains[132,133]. Thereby, biglycan contributes to fibrillogenesis and fibril structure and regulates matrix assembly without being part of the fibrils themselves, while simultaneously becoming sequestered in the ECM[134]. Besides serving structural purposes, biglycan can interact with numerous cell surface receptors and modulate cell-matrix interactions due to its location in the pericellular compartment[135]. For instance, there is interplay with growth factors or cytokines, such as transforming growth factor β (TGFβ)[136], TNFα[137] or BMP2 and 4[138-140], as well as involvement in Wnt signaling[141-143]. Yet, for most direct interactions biglycan has to regain its soluble state, either by release from the matrix via proteolysis upon tissue stress or injury or by *de novo* synthesis through resident cells or macrophages[144,145].

As indicated by the diversity of interacting partners, biglycan has been implicated as a factor in many biological processes. Mainly transgenic mouse models contributed new evidence to the versatile roles of biglycan. Loss of biglycan results in an osteoporosis-like phenotype[146] crucially impacting skeletal bone formation[138,147-150] by modulating TGFβ/BMP and Wnt

signaling pathways[127,151]. Further, biglycan has been shown to be of similar importance in tendon[152-155] and cartilage[156] formation and atherosclerosis prevention[157,158] as well as a stabilizer of muscle[159-161] and neuromuscular synapses[162]. In contrast, its part in tissue fibrosis remains unresolved, although accumulation and deposition of biglycan in renal, hepatic or pulmonary fibrosis have been established[163-166]. Biglycan does not exhibit antifibrotic potential like its closely related sister molecule decorin[167], but has been suggested to promote fibrogenesis via inflammatory signaling[163,168,169]. Still, it is beneficial in fibrotic scar remodeling after myocardial tissue injury[170]. Meanwhile its pro-inflammatory signaling properties, namely the interaction with TGFβ and Wnt[143,171], as well as regulation of the cell cycle[172,173] have linked biglycan to cell growth and proliferation and thus, tumorigenesis. In this context, promotion of angiogenesis via, for instance, biglycan-regulated VEGF (Vascular endothelial growth factor)[174-176] has, together with biglycan overexpression, formed a connection of biglycan with tumor progression[177-179].

1.2.2 Biglycan in inflammatory signaling

Besides its structural abilities as extracellular matrix stabilizer, biglycan has emerged as regulator of immune signaling acting as a danger-associated molecular pattern (DAMP) in both, the innate and the adaptive immune response[127,165,180]. These actions were thus mainly deciphered in immune cells, primarily macrophages. In injury or stress conditions, sequestered biglycan and fragments thereof can be liberated from the extracellular matrix by matrix degradation through metalloproteinases[165]. Soluble biglycan binds TLR2 and TLR4 (Figure 1.4) on the surface of immune cells via the central domain[169,181] mimicking recognition features of the native pathogenic TLR ligands[180,182]. At least the core domain and one GAG chain of biglycan are needed for TLR activation[169] rendering some of the released fragments ineffective in introducing an inflammatory response, therefore supporting speculation that in addition to proteolysis *de novo* synthesis of biglycan might be necessary[180]. Since biglycan triggers activation of both, TLR2 and 4, it is able to amplify the immune response in pathogen-induced inflammation through the non-pathogen-sensing TLR[183]. Via TLRs biglycan indirectly activates mitogen-activated protein kinases (MAPK) p38 and extracellular-signal regulated kinase (ERK) 1/2 or nuclear factor kappa B (NFκB) signaling leading to expression of the pro-inflammatory cytokines and chemokines interleukin (IL) 1β, CCL2, 3, 5 and 20, CXCL1, 2, 10 and 13 and TNFα[169,181,184-186].

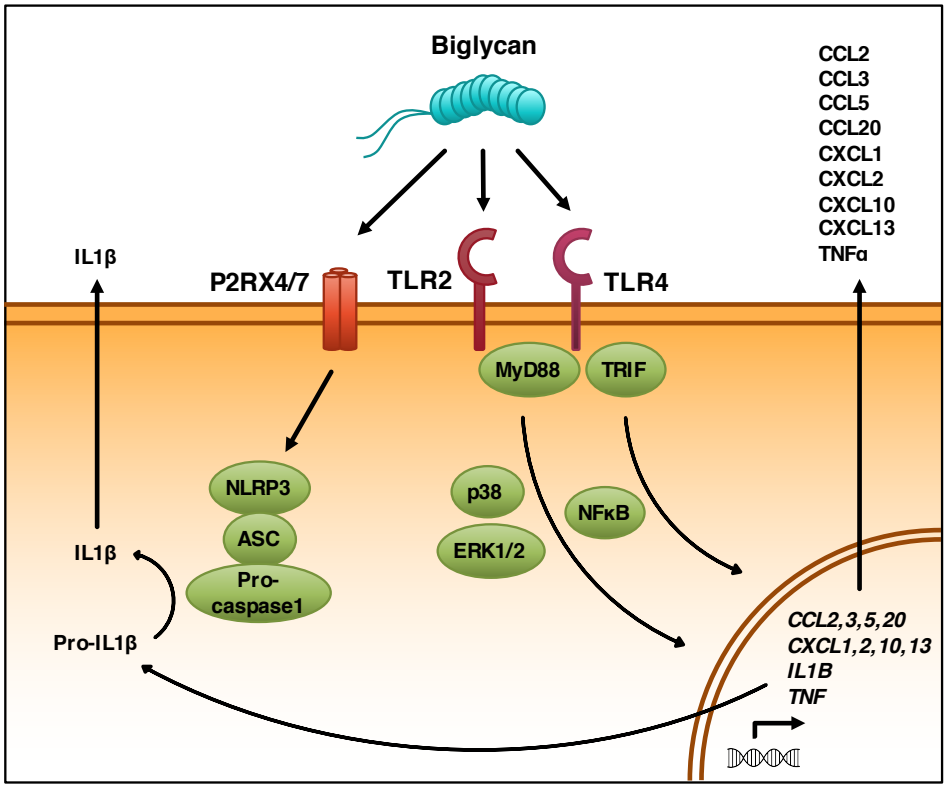

Figure 1.4 Biglycan autonomously triggers inflammatory signaling.
Soluble biglycan activates TLR2 and 4 thereby inducing expression and secretion of cytokines and chemokines via p38/ERK or NFκB signaling as it has been discovered in macrophages. CCL2 and 20 and CXCL1 and 2 are synthesized dependent on MyD88, whereas CCL5 and CXCL10 production is solely achieved via the TLR4/TRIF axis. Biglycan prompts clustering of TLRs with P2RX4/7 leading to activation of the NLRP3 inflammasome followed by IL1β maturation and subsequent release. Modified on the basis of [163,180,186].

Secretion of cytokines and chemokines contributes to the inflammatory environment and to gradient formation attracting immune cells to the site of injury, thereby connecting innate and adaptive immune response[127]. For instance, B cells can be recruited via biglycan-controlled CXCL13[184]. CCL2, CXCL1 and CXCL2 production depends on the TLR adaptor and signaling molecule MyD88 (myeloid differentiation primary response 88) and recruits macrophages and neutrophils, while MyD88-dependent CCL20 synthesis leads to Th17 chemoattraction. TLR4 can additionally signal through the adaptor TRIF (TIR-domain-containing adapter-inducing interferon β) inducing CCL5 and CXCL10 expression and consecutive T cell migration[185,186]. More additional determinants of activation and regulation of these signaling processes, e.g. interferon γ receptor[186] or sphingosine kinase 1[187], become unraveled, although it will take considerable time and effort to reveal all factors in this complex signaling network. Besides binding Toll-like receptors, biglycan is able to introduce clustering of TLR2 and 4 with purinergic receptors P2RX4 or 7. This interaction promotes NLRP3 (NLR family pyrin domain containing 3) inflammasome activation and subsequent IL1β maturation and release[188]. Biglycan further modulates this process dependent on NADPH oxidases and heat shock proteins[188,189].
Consequently, biglycan knock-out mice exhibit reduced caspase 1 activation via the NLRP3 inflammasome and lower cytokine levels in non-infectious inflammation models causing

less inflammatory damage[188,189]. Hence, biglycan is viewed as autonomous trigger of sterile inflammation.

1.3 The system of purinergic signaling

1.3.1 Purinergic receptors

The system of purinergic receptors has originally been classified into two subgroups, P1 and P2 receptors, according to their ligands. P1 receptors bind adenosine, whereas P2 receptors recognize various nucleotides, prevalently adenosine triphosphate (ATP) and adenosine diphosphate (ADP)[190]. P2 receptors were subsequently divided into ligand-gated ion channels (P2X receptors) activated by ATP and G-protein coupled receptors (GPCRs; P2Y receptors; Figure 1.5)[191,192]. Activation of all purinergic receptors is interconnected. Extracellular ATP can be converted into its metabolites ADP, adenosine monophosphate (AMP) and finally adenosine by ectonucleotidases. Thus, activation of P2Y or adenosine receptors can occur as a downstream effect of ATP signaling as well[193].

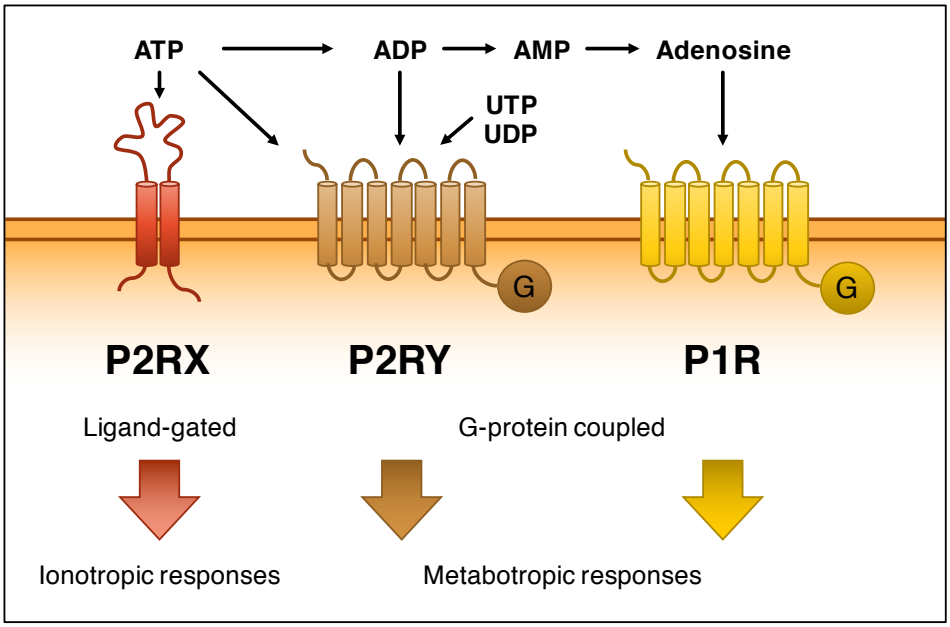

Figure 1.5 Purinergic receptor signaling.

The purinergic receptors are subdivided into receptor families, P1, P2X and P2Y receptors. P2RX monomers consist of two transmembrane domains, which assemble in trimers to form ligand-gated ion channels initiating ionotropic responses. P2RX are activated by ATP as their natural ligand. P2RY and P1R are both seven transmembrane domain G-protein coupled receptors mediating metabotropic responses. P2RY subtypes display different affinities to their ligands, the most common ones being ATP, ADP, UTP and UDP. P1R are activated by adenosine solely. Ectonucleotidases are able to metabolize ATP to ADP, AMP and finally adenosine, thus linking purinergic actions induced by different ligands. Modified on the basis of [194].

P1 receptors or adenosine receptors are comprised of a family of four GPCRs, A1, A2A, A2B and A3[195,196]. A1 and A2A display high affinity to their ligand adenosine, whereas A2B and A3 are of low affinity[197]. All four P1 receptors possess a seven transmembrane helix domain structure coupled to G_s protein in case of A2A and A2B and to $G_{i/o}$ protein in case

of A1 and A3. This means A2A and A2B positively stimulate adenylate cyclase (AC) via G_s leading to cyclic adenosine monophosphate (cAMP) formation and consecutive downstream signaling. On the contrary, A1 and A3 activation inhibits adenylate cyclase signaling via $G_{i/o}$[197].

P2Y receptors are also seven transmembrane helix domain GPCRs, similar to P1 receptors. Eight subtypes have been identified, P2RY1, P2RY2, P2RY4, P2RY6, P2RY11, P2RY12, P2RY13 and P2RY14[198]. P2RY12-14 prevalently couple to $G_{i/o}$ protein thereby preventing AC activation. The other five P2RY subtypes mainly induce phospholipase C (PLC) signaling via G_q protein resulting in cytosolic inositol triphosphate (IP_3) increase and subsequent Ca^{2+} mobilization from intracellular stores[198,199] with the exception of P2RY11, which can couple to G_s protein and thus, signal through AC, too[200,201]. In contrast to P1 and P2X receptors, P2Y receptors recognize more than one native agonist, purines as well as pyrimidines and derivatives, albeit with considerably different affinities. While P2RY1, P2RY12 and P2RY13 exhibit their highest affinity to ADP[202-204], P2RY11 is most efficiently activated by ATP[205]. Uridine triphosphate (UTP) is the most potent ligand on P2RY2 and P2RY4, closely followed by ATP in case of P2RY2[206]. P2RY6 possesses topmost affinity to uridine diphosphate (UDP)[206] and P2RY14 is primarily activated by UDP-glucose[207].

Contrary to the GPCR structure of P1 and P2Y receptors, P2X receptor monomers consist of two transmembrane-spanning domains with intracellular N- and C-termini connected by an extracellular loop[208-211]. Dependent on the subtype, they assemble as homo- or heteromeric trimers to form cation permeable channels. Seven members have been assigned to the P2X receptor family, P2RX1-7[191,197]. Homotrimers have been detected for each member and a variety of heterotrimers has been established, for instance P2RX1/2, P2RX1/4, P2RX1/5, P2RX2/3, P2RX2/5, P2RX2/6 and P2RX4/6[212-214]. Heterotrimer formation by P2RX7 is a current topic of discussion, but accumulating evidence suggests that it forms heterotrimers with P2RX4[215,216]. All P2X receptors share ATP as physiological ligand, yet effective concentrations (EC) of ATP stretch from low-nanomolar to mid-micromolar range[217]. Activation of P2X receptor trimers occurs via ATP binding to the interface of two subunits in a cooperative manner[218-220] inducing a conformational change and rearrangement of the subunits that leads to channel opening[221,222]. In the open state, the channel pore is permeable to sodium and calcium influx and potassium efflux inducing membrane depolarization and a rise in intracellular Ca^{2+} concentration[223-225]. Channel activation is followed by desensitization and a final cease of the ion flow. Desensitization kinetics highly depend on the involved P2RX subtypes. While P2RX1 and P2RX3 desensitize rapidly, the process occurs slowly for P2RX2, P2RX4 and P2RX5. P2RX7, however, does not appear to desensitize[217,224]. Prolonged ATP stimulation leads to enhanced membrane permeability for large cations therefore termed pore dilation. This hallmark of P2X receptor activation has been observed for P2RX2, P2RX4 and P2RX7 as well as several heterotrimers[226-228]. Whether the P2X-formed channel pore can actually dilate to the required diameter to allow the passage of large cations remains to be determined. A second option is the interaction of activated P2RXs with a separate membrane channel mediating large cation influx[229,230].

In the testis, presence of different purinergic receptors was confirmed mostly based on studies conducted in the rodent. P1 receptors were found to be expressed in the testis[231,232] suggesting a role in sperm physiology[233-236]. P2 receptors display a diverse expression pattern, which is oftentimes inconsistent between reports[237,238]. Murine spermatogonia exhibit functional P2RX4 and P2RX7 signaling as part of a paracrine signaling network in spermatogenesis[239], whereas stage-dependent expression of P2RX2, P2RX3 and P2RX5 has been shown in postmeiotic germ cells in the rat[240]. In murine sperm, P2RX2 signaling was found to be crucial in preserving fertility[241], while the human sperm transcriptome revealed the presence of P2RX3, P2RX4, P2RX5 and P2RX7 transcripts[242]. In Sertoli cells, P2RX and P2RY signaling intermingles[243-245] exemplified by expression of P2RY1, P2RY2, P2RX2, P2RX3, P2RX4, P2RX5 and P2RX7 in rat Sertoli cells[240,246]. In mouse Sertoli cells, P2RX2 and P2RY2 were recently identified as purinergic signal mediators of ATP[247]. P2RX2, P2RX4, P2RX6 and P2RX7 were discovered in Leydig cells, which predominantly exhibit pharmacological properties of P2RX2[248,249]. In regard to peritubular cells, until now solely faint and infrequent expression of P2RX2 and P2RX5 was described[240]. Hence, distinguishing purinergic signaling contributors and resulting physiological impact in the testis remains a challenging field.

1.3.2 Purinergic signaling in physiology and pathophysiology

Purinergic signaling is an omnipresent mechanism found throughout tissues. Thus, it engages in numerous processes establishing and maintaining tissue function[250]. The concept of purinergic signaling was first introduced when the purine nucleotide ATP was discovered as a neurotransmitter acting in extracellular space[251,252]. Consequently, ATP is now established as co-transmitter in synaptic transmission of neurons in the central nervous system, but also known to modulate synaptic interaction with glial cells or astrocytes, which are all affected via their different repertoire of purinoceptors[253]. This process belongs to the short-term, i.e. directly effective purinergic actions. Another major short-term effect is the control of smooth muscle cell contraction. In the periphery, ATP release by sympathetic neurons causes smooth muscle contraction, while simultaneously promoting relaxation via endothelial cells[254,255]. In the male reproductive system, purinergically controlled smooth muscle contraction in the vas deferens is crucial to sperm ejaculation[256,257] supported by the notion that P2RX1 knock-out mice are significantly less fertile due to declined contraction ability of the vas deferens[258]. It contributes to penile erection via contraction and relaxation events and ATP signaling has been indicated in sperm motility and fertilizing capacity[238]. Short-term purinergic actions further comprise induction of endocrine and exocrine secretion, chemoattraction and acute inflammation and nociception[259,260].

Long-term or trophic purinergic signaling is executed through the vast variety of intracellular signaling cascades that are activated by purinergic receptors and it is related to fundamental processes, such as cell proliferation, differentiation, motility and death[261]. Substantial roles have been identified in development starting from the early embryo via differentiation of organ structures and systems and ending with ageing process[262]. Purinergic signaling participates for instance in synaptic plasticity[263,264] or bone formation and resorption[265,266]. At the same time it is indicated in pathophysiologic conditions, which renders purinergic

receptors putative targets for treatment of these conditions[267]. Depending on the involved subset of purinergic receptors, extracellular purines can promote or constrain processes like atherosclerosis[268], brain injury and neurodegenerative diseases[253], tumor progression[269-271] or tissue regeneration versus chronic inflammation and pain[272-274]. Generally speaking, ATP-mediated signaling rather fosters the pathological conditions, while adenosine actions exert a protective effect counterbalancing the ATP-induced processes[275].

1.3.3 Purinergic signaling in inflammation

Under physiologic conditions concentrations of extracellular nucleotides are marginal[276-278]. Upon injury, ATP is released from damaged cells e.g. via exocytosis or the opening of plasma membrane channels[279] and eventually through apoptotic cell death[280]. Extracellular ATP is able to act as a danger signal activating autocrine or paracrine purinergic signaling thereby attracting immune cells[281-283]. Response of immune cells to ATP is shaped by their distinct repertoires of purinergic receptors. Thus, dependent on the extracellular ATP concentration different purinoceptors become activated mediating e.g. neutrophil or macrophage migration to the site of cellular damage to induce phagocytic clearance[280,282-284]. Recruitment of immune cells is further promoted indirectly by ATP-dependent release of chemoattractants like CCL2, CXCL8 or IL6 from fibroblasts or endothelial cells[285,286].

Among the P2X receptors, P2RX7 has been found to be particularly involved in inflammatory processes through both, its ion channel permeability and its intracellular signaling properties[287]. Most prominently, P2RX7 activation triggers formation of the NLRP3 inflammasome via potassium efflux or potentially direct interaction[288] including subsequent IL1β and IL18 maturation and release[289-291]. Moreover, P2RX7 initiates pro-inflammatory gene expression through MyD88-dependent activation of NFκB[292-294], which is the primary inducer of *IL1B* transcription, but also of a variety of other pro-inflammatory cytokines and chemokines[295]. Via NLRP3 inflammasome signaling, P2RX7 has been identified as crucial to pyroptotic cell death[296], but has also been implicated in other forms of cell death, namely apoptosis[297,298], necrosis[299,300] and autophagy[301], depending on the cell type[287]. In contrast, P2RX7 can act as mediator of cell proliferation and growth[270,302,303]. In chronic inflammation, P2RX7 substantially contributes to tissue fibrosis[304,305].

P2RX4-mediated ATP-dependent responses came into focus more recently. P2RX4 is co-expressed with P2RX7 in most types of immune cells[284] where it has been found to exhibit significant impact on the ionotropic Ca^{2+} response in monocytes and macrophages[306] or amplify the immune response in T cell activation[307]. Like P2RX7, P2RX4 has been uncovered as an activator of the inflammasome[308-310]. P2RX4 and P2RX7 cooperate through direct functional interaction[215,311-313], yet it appears that P2RX4 acts as regulator of P2RX7-mediated inflammatory functions[314-316].

1.4 The NLRP3 inflammasome

1.4.1 NLRP3 inflammasome structure and assembly

Inflammasomes are multiprotein complexes composed of sensor, adaptor and effector components, which assemble in the cytosol of immune cells for the purpose of inflammatory caspase activation[317]. Sensor proteins were established as intracellular pattern recognition receptor (PRR) of the innate immune system detecting pathogen-associated molecular patterns (PAMPs) and danger- associated molecular patterns (DAMPs). The concept of pattern recognition evolves around the invariability of exogenous signals shared by innumerous pathogens (PAMPs) and endogenous signals of cellular or tissue damage and thus sterile inflammation (DAMPs). Due to their invariability, PAMPs and DAMPs can be sensed by a constant repertoire of innate immune receptors (PRRs)[318-320].

Several different sensor proteins of inflammasomes have been described, most of them belonging to the NOD-like receptor (NLR) family[321]. One of them is NLR family pyrin domain containing 3 (NLRP3; 118 kDa) consisting of three major domains, an N-terminal Pyrin domain (PYD), a central nucleotide-binding and oligomerization domain called NACHT (AIP, CIITA, HET-E and TP1 domain with NTPase activity) and a C-terminal leucine-rich repeat domain[322]. Together with the adapter protein ASC (apoptosis associated speck-like protein containing a caspase activation and recruitment domain (CARD)) and the effector protein pro-caspase1, it forms the NLRP3 inflammasome[323].

Its canonical activation mechanism requires two independent hits by a priming and an activating stimulus, respectively (Figure 1.6). In the priming step, PAMPs or DAMPs trigger NFκB-dependent transcription of *NLRP3* itself and cytokines of the IL1 family, *IL1B* and *IL18*, resulting in increased availability of NLRP3, pro-IL1β and pro-IL18 in the cytosol[324-328]. In addition, cytosolic NLRP3 becomes deubiquitinated by BRCC3 (BRCA1/BRCA2-containing complex subunit 3)[329,330]. Prototypical priming is achieved, for instance via activation of TLRs, IL1 receptor or TNFα receptor and their downstream signaling molecules by their respective ligands[321]. As a second and activating stimulus, a vast range of triggers has been identified. PAMPs like viral or bacterial products, especially lipopolysaccharide (LPS) or pore-forming toxins, induce inflammasome formation[331]. A particular broad spectrum of activating DAMPs includes particulates like uric acid crystals[332] or silica[333] and extracellular ATP triggering P2RX7 pore formation[290,334], which result in potassium efflux from the cytosol. Further, mitochondrial dysregulation leading to mitochondrial reactive oxygen species (mROS)[335] or oxidized mitochondrial DNA[336] has been uncovered. Alternatively, calcium sensing receptor (CASR) can induce an increase of cytosolic Ca^{2+}, which evokes inflammasome assembly either directly or via mitochondrial damage[337,338] to name some examples among the inflammasome activating triggers[331].

Still, direct binding of a stimulus to NLRP3 for activating purposes has not been confirmed, arguing that NLRP3 rather senses and integrates a consensus signal of altered cell homeostasis induced by the varying second stimuli[339]. Potassium efflux was proposed to be the sought consensus trigger since it is the common downstream effect of multiple activating stimuli including pore-forming toxins, P2RX7 activation or lysosomal disintegration[340,341].

However, the immediate connection between potassium efflux and NLRP3 activation remains elusive. Identification of NIMA-related kinase 7 (NEK7), which directly binds NLRP3 and is critical for inflammasome assembly, but acts downstream of the potassium efflux[342-344] could be the next step in determining this link[340].

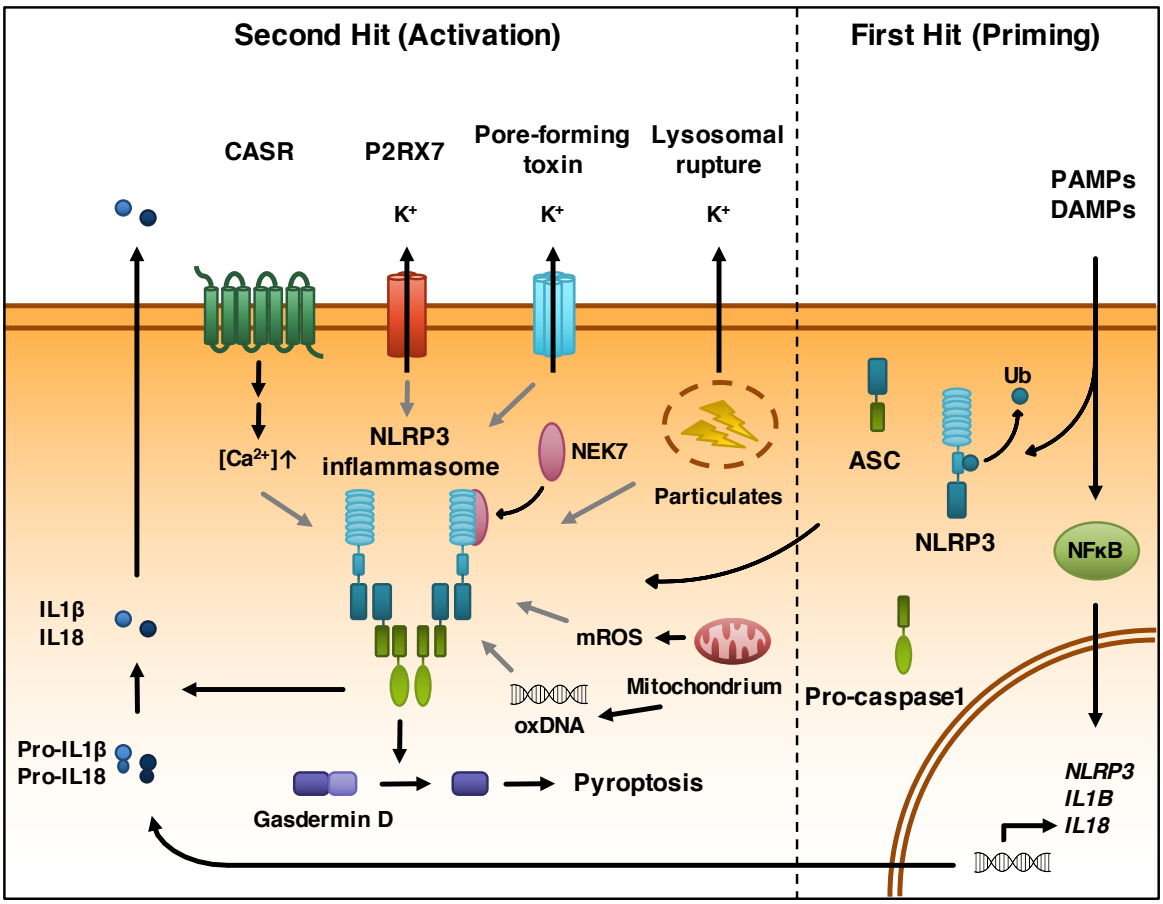

Figure 1.6 Canonical activation of the NLRP3 inflammasome.
The NLRP3 inflammasome activation occurs according to a two-hit hypothesis. As a first, priming hit, PAMPs or DAMPs increase *NLRP3*, *IL1B* and *IL18* transcription dependent on NFκB. In addition, NLRP3 becomes deubiquitinated. The second, activating hit can be triggered by a variety of stimuli: For instance, intracellular calcium recruitment due to CASR signaling, potassium efflux due to P2RX7 activation, pore-forming toxins or lysosomal damage caused by particulates, mitochondrial ROS (mROS) production and oxidized mitochondrial DNA (oxDNA) can induce the inflammasome assembly, but not through direct interaction (indicated by grey arrows). Binding of NEK7 to NLRP3 is also critical. Thus, NLRP3, ASC and pro-caspase1 assemble via homotypic domain interactions to form a functional inflammasome (here illustrated by dimerization). Upon assembly, caspase1 is proteolytically activated from pro-caspase1. Caspase1 cleaves GasderminD resulting in pyroptosis and maturates pro-IL1β and pro-IL18 into IL1β and IL18, respectively, which are then released into extracellular space. Modified on the basis of [345,346].

In response to the second hit, the NLRP3 inflammasome assembles from its components in the cytosol. Via a homotypic PYD-PYD interaction, NLRP3 can associate with ASC, which comprises a PYD and a CARD[347-349]. In turn, ASC recruits pro-caspase1 via a homotypic CARD-CARD interaction[350]. After nucleation of NLRP3 by oligomerization via the NACHT domains, ASC can adhere to the multimeric complex and polymerize in helical filament-like structures also known as the ASC speck[347,351]. Thereby ASC filaments provide

a scaffold for pro-caspase1 recruitment and filament formation resulting in caspase dimerization and activation[352]. Once assembled, the NLRP3 inflammasome is a director of two main effector pathways, interleukin synthesis and inflammatory cell death termed pyroptosis. In the inflammasome complex, pro-caspase1 becomes activated due to autocatalytic cleavage[353]. Active caspase1, in turn, is able to convert pro-IL1β and pro-IL18 into their mature forms by N-terminal cleavage[354-357]. In addition, active caspase1 promotes pyroptosis by Gasdermin D (GSDMD) cleavage[358,359]. The N-terminal GSDMD fragment then forms a membrane-spanning pore resulting in a collapse of the osmotic gradient across the plasma membrane and thus, cell death by cell swelling, membrane damage and release of cytosolic content[360,361].

A non-canonical mode of NLRP3 inflammasome activation has additionally been identified. This pathway starts with oligomerization of human caspases4 and 5, homologous to murine caspase11, upon encounter of intracellular LPS and their subsequent activation[362-365]. Active caspase4/11 requires potassium efflux for canonical NLRP3 inflammasome assembly and consecutive caspase1-mediated IL1β maturation[366-369] whereas cleavage of Gasdermin D and thus pyroptosis induction can also proceed in a caspase1-independent manner[370,371].

1.4.2 Role of NLRP3 in inflammation

NLRP3 inflammasome signaling is crucial to both, sterile and pathogen-induced inflammation rendering NLRP3 inflammasome mediated interleukin production and release as well as pyroptosis early signals in the line of host defense[372]. Release of mature IL1β and IL18 can occur via several pathways, for instance, exocytosis of secretory lysosomes[373,374], shedding of microvesicles[375,376] or exosome liberation[377]. Apart from these mechanisms, direct release via transporters[378], membrane pores[379] or Gasdermin D induced pore formation[359,360,380] were identified. Extracellular IL1β and IL18 serve as triggers for activation of innate immune cells like macrophages, mast cells or dendritic cells. Secondly, along with cytokines secreted by the activated innate immune cells, IL1β and IL18 contribute to recruitment and proliferation of adaptive immune cells, for instance T helper cells or B cells thereby connecting innate with adaptive immune response. Ultimately clearance of injured cells is induced via both lines of immune response[381].

Another mechanism identified in mediating inflammation across cell membranes has been termed inflammasome spreading. In case of cell death due to pyroptosis, ASC specks are released into the extracellular space, where they continue to persist and maturate IL1β. Phagocytosis allows ASC specks to re-enter the cytosol and propagate inflammatory signaling to bystander cells as means of enhancing inflammatory signaling beyond the damaged cell[382-385].

As both, the canonical and the non-canonical NLRP3 inflammasome activation pathways are highly complex processes, each step is tightly regulated to prevent unnecessary activation[321]. Consequently, constant inflammasome activity prompts loss of tissue homeostasis and chronic inflammation. Involvement of the deregulated NLRP3 inflammasome has been shown in various cardiovascular, metabolic or neurologic disorders. For example, NLRP3 inflammasome activation via internalized cholesterol crystals causing

lysosomal disintegration has been implicated in the progression of plaque formation and rupture in atherosclerosis[386-389]. In type 2 diabetes mellitus (T2D), hyperglycemia can promote NLRP3 activation in pancreatic β cells probably via the intracellular stimulus TXNIP[390,391], whereas saturated fatty acids and soluble islet amyloid polypeptide (IAPP) or its amyloid aggregates induce inflammasome activation in myeloid cells through different mitochondrial ROS production and lysosome disintegration, respectively[392-395]. Thereby generated IL1β release significantly contributes to β-cell loss and thus, insulin resistance in T2D pathogenesis[396,397]. Similar to IAPP, the amyloid-β peptide is internalized and triggers inflammasome activation through lysosomal perturbation in Alzheimer's disease development[398-400]. Comparable observations have been established for deposited uric acid crystals in gout[332,401].

In contrast to these chronic inflammatory diseases, cyropyrin-associated periodic syndrome (CAPS) is caused by constant NLRP3 inflammasome activity due to gain-of-function mutations predominantly occurring in the nucleotide binding site of the *NLRP3* gene[402-404]. Permanent NLRP3 inflammasome activity with consecutive IL1β overproduction results in familial autoinflammatory diseases, namely familial cold autoinflammatory syndrome (FCAS)[405], Muckle-Wells syndrome (MWS)[406,407] and chronic infantile neurological cutaneous articular (CINCA) syndrome[408]. Fever and rash due to inflammation are characteristic symptoms common in all three disease manifestations, often accompanied by hearing loss, bone defects, renal amyloidosis or abnormalities in the central nervous system depending on the severity of the disease[402,409,410]. The Muckle-Wells syndrome is of particular interest since it has been connected to perturbed spermatogenesis and infertility in men. Yet, the extent of infertility has not been investigated in detail and molecular mechanisms remain undetermined[406,411-413].

1.4.3 Non-classical roles of NLRP3

Beyond its classical role in inducing inflammation and pyroptosis, the NLRP3 inflammasome has been found to engage in regulation of additional cellular processes independent of interleukin-mediated effects[414]. The NLRP3 inflammasome has been identified to e.g. participate in a negative autoregulatory loop with autophagy. NLRP3 inflammasome activation induces mitochondrial dysfunction and inhibits mitochondrial autophagy[415], whereas autophagy proteins prevent NLRP3 and subsequent caspase 1 activation[416] implying an impact on cellular homeostasis. NLRP3-dependent caspase 1 promotes phagosome maturation[417], while caspase 4/11 facilitate phagolysosomal fusion[414,418], thereby enhancing the anti-microbial response. NLRP3-dependent caspase 1 further influences lipid metabolism[419,420].

Inflammasome activation and signaling is a mechanism prevalently described in myeloid cells supported by the fact that NLRP3 expression previously has been confined to the myeloid lineage[421]. Meanwhile NLRP3 expression has been found in lymphoid cells of the immune system[422-425] as well as somatic cell types. This includes mesenchymal cells like osteoblasts or chondrocytes[426-429], cardiac fibroblasts[430,431] or vascular smooth muscle cells[432]. Further, epithelial expression of NLRP3 has been revealed in kidney[433,434],

lung[333,435] or retina[436]. In this context, it is noteworthy that NLRP3 expression in human and mouse testis has been established[437,438]. In a mouse model of testicular ischemia/reperfusion injury, NLRP3 knock-out or inhibition proved beneficial for preservation of histological integrity and spermatogenesis and displayed less inflammatory gene activation[438]. In addition, a functional NLRP3 inflammasome inducing IL1β production and release has been described in murine Sertoli cells[439]. Both studies related inflammatory actions to NLRP3 and indicated a putative role in the onset of male infertility.

In parallel to the finding of NLRP3 inflammasome actions in somatic cells, inflammasome-independent functions of NLRP3 have begun to emerge. In the lung, NLRP3 can promote post-injury inflammation via the STAT3 pathway without IL1β induction[440]. In terms of non-inflammatory roles, NLRP3 is involved in preserving epithelial barrier integrity via cell adherence in the lung[441], but contribution to epithelial barrier functioning has been revealed in kidney[442] and testis[439] as well. TGFβ-induced NLRP3 has been reported to contribute to epithelial-mesenchymal transition in kidney epithelium[443] and colon cancer cells[444]. Moreover, TGFβ-dependent NLRP3 fosters fibrogenesis in cardiac myofibroblasts[445]. In contrast, NLRP3 can act as transcription factor in T helper type 2 cell differentiation[425]. Unraveling NLRP3-mediated effects in inflammatory and inflammation-associated processes, but simultaneously in a diverse set of cellular mechanisms introduces a new perspective to NLRP3 signaling.

1.5 Objective

Impairment of spermatogenesis is often accompanied by fibrosis and both are exemplary hallmarks of male sub- and infertility. Fibrosis may result from sterile inflammation of the testis, yet underlying molecular mechanisms of have sparsely been investigated. The tubular wall is the testicular compartment that is critically affected through fibrotic remodeling and infiltrating immune cells. It may thus be involved in development of sterile inflammation, which putatively leads to male infertility.

(1) The first goal of the thesis will be to discover and assess the role of the extracellular matrix molecule biglycan and biglycan signaling in the testis. Since biglycan is implicated in initiating inflammatory processes, biglycan and associated inflammation-mediating receptors (TLRs and P2X receptors) are to be identified and evaluated in an inflammatory context. Therefore, a previously described mouse model of male infertility associated with chronic sterile inflammation in the testis, the *AROM*$^+$ mouse, will be employed. Besides assessing the *AROM*$^+$ mouse as suitable model for this study, the mechanistic actions of biglycan will specifically be addressed by introducing a biglycan knock-out in the *AROM*$^+$ mouse model.

(2) As next step, the probability of purinergic receptors and signaling contributing to testicular inflammation will be examined. For this purpose, human testicular peritubular cells (HTPCs) as cell culture model for mechanistic studies will be exploited. The repertoire of purinergic receptors and their functionality in HTPCs is to be revealed. Inflammatory conditions in the testis provide increased availability of the physiological purinergic ligand ATP. Subsequently, the impact of purinergic signaling through ATP in terms of inflammatory gene regulation and the characteristic HTPC phenotype is to be assessed.

(3) Third, as a putative downstream pathway of inflammatory signaling, NLRP3 expression in human and mouse testes will be inspected. Putative correlation of NLRP3 with phenotypic alterations in testicular pathophysiology is to be examined. To reveal an association of NLRP3 with testicular inflammation, the *AROM*$^+$ mouse as a systemic mouse model of sterile inflammation will again be employed.

Thus, precise investigation of biglycan, purinergic receptors and NLRP3 is to participate in the identification and clarification of sterile inflammatory processes and reveal mechanisms putatively contributing to subfertile testicular pathologies.

2 RESULTS

2.1 Biglycan – an inducer of sterile inflammation in the testis?

Biglycan is expressed ubiquitously throughout the body[128]. In the testis, it is located in the extracellular matrix of the seminiferous tubular wall in particular[129]. It has further been associated with fibrotic remodeling of the tubular wall in subfertility patients[95]. Biglycan has been implicated as inducer of sterile inflammation via TLRs and purinergic receptors in cells of the innate immune system[180]. Abundance and functionality in the testis was evaluated using human testicular tissue and a mouse model of sterile inflammation and male infertility.

2.1.1 Correlation of biglycan expression with sterile inflammation in the human testis

Biglycan expression in human testis was assessed using immunohistochemistry of testicular sections from patients displaying normal morphology and mixed atrophy (Figure 2.1).

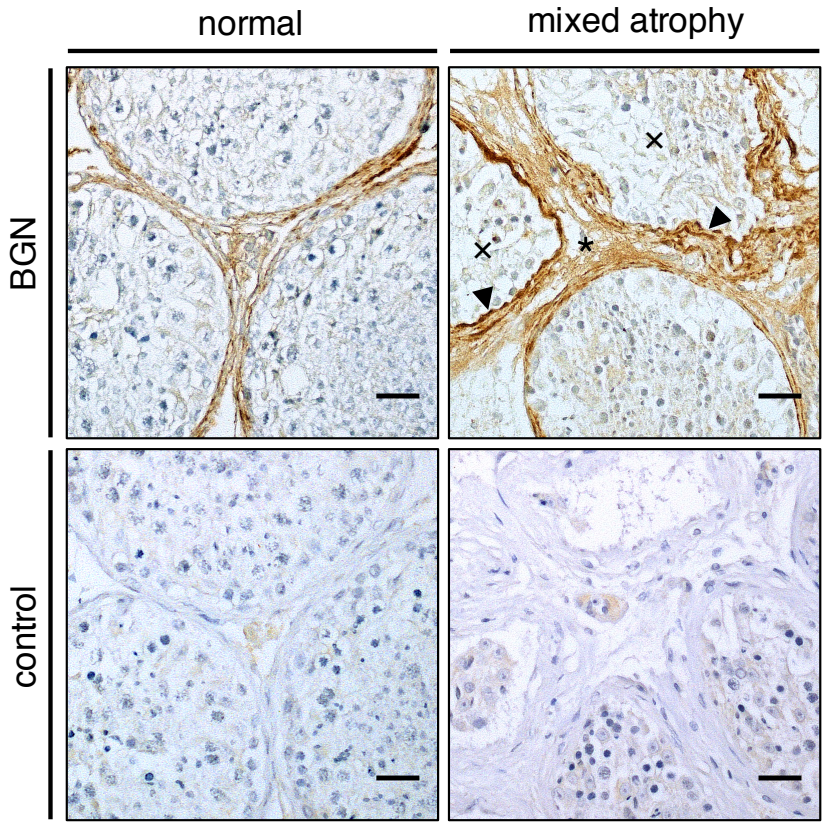

Figure 2.1 Biglycan expression in the human testis.

Representative testicular sections displaying normal morphology (left panel) and mixed atrophy (right panel) were stained for BGN expression. Mixed atrophy samples were characterized by tubules showing normal spermatogenesis next to tubules with deteriorating spermatogenesis (crosses) and thickened tubular walls (arrowheads) as well as excess interstitial tissue (asterisk). BGN staining was present in the tubular wall and the interstitial tissue (upper panel) and appeared more prominent in morphologically altered samples from mixed atrophy patients. Controls (lower panel) consisted of primary antibody omission in consecutive sections. Staining was performed for n = 3 normal patients and n = 3 mixed atrophy patients. Bar = 25 µm.

In both sections, distinguished staining became obvious in the tubular wall and the interstitial tissue. In mixed atrophy patients, the wall of tubules displaying signs of impaired spermatogenesis was profusely altered regarding thickness and structural integrity indicating ongoing testicular remodeling[33,38]. Evidently, staining appeared more prominent in fibrotically thickened tubular walls as well as in the ample interstitial tissue of mixed atrophy patients.

Fibrotic remodeling includes extensive ECM abundance and is considered a phenotypic sign following inflammation[446], that can be observed in the tubular wall of the testis as well[47,95]. In a previous study, testicular biglycan expression has already been associated with fibrotic tubular walls and biglycan action in HTPCs was identified to induce pro-inflammatory cytokine production via TLR2[95]. Together, these findings link enhanced biglycan expression to an inflammatory testicular state supporting the hypothesis that biglycan is not only a result, but also a putative cause of testicular inflammation.

2.1.2 Increase of biglycan, TLRs and purinergic receptors in in the *AROM*$^+$ mouse

The *AROM*$^+$ transgenic mouse line was chosen as a systemic model to investigate biglycan in a context of sterile inflammation. Initial examination of expression levels in the *AROM*$^+$ mouse line revealed significantly increased abundance of *Bgn* transcripts in the testes of *AROM*$^+$ animals compared to age-matched WT animals at five months of age (Figure 2.2). Similar observations were made for the cell surface receptors known for their interaction with biglycan. *Tlr2* and *Tlr4* as well as *P2rx4* and *P2rx7* relative expression levels were increased, albeit only significantly for *Tlr4* and *P2rx4*. These findings support the hypothesis of biglycan and its associated cascade being involved in sterile inflammation of the testis.

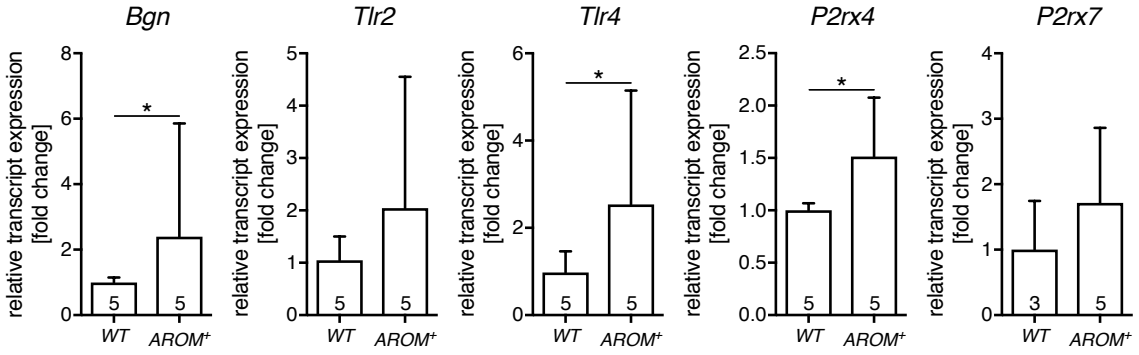

Figure 2.2 Elevated *Bgn* transcript expression and associated receptors in testes of *AROM*$^+$ mice. Relative amounts of *Bgn*, *Tlr2*, *Tlr4*, *P2rx4* and *P2rx7* were increased in five months old *AROM*$^+$ transgenic mice compared to WT littermates. Transcript levels are depicted normalized to WT control levels. Numbers of animals analyzed are denoted in the graphs. Data represent geometric means + 95% confidence interval. Asterisks denote statistical significance (unpaired *t*-test, $p < 0.05$).

2.1.3 Biglycan deficiency fails to rescue the inflammatory *AROM*$^+$ phenotype

The putative role of biglycan in sterile inflammation of the testis was further evaluated in the *AROM*$^+$ mouse line. Biglycan knock-out mice ($Bgn^{-/0}$)[146] were crossed with the *AROM*$^+$ mouse line to investigate, if biglycan deficiency was able to counteract the inflammatory phenotype of this mouse line. Mice were evaluated at the age of four and ten months,

respectively. Differences in body and testis weights were assessed, as were histology and seminiferous tubule diameters. In addition, hormonal levels in the testes were determined at ten months of age. To complement the analysis, testicular mRNA expression levels of characteristic marker genes for relevant testicular cell types and inflammatory parameters were compared. Body weights were not significantly altered between mice of different genotypes in both age groups (Figure 2.3). At four months of age, testis weights were decreased in *AROM*$^{+}$ *Bgn*$^{-/0}$ and *AROM*$^{+}$ animals compared to *Bgn*$^{-/0}$ animals, yet there were no differences between WT animals and any other genotype. In contrast, at ten months of age testis weight differences could not be observed. Seminiferous tubule diameters did not display inter-genotype changes in both age groups.

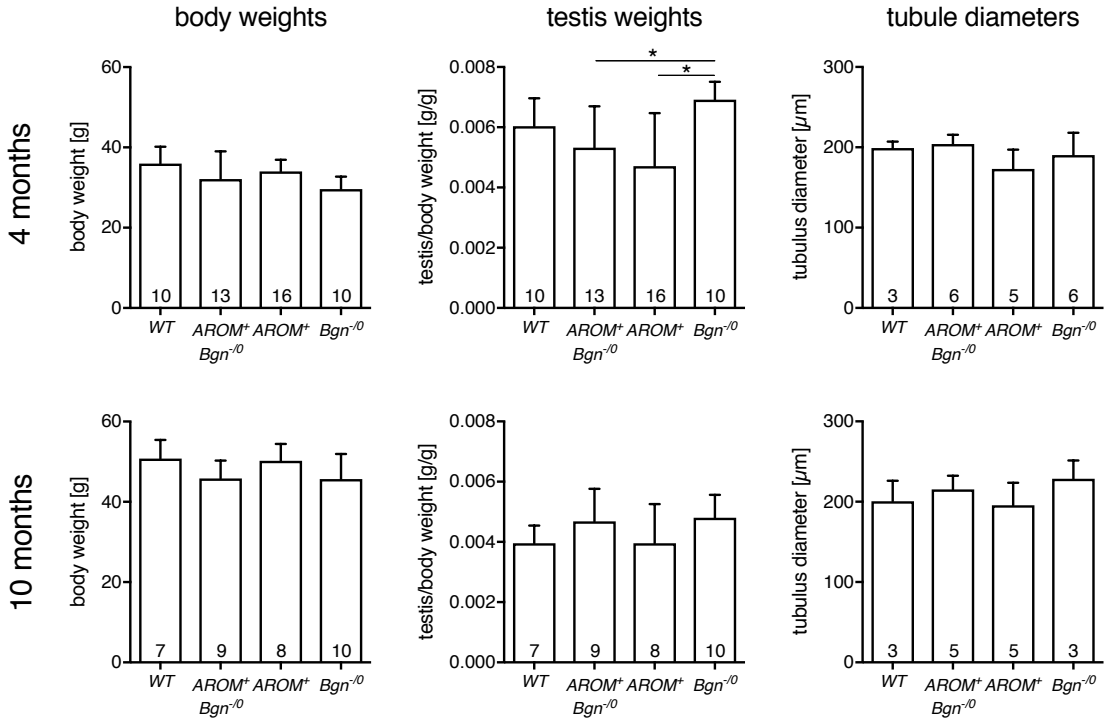

Figure 2.3 Comparison of body weights, testis weights and tubule diameters of mice from *AROM*$^{+}$ x *Bgn*$^{-/0}$ crossings.

Body weights, testis weights and seminiferous tubule diameter were evaluated according to genotype of the *AROM*$^{+}$ x *Bgn*$^{-/0}$ F2 offspring at four and ten months, respectively. Numbers of animals analyzed are denoted in the graphs. Data represent means + SD. Asterisks denote statistical significance (ANOVA with Tukey's post-test, $p < 0.05$).

After discovering almost no differences in the general parameters, histological analysis of the genotypically different testes was performed (Figure 2.4). At four months of age, WT and *Bgn*$^{-/0}$ mice testes were of regular appearance including spermatogenesis, yet *AROM*$^{+}$-containing genotypes comprised a visible increased abundance of interstitial tissue. In contrast, at ten months of age testicular phenotypes appeared heterogeneous even among animals of the same genotype. In *AROM*$^{+}$ (*Bgn*$^{-/0}$) mice, some animals maintained an almost intact tubular organization, while others displayed massive intratubular degeneration comprising germ cell vacuolization and loss of spermatogenesis. Interestingly, in some cases tubules with intact spermatogenesis were found directly besides tubules with completely disrupted structure. All *AROM*$^{+}$ (*Bgn*$^{-/0}$) animals displayed an excess of interstitial tissue

consisting putatively of infiltrating macrophages and hypertrophic Leydig cells, but differences between *AROM*$^{+}$ *Bgn*$^{-/0}$ and *AROM*$^{+}$ testicular sections did not become evident. In comparison, *Bgn*$^{-/0}$ and WT testes exhibited intact testicular morphology without obvious alterations.

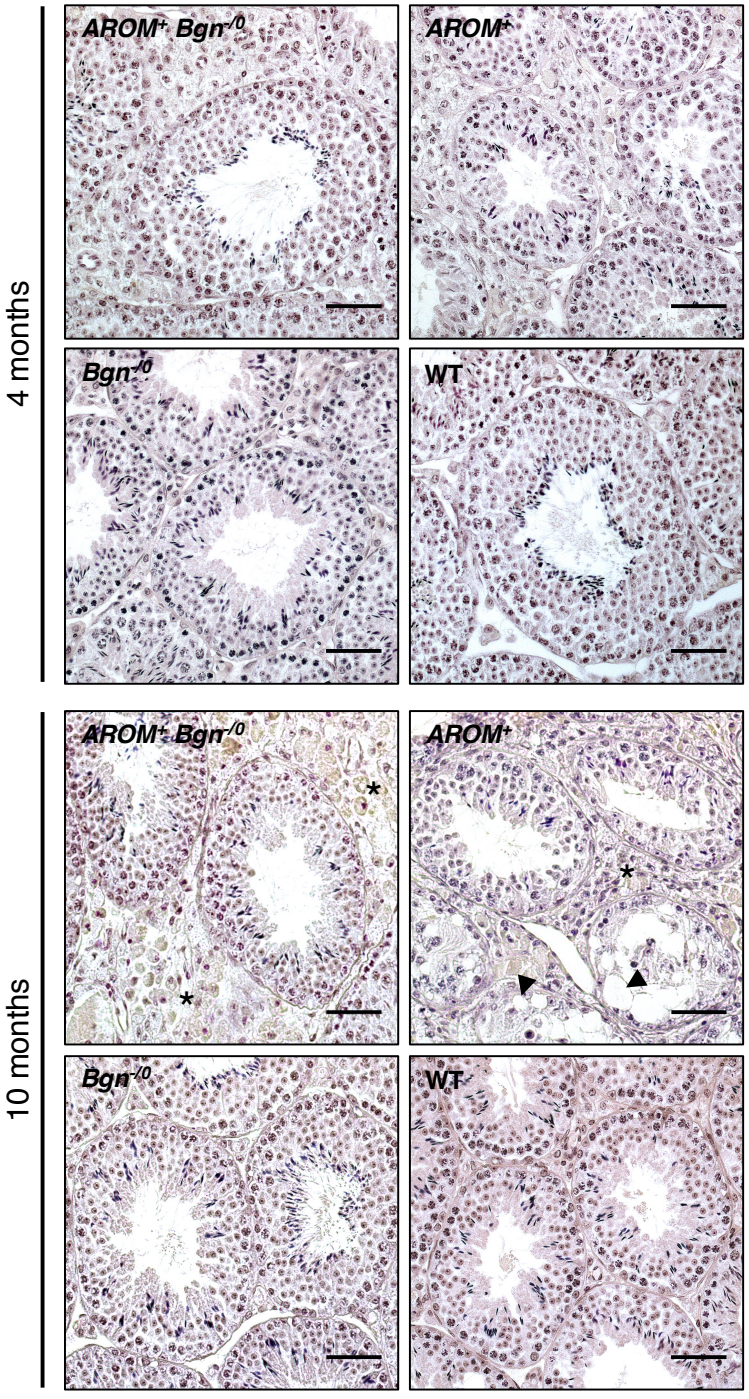

Figure 2.4 Testicular histology of mice from *AROM*$^{+}$ x *Bgn*$^{-/0}$ crossings.
Hematoxylin and eosin staining of representative testicular sections from each genotype of the *AROM*$^{+}$ x *Bgn*$^{-/0}$ F2 offspring at four (left panel) and ten months (right panel). Differences in testicular morphology were hardly apparent at four months, but at ten months of age *AROM*$^{+}$ *Bgn*$^{-/0}$ and *AROM*$^{+}$ mice displayed an altered testicular structure including interstitial infiltrates (asterisks), germ cell vacuolization (arrowheads) and disturbed tubular organization. Bar = 50 µm.

To complete the analyses of the testes, steroid hormonal levels of testosterone and estradiol were assessed in the testes of ten months old mice (Figure 2.5). Testosterone levels appeared scarcely but not significantly lower in all genotypes different from WT. In contrast, estradiol levels were considerably and significantly elevated in *AROM*$^+$-containing genotypes regardless of the *Bgn* knock-out.

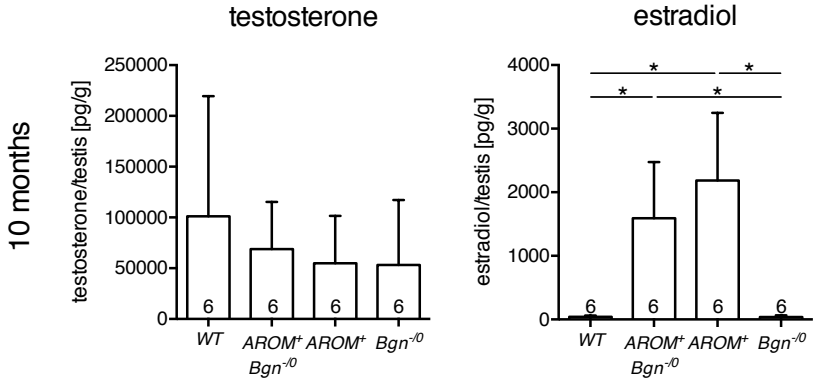

Figure 2.5 Comparison of steroid hormone levels of mice from *AROM*$^+$ x *Bgn*$^{-/0}$ crossings.
Testosterone and estradiol levels were determined from testicular lysates by MS/MS at ten months of age. Results are depicted according to genotype of the *AROM*$^+$ x *Bgn*$^{-/0}$ F2 offspring. Numbers of animals analyzed are denoted in the graphs. Data represent means + SD. Asterisks denote statistical significance (ANOVA with Tukey's post-test, $p < 0.05$).

Since general traits did not reveal a rescue of the *AROM*$^+$ phenotype by *Bgn* deficiency, more detailed insight into alterations of testicular cell types and inflammatory parameters was obtained via transcription level analysis from whole testes.

Biglycan transcripts were almost undetectable in the knock-out genotypes of both age groups, but *Bgn* levels in *AROM*$^+$ mice were significantly elevated compared to WT as seen in the original mouse line. The SLRP decorin, which is a sister molecule to biglycan, displayed increased levels in all *AROM*$^+$-containing animals, but differences between *AROM*$^+$ mice with or without *Bgn* could not be observed (Figure 2.6). Hence, the hypothesis of a compensation of *Bgn* deficiency by *Dcn*, as previously discovered in *Bgn*- and/or *Dcn*-deficient mouse models[447,448], was rejected.

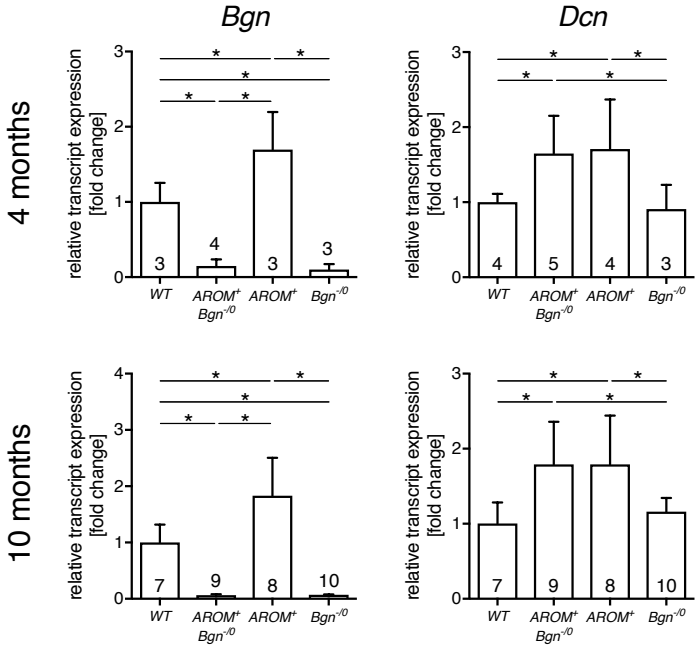

Figure 2.6 Comparison of *Bgn* and *Dcn* transcript levels in testes of mice from *AROM*$^{+}$ x *Bgn*$^{-/0}$ crossings.

Bgn and *Dcn* transcript levels were evaluated according to genotype of the *AROM*$^{+}$ x *Bgn*$^{-/0}$ F2 offspring at four and ten months, respectively. Transcript levels are depicted normalized to WT control levels. Numbers of animals analyzed are denoted in the graphs. Data represent geometric means + 95% confidence interval. Asterisks denote statistical significance (ANOVA with Tukey's post-test, $p < 0.05$).

Germ cell lineage and therefore spermatogenesis-specific marker gene DEAD-box helicase 4 (*Ddx4*)[449,450] levels remained unaltered at four months of age, whereas they decreased in *AROM*$^{+}$-containing mice at ten months, albeit only significantly to the *Bgn*$^{-/0}$ genotype. Although Ddx4 levels appeared reduced in *AROM*$^{+}$ compared to *AROM*$^{+}$ *Bgn*$^{-/0}$ mice, this trend was not statistically significant. In comparison, transcript levels of spermatogonial stem cell marker fibroblast growth factor receptor 3 (*Fgfr3*)[451] did not display significant changes in any age group. Levels of *Cyp17a1* (Cytochrome P450 family 17 subfamily A member 1), a Leydig cell marker gene[452,453], were heterogeneous within each genotype in both age groups, so no tendency became evident. In contrast, *Cd68* levels indicating Cd68-positive macrophages[454] at four and ten months were markedly increased in *AROM*$^{+}$ (*Bgn*$^{-/0}$) testes compared to both, *Bgn*$^{-/0}$ and WT testes. Yet, differences between *AROM*$^{+}$ *Bgn*$^{-/0}$ and *AROM*$^{+}$ mice could not be identified (Figure 2.7). These marker-based results imply that spermatogonial germ cell and spermatogenesis levels are not substantially altered in the *AROM*$^{+}$ x *Bgn*$^{-/0}$ crossings, nor is the abundance of Leydig cells, although levels are inhomogeneous. However, Cd68-positive macrophages are significantly more frequent in *AROM*$^{+}$ overexpressing mice and independent of the *Bgn* knock-out.

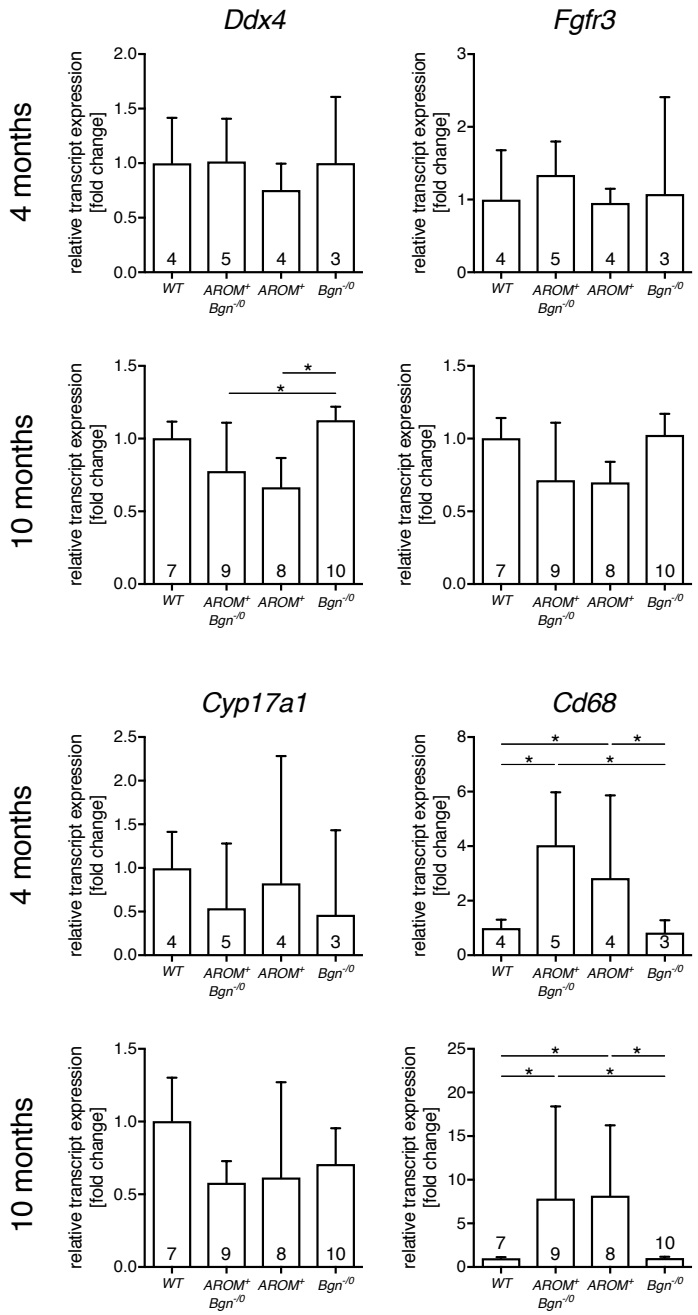

Figure 2.7 Comparison of testicular cell type-specific transcript levels in testes of mice from *AROM*$^+$ x *Bgn*$^{-/0}$ crossings.

Ddx4, Fgfr3, Cyp17a1 and *Cd68* transcript levels were evaluated according to genotype of the *AROM*$^+$ x *Bgn*$^{-/0}$ F2 offspring at four and ten months, respectively. Transcript levels are depicted normalized to WT control levels. Numbers of animals analyzed are denoted in the graphs. Data represent geometric means + 95% confidence interval. Asterisks denote statistical significance (ANOVA with Tukey's post-test, $p < 0.05$).

To characterize inflammatory events in the testes of the *AROM*$^+$ x *Bgn*$^{-/0}$ offspring, receptor expression levels previously evaluated in the *AROM*$^+$ mouse line were compared (Figure 2.8). At four months of age, *Tlr2* and *Tlr4* levels were elevated in *AROM*$^+$-containing mice compared to WT mice, but also in *AROM*$^+$ *Bgn*$^{-/0}$ animals compared to *AROM*$^+$ animals. The same pattern was detected for *P2rx7*, but not for *P2rx4*, where levels between *AROM*$^+$ *Bgn*$^{-/0}$ and *AROM*$^+$ mice were not significantly dissimilar. These findings in four months old mice

could not be recapitulated in the ten months old. While *AROM*$^+$ (*Bgn*$^{-/0}$) animals constantly exhibited higher receptor levels than WT and *Bgn*$^{-/0}$ animals, differences between the two could no longer be observed leading to the conclusion that the *Bgn* deficiency in *AROM*$^+$ mice at four months rather fosters the inflammation-associated receptor expression, whereas there appears to be no difference between these two genotypes at ten months.

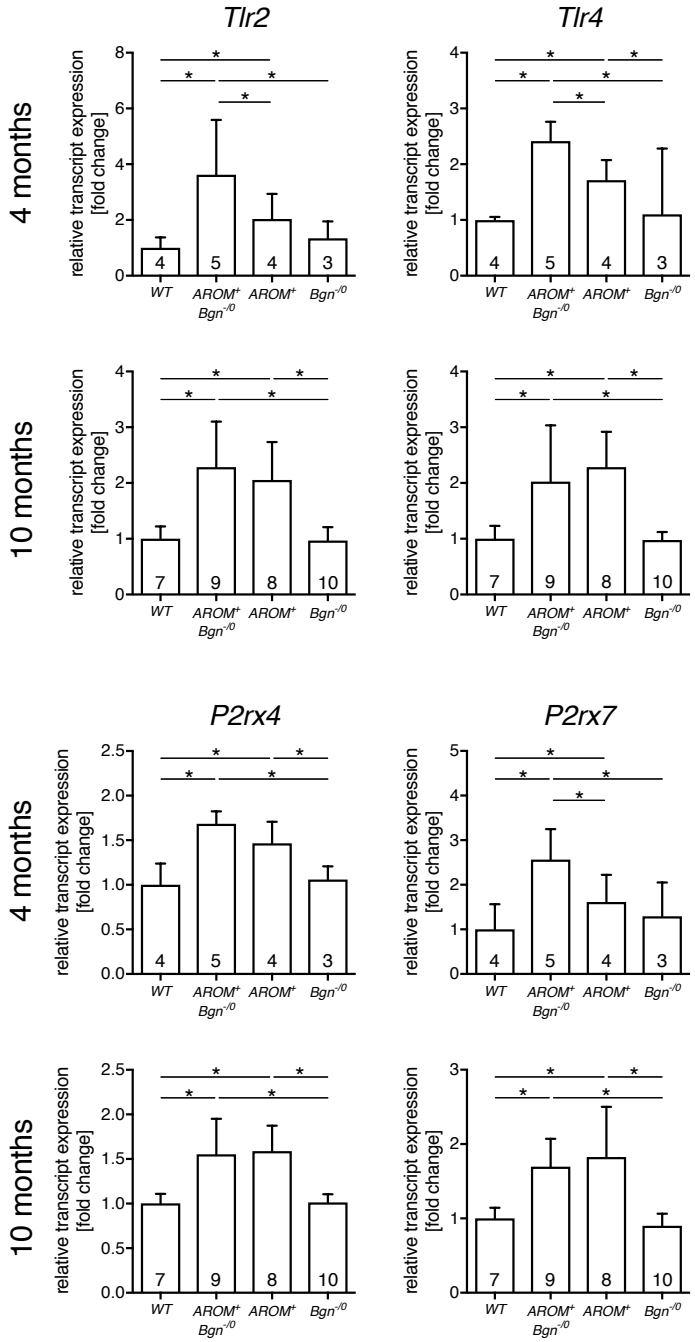

Figure 2.8 Comparison of Toll-like and purinergic receptor transcript levels in testes of mice from *AROM*$^+$ x *Bgn*$^{-/0}$ crossings.

Tlr2 and *4* and *P2rx4* and *7* transcript levels were evaluated according to genotype of the *AROM*$^+$ x *Bgn*$^{-/0}$ F2 offspring at four and ten months, respectively. Transcript levels are depicted normalized to WT control levels. Numbers of animals analyzed are denoted in the graphs. Data represent geometric means + 95% confidence interval. Asterisks denote statistical significance (ANOVA with Tukey's post-test, $p < 0.05$).

Possible implications of elevated inflammation-associated receptor expression were determined via a selected panel of presumably affected inflammatory cytokines and chemokines (Figure 2.9). Transcript levels of the prototypical pro-inflammatory *Il1b* revealed heterogeneous expression in both age groups, albeit without significant changes. Consistently, pro-inflammatory cytokine *Il6* levels were unaltered or even decreased between *AROM*$^{+}$ *Bgn*$^{-/0}$ and *Bgn*$^{-/0}$ mice at ten months of age. In contrast, *Tnfa* transcript expression increased in *AROM*$^{+}$ (*Bgn*$^{-/0}$) ten months old animals compared to controls. A similar development was witnessed for chemokine *Ccl2*. Its transcript levels were significantly elevated in *AROM*$^{+}$-containing mice at four and ten months of age, but as for *Tnfa* no difference between *AROM*$^{+}$ *Bgn*$^{-/0}$ and *AROM*$^{+}$ mice was uncovered. Consequently, increased cytokine expression, if detectable, appears to be entirely dependent on the *AROM*$^{+}$ genotype and independent of the *Bgn* knock-out.

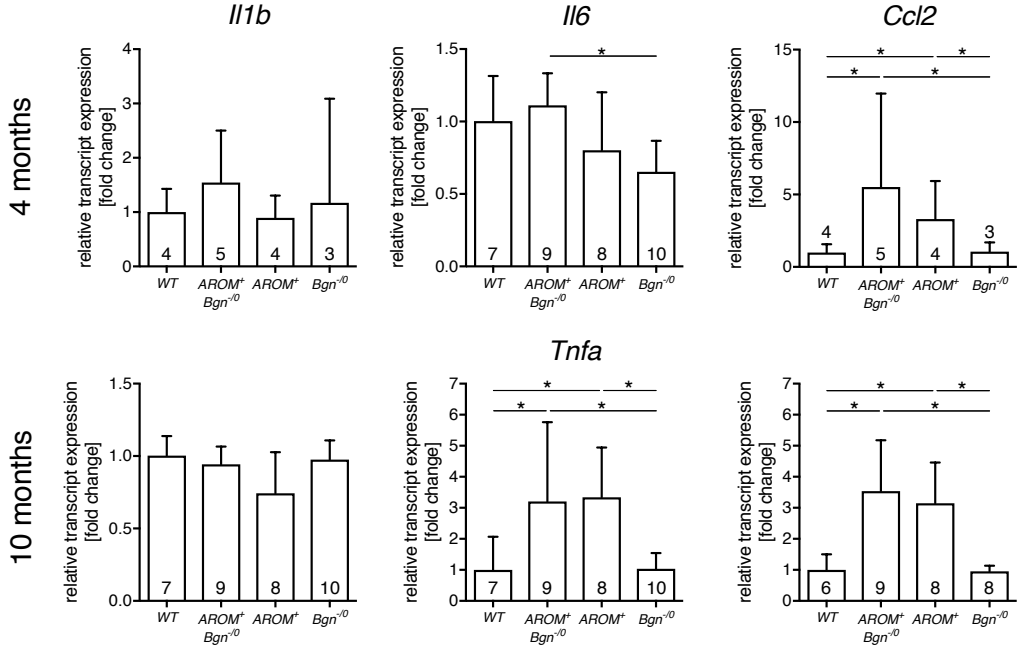

Figure 2.9 Comparison of pro-inflammatory cytokine and chemokine transcript levels in testes of mice from *AROM*$^{+}$ x *Bgn*$^{-/0}$ crossings.

Il1b, Ccl2, Il6 and *Tnfa* transcript levels were evaluated according to genotype of the *AROM*$^{+}$ x *Bgn*$^{-/0}$ F2 offspring at four and ten months for *Il1b* and *Ccl2* and at ten months only for *Il6* and *Tnfa*. Transcript levels are depicted normalized to WT control levels. Numbers of animals analyzed are denoted in the graphs. Data represent geometric means + 95% confidence interval. Asterisks denote statistical significance (ANOVA with Tukey's post-test, $p < 0.05$).

Taken together, *Bgn* deficiency did neither alter testicular morphology including cellular composition and steroid hormone levels nor inflammation-associated gene expression when comparing *AROM*$^{+}$ *Bgn*$^{-/0}$ and *AROM*$^{+}$ mice. Hence, the *Bgn* knock-out did not gravely influence all parameters examined and thus, did not rescue the inflammatory phenotype of the *AROM*$^{+}$ mouse line.

2.2 Purinergic receptors – involved in testicular inflammation?

In a chronic inflammatory environment as provided in testes of the *AROM*$^+$ mouse line, purinergic receptor levels *P2rx4* and *P2rx7* in the testes were markedly elevated (Figure 2.2). The receptors of the purinergic system, especially P2RX4 and P2RX7, have previously been linked to inflammatory events and fibrosis in various scenarios[455,456]. Hence, purinergic signaling presumably contributes to testicular inflammation, also in the human. This hypothesis was tested utilizing human testicular peritubular cells as a human *in vitro* model. Since biglycan could not be identified as a key factor of testicular inflammation in the *AROM*$^+$ mice, purinergic signaling in peritubular cells was assessed by employing the physiologically omnipresent and prevalent purinergic ligand ATP.

2.2.1 Expression profile of purinergic receptors in HTPCs

As first step, the expression profile of the known seven P2X and eight P2Y receptor isoforms was evaluated in HTPCs. For that purpose, HTPCs from four representative individuals were assessed employing whole testis lysate as a positive control (Figure 2.10). Expression of *P2RX2*, *P2RX3* and *P2RY4* mRNAs was found in none of the HTPCs from the four patients examined, but in the whole human testis sample. *P2RX1*, *P2RX6*, *P2RY2*, *P2RY11*, *P2RY12*, *P2RY13* and *P2RY14* transcript expression was dependent on the individual patient and no general pattern among the four patients was discovered. Consistent expression was only detected for *P2RX4*, *P2RX5*, *P2RX7*, *P2RY1* and *P2RY6*. These results indicate expression of various receptor isoforms providing the possibility of purinergic signaling in HTPCs.

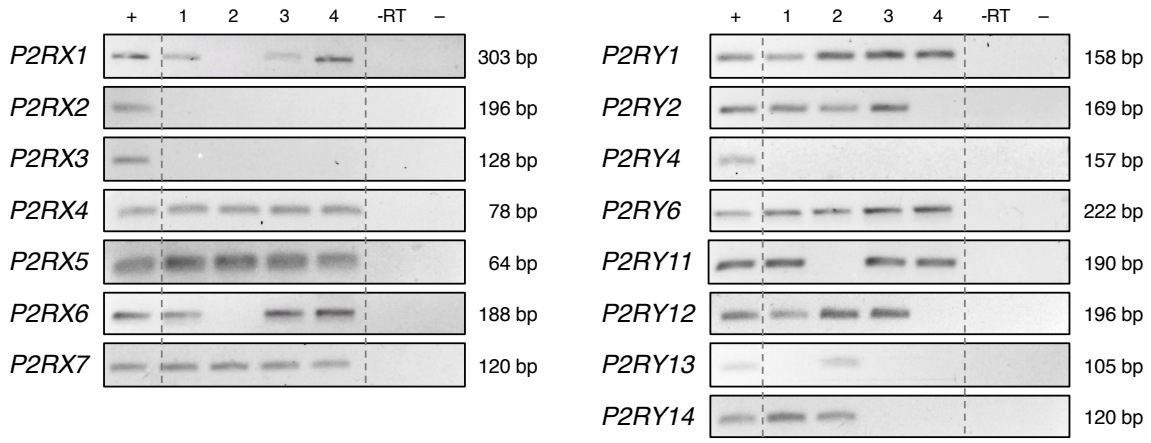

Figure 2.10 Qualitative expression of purinergic receptor transcripts in whole human testis and HTPCs.

Transcript expression of seven *P2RX* and eight *P2RY* subtypes in whole human testis lysate (+) and HTPCs from four individual patients (1-4) revealed ubiquitous expression for *P2RX4*, *P2RX5*, *P2RX7*, *P2RY1* and *P2RY6*, patient-dependent expression for *P2RX1*, *P2RX6*, *P2RY2*, *P2RY11*, *P2RY12*, *P2RY13* and *P2RY14* and whole testis expression solely for *P2RX2*, *P2RX3* and *P2RY4*. Figure shows RT-PCR reaction fragments visualized on agarose gels. Negative controls consisted of non-reverse transcribed RNA as template (-RT) and a non-template reaction (–). Amplicon lengths are indicated to the right of the corresponding fragments.

2.2.2 Testicular expression of P2RX4 and P2RX7

Since P2RX4 and P2RX7 are the receptor subtypes that have been associated with inflammatory signaling and tissue fibrosis[304,456,457], these two isoforms were examined more closely. In addition to consistent basal *P2RX4* and *P2RX7* transcript expression in cultured peritubular cells, transcript level variation was analyzed. In comparison to the mean expression, inter-individual *P2RX4* levels were similar, whereas inter-individual *P2RX7* levels varied considerably under control conditions. This was observed for control conditions at both time points, 6 h and 24 h, that were chosen for RNA evaluation after HTPC treatment (only shown at 24 h, Figure 2.11A). Expression of the mature protein in HTPCs was found for P2RX4 and P2RX7 in all individuals considered (Figure 2.11B).

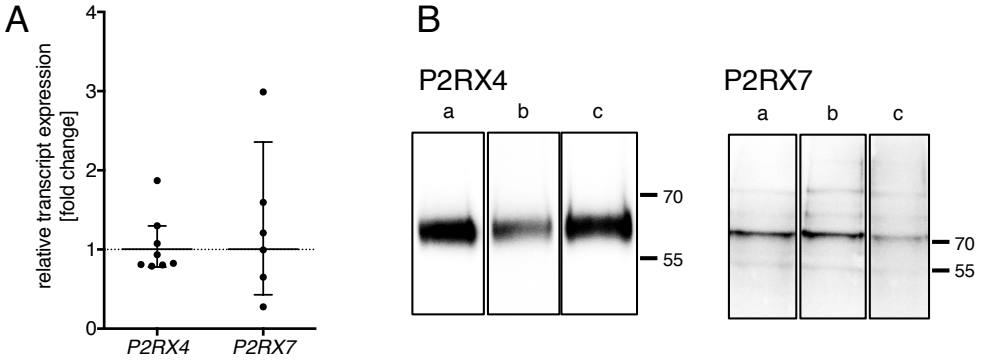

Figure 2.11 P2RX4 and P2RX7 expression in cultured peritubular cells.

A. Basal transcript levels variation among individual patients compared to a hypothetical patient mean was moderate for *P2RX4* (n = 8) and relatively high for *P2RX7* (n = 5) under control conditions (24 h). Data represent geometric means ± 95% confidence interval. **B.** P2RX4 and P2RX7 expression was confirmed on protein level in three individual HTPC samples (a-c) via Western blotting. Labels indicate corresponding protein ladder weight in [kDa]. A pre-absorption control for P2RX4 expression in HTPCs can be found in the Appendix, Supplementary Figure 1. Reproduced and modified from [458] under a Creative Commons BY license.

In human testicular sections receptor protein expression was verified by immunohistochemistry (Figure 2.12). P2RX4 staining was found in peritubular cells, but also in cells of the tubular compartment and in the interstitial tissue. Specificity of the P2RX4 staining was demonstrated by pre-adsorbed control staining. P2RX7 staining was confined to peritubular cells. In sections from patients displaying fibrotically altered tubular wall structure, both P2RX4 and P2RX7 expression appeared enhanced in these fibrotically thickened wall segments implying a possible association of P2RX4 and P2RX7 expression with subfertility-related fibrosis.

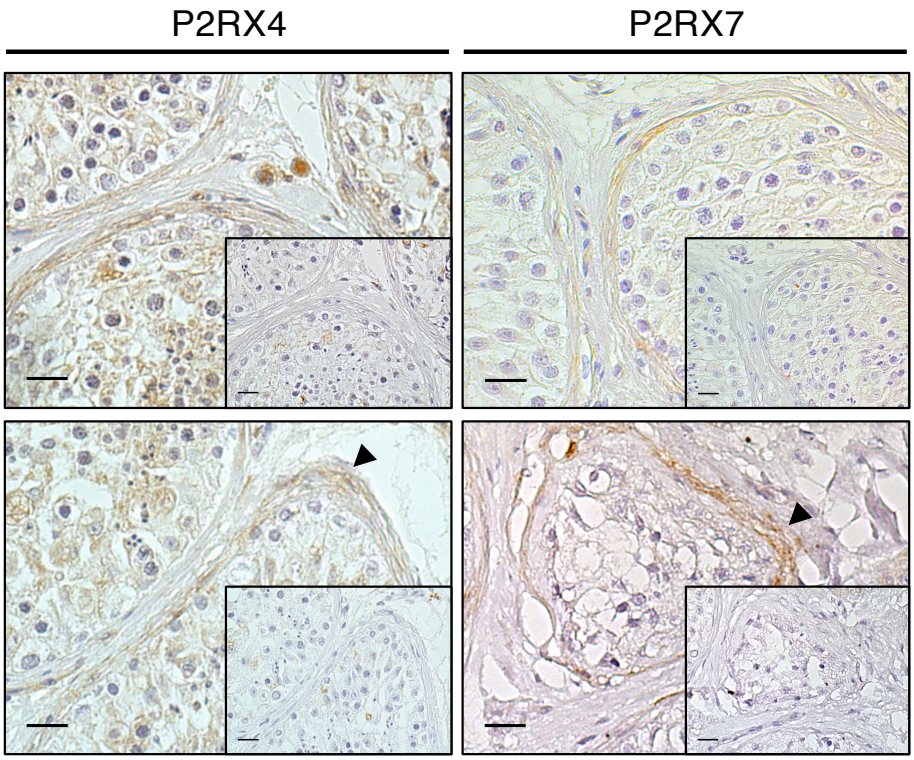

Figure 2.12 P2RX4 and P2RX7 expression in the human testis.
Immunohistochemical staining indicating P2RX4 expression in peritubular cells as well as in tubular and interstitial compartment (left panel). Staining for testicular expression of P2RX7 was restricted to cells of the tubular wall (right panel). In patients exhibiting fibrotically thickened segments of the tubular wall (lower panel), receptor staining intensified in these areas (arrowheads). Insets: Negative controls (pre-adsorption for P2RX4, omission of primary antibody for P2RX7). Staining was performed for n = 4 patients. Bars = 20 µm. Reproduced and modified from [458] under a Creative Commons BY license.

2.2.3 Functional purinergic receptor assessment by Ca^{2+} imaging in HTPCs

To explore purinergic receptor functionality, especially potential P2RX4 and P2RX7 functionality, in HTPCs and thus, putative signal transduction, Ca^{2+} imaging via an intracellular fluorescent dye was employed (Figure 2.13). Since the native purinergic ligand ATP activates almost all purinergic receptors except P2RX7 in the low micromolar range[217], its more specific derivative BzATP was used as agonist for characterization purposes. P2RX4 and P2RX7 are sensitive to BzATP (EC_{50} ~3 µM for P2RX4 and ~5 µM for P2RX7)[459,460] in particular, yet the applied concentration of 100 µM is also effective on further members of the P2X family (EC_{50} ~1-50 µM)[217], but putatively not on members of the P2Y family except for P2RY11[205,461].

Response of HTPCs to BzATP as agonist was firmly established since the cells showed immediate and transient [Ca^{2+}] elevations as long as exposed to the stimulating agent (Figure 2.13A1/B1) thereby pointing to the presence of functional purinergic receptors. To distinguish, if BzATP-induced Ca^{2+} signals were mediated via P2X or P2Y receptors, external [Ca^{2+}] was removed from the environment. Since P2X receptors are ligand-gated ion channels, activation induces pore opening of the receptor to cations in the extracellular environment leading to Ca^{2+} influx into the cytosol.

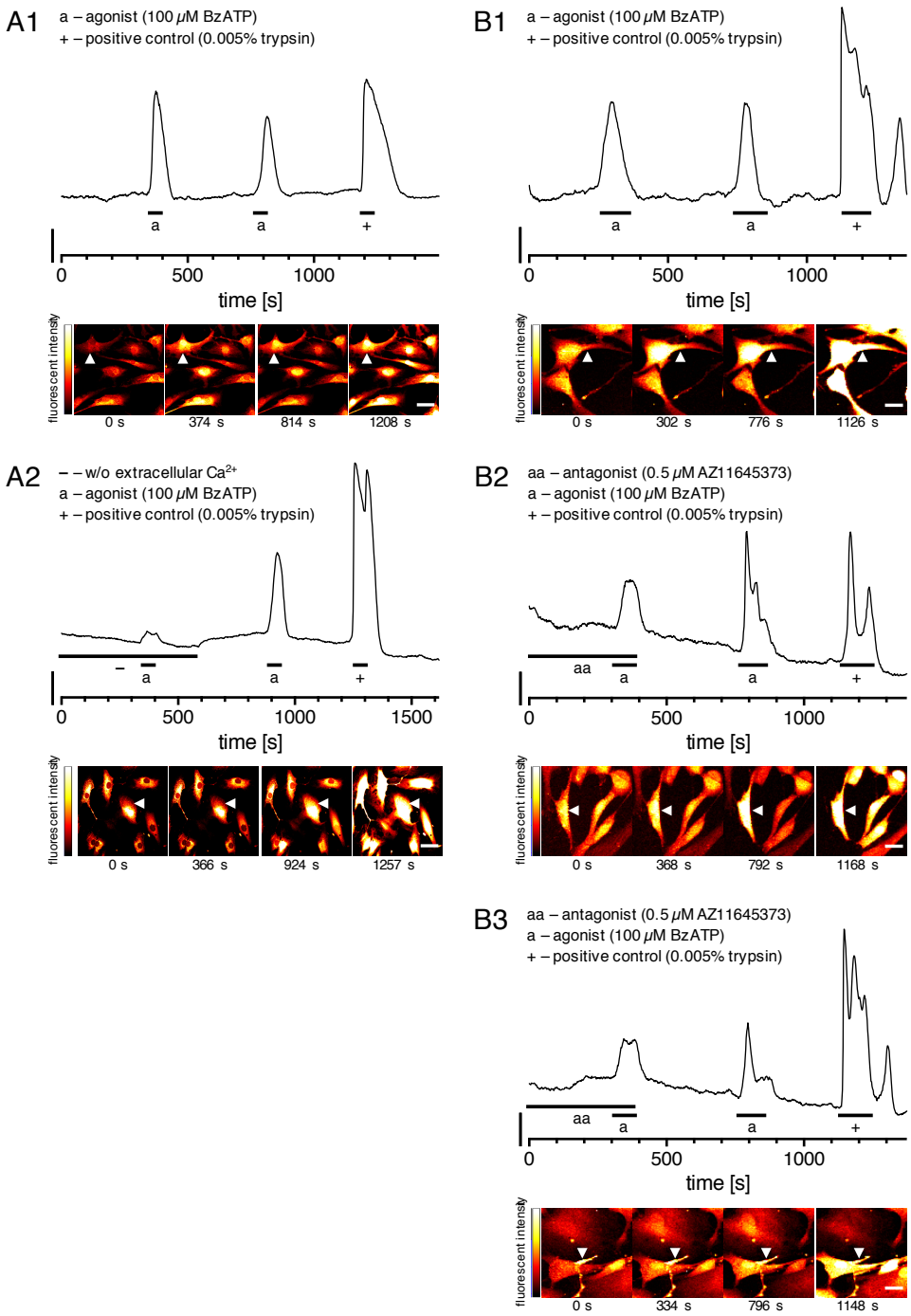

Figure 2.13 Functional purinergic receptor assessment in HTPCs via calcium imaging.
Top: Graphic representation of representative Ca^{2+}-dependent fluorescent signals in individual HTPCs loaded with Fluo4 or Fluoforte (5 µM) over time when exposed to different conditions. Stimulation time periods are indicated by horizontal bars. 0.005% trypsin was used as a positive control (+) in all experiments. y axis bar represents 20 a.u. fluorescent intensity. Bottom: Pseudocolor single frame images of fluorescent intensity at the beginning of the experiment (0 s) and at peak elevations during agent and positive control exposure depict the response of the measured HTPCs (arrowhead). Bars = 50 µm. **A1/B1.** Response to agonist exposure (a, 100 µM BzATP) revealed robust Ca^{2+} transients in HTPCs of two different patients. **A2.** Response to the agonist BzATP was nearly abolished by removal of extracellular Ca^{2+}(–), but reestablished after addition of Ca^{2+} (1.8 mM). **B2/B3.** Response to the agonist BzATP in antagonist (aa, 0.5 µM AZ11645373) pre-treated cells appeared to be of lower intensity compared to Ca^{2+} signals during agonist exposure after antagonist washout.

P2Y receptors, however, are G-protein coupled transmembrane receptors. Their activation entails signaling processes that eventually lead to the depletion of intracellular Ca^{2+} stores into the cytosol. Thus, Ca^{2+} signals in the absence of extracellular [Ca^{2+}] indicate involvement of the P2RY family, whereas signal abrogation points to P2RX signaling. As Figure 2.13A2 illustrates, in the absence of external [Ca^{2+}], the fluorescent signal was almost abolished, but recovered when [Ca^{2+}] was added to the environment. This finding implies that P2X receptors are the predominant functional receptors in HTPCs. To investigate, if P2RX7 is the responsible ion channel in response to BzATP, imaging with the specific P2RX7 inhibitor AZ11645373 (0.5 µM; K_B = 5-20 nM)[462,463] was carried out. Pre-treatment of HTPCs with the antagonist led to an attenuated [Ca^{2+}] elevation during BzATP exposure compared to the BzATP response without the presence of the inhibitor (Figure 2.13B2-3). This suggests, that P2RX7 is a contributing factor, but not the prevalent P2X receptor in HTPCs.

In collaboration with the Spehr Lab at RWTH Aachen University, these findings in HTPCs were confirmed and expanded. ATP was applied as agonist and found to induce concentration-dependent [Ca^{2+}] elevations in HTPCs (EC_{50} = 41 µM). Treatment with two further antagonists excluded major signal mediation by P2RX1, P2RX2, P2RX3 and P2RX5. Together with electrophysiological recordings, which suggested involvement of a highly ATP-sensitive P2X receptor, P2RX4 was putatively identified as the prevalently acting purinergic receptor in HTPCs[458].

2.2.4 ATP-mediated effects in HTPCs

To correlate ATP activation of purinergic receptors with regulation of cellular mechanisms and functions in the human testis, the impact of ATP was evaluated in HTPCs. As prerequisite, the possibility of ATP being an endogenous ligand at purinergic receptors of peritubular cells was examined. In the testis, extracellular ATP can originate from various sources. Sertoli cells have been described to release ATP as physiologic stimulus in presumably paracrine activity[464,465]. In contrast, ATP is also able to act as a danger signal, if released from cells undergoing apoptosis[280], infiltrating macrophages or mast cells[284,466,467]. While apoptosis is an omnipresent yet tightly controlled process that recruits macrophages amongst others[281,468], macrophages per se are not common in the healthy human testis and their presence has been associated with infertility[45]. Mast cells, however, are more abundant in the testis and increased numbers and localization in and around the peritubular compartment have been observed in subfertile patients[47,66]. Thus, extracellular ATP levels are hypothesized to be elevated in the testis under pathophysiologic conditions.

Immunohistochemical staining for the mast cell marker tryptase in human testicular sections confirmed that tryptase-positive mast cells reside in the immediate vicinity of the seminiferous tubular wall or even within the tubular wall (Figure 2.14). Hence, they represent a natural origin of extracellular ATP in the testis, capable to act on peritubular cells. This hypothesis was evaluated using HTPCs as *in vitro* model.

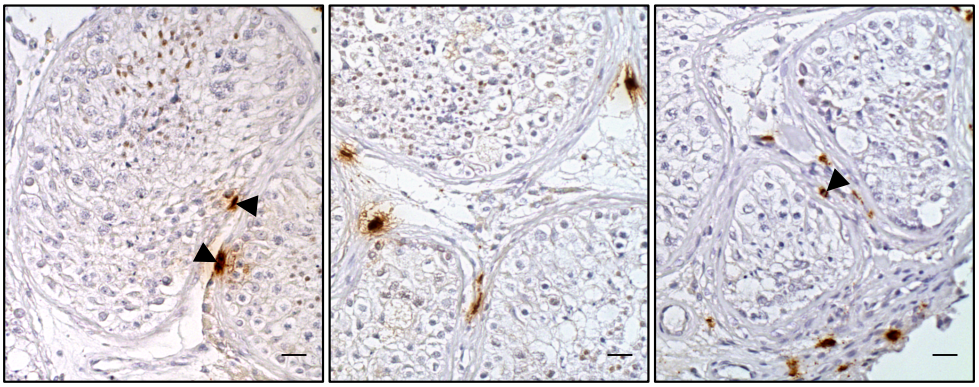

Figure 2.14 Presence of mast cells in and near the tubular wall of the human testis.
Immunohistochemical staining of the mast cell marker tryptase in testicular sections derived from three individual patients revealed presence of tryptase-positive mast cells near and embedded into (arrowheads) the tubular wall. Bars = 20 µm.

Cell viability of HTPCs in response to ATP treatment (1 mM) was assessed (Figure 2.15). Via live cell imaging cell number and confluence were determined over a period of 72 h exhibiting no significant difference between treated and untreated HTPCs, except that cell number at 6 h was even increased in ATP-treated compared to untreated cells. ATP-mediated cytotoxicity was monitored via lactate dehydrogenase (LDH) release as a means to detect disruption of cellular membranes. ATP-treated HTPCs displayed slightly lower LDH release at all time points examined. Although this finding did not reach statistical significance, it coincides with marginally elevated cell counts and confluence in ATP-treated HTPCs. Altogether, this definitely supports the conclusion that ATP at the concentration used in the following studies did not affect HTPC proliferation or viability.

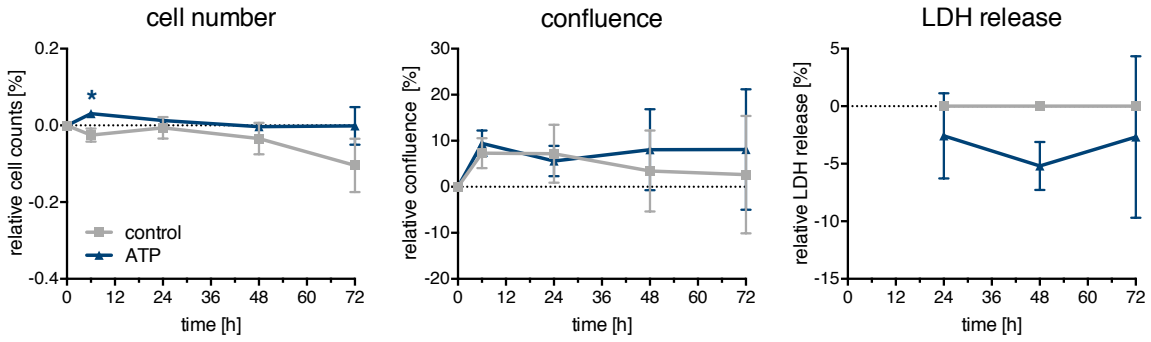

Figure 2.15 Viability of HTPCs during ATP treatment.
ATP treatment (1 mM) did not negatively alter HTPC viability assessed via determination of cell number, confluence and LDH release. Cell number and confluence (n = 4 individual patients) were evaluated at 6 h, 24 h, 48 h and 72 h post treatment, LDH release (n = 3 individual patients) was measured 24 h, 48 h and 72 h after treatment. Data represent means ± SEM relative to starting point (cell number, confluence) or control conditions (cytotoxicity). Asterisks denote statistical significance (paired *t*-test for cell number and confluence, one-sample *t*-test for LHD release, $p < 0.05$). Reproduced and modified from [458] under a Creative Commons BY license.

To identify parameters altered by ATP treatment of HTPCs, transcript expression of purinergic receptors, peritubular cell characteristic markers and putatively affected pro-inflammatory cytokines and chemokines was quantified after 6 h and 24 h (Figure 2.16).

Transcript levels of purinergic receptors *P2RX4* and *P2RX7* significantly declined due to ATP treatment (Figure 2.16A) implying a negative feedback of ATP on its receptors. Concomitantly, transcript levels of smooth muscle cell markers, smooth muscle actin (Actin, aortic smooth muscle, *ACTA2*) and calponin 1 (*CNN1*) and therefore indicators of characteristic peritubular features were significantly decreased as well (Figure 2.16B).
The known HTPC-secreted stem cell niche regulatory factors CXCL12 and GDNF were investigated, too (Figure 2.16C). *CXCL12* transcript levels were diminished after 6 h of ATP treatment, but restored at 24 h, whereas *GDNF* transcript levels were increased after 6 h and also restored at 24 h.

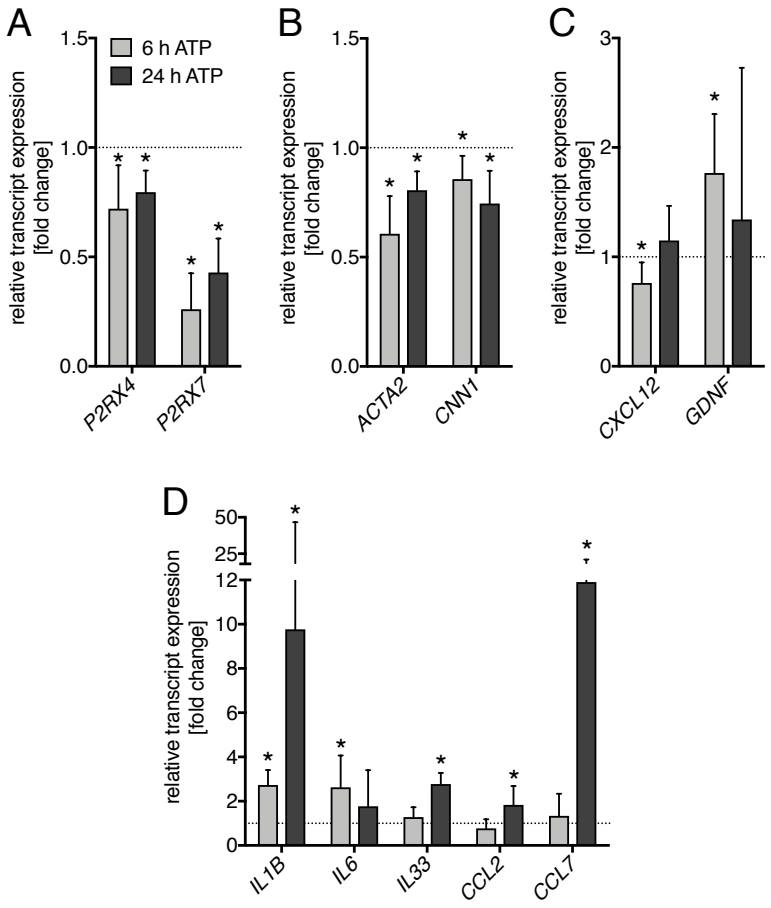

Figure 2.16 Transcript regulation by ATP treatment of HTPCs.
A. Purinergic receptor *P2RX4* and *P2RX7* transcript levels significantly decreased by ATP treatment at both time points. **B.** Smooth muscle cell marker *ACTA2* and *CNN1* transcript levels were significantly diminished after ATP treatment at 6 h and 24 h. C. Stem cell niche regulatory factor *CXCL12* and *GDNF* transcript levels were up-regulated and down-regulated, respectively, after 6 h of ATP treatment, but unaltered at 24 h. **D.** Cytokine *IL1B*, *IL6* and *IL33* and chemokine *CCL2* and *CCL7* transcript levels were all significantly elevated at 24 h of ATP treatment except for *IL6*, but only *IL1B* and *IL6* transcript levels displayed significant increase at 6 h. HTPCs from eight patients were analyzed except for four transcripts at 24 h (n = 6 for *P2RX7*, *GDNF* and *CCL7* and n = 5 for *IL1B*). Data represent geometric means + 95% confidence interval relative to controls. Asterisks denote statistical significance (one-sample *t*-test, $p < 0.05$). Reproduced and modified from [458] under a Creative Commons BY license.

These results suggest that ATP-mediated processes may be involved in modulation of stem cell niche regulatory factors, albeit in a time-dependent manner. The ultimately expected effect of stimulating cells with the danger molecule ATP was an induction in inflammation-associated molecules, so transcript levels of cytokines *IL1B*, *IL6*, *IL33* and chemokines *CCL2* and *CCL7* were assessed (Figure 2.16D). Transcript levels of the pro-inflammatory *IL1B* were the only ones significantly up-regulated at both examined time points, while the other cytokine and chemokine transcript levels were obviously underlying a time-dependent regulation. *IL6* transcript levels were significantly elevated solely after 6 h of ATP treatment, *IL33*, *CCL2* and *CCL7* only after 24 h of ATP treatment.

To confirm transcriptional results and correlate it with protein secretion of cytokines and chemokines, a cytokine profiling assay was used to analyze supernatants of ATP-treated HTPCs after 48 h (Figure 2.17 and Figure 2.18). Among the cytokines and chemokines altered on transcript level, IL1β and IL33 signals could not be detected in the assay. CXCL12, IL6 and CCL2 secretion levels did not seem to be increased, yet CCL7 secretion appeared to be augmented, albeit not significantly. An additional chemokine that stood out in the profiling assay was CXCL5. Although its protein levels in the supernatant were not significantly elevated (Figure 2.17A), a significant increase of *CXCL5* transcript abundance after 24 h, but not 6 h of ATP treatment became evident (Figure 2.17B). Altogether, transcript and supernatant data indicate an ATP-mediated increase in cytokine and chemokine production and secretion. However, the underlying processes seem to be regulated in a time-dependent manner.

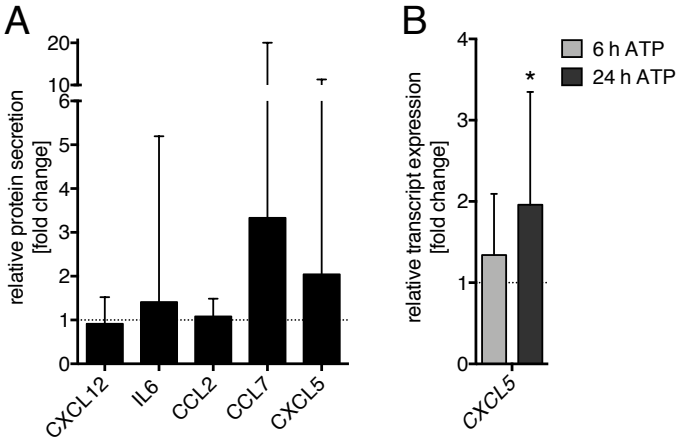

Figure 2.17 Influence of ATP treatment on cytokine and chemokine secretion in HTPCs.
A. Secreted CXCL12, IL6, CCL2, CCL7 and CXCL5 protein levels were not significantly increased in ATP-treated supernatants after 48 h of incubation (n = 4). **B.** The newly identified *CXCL5* was also elevated on transcript level by ATP treatment, yet significantly only at 24 h (n = 6) but not 6 h (n = 8). Data represent geometric means + 95% confidence interval relative to controls. Asterisks denote statistical significance (one-sample *t*-test, $p < 0.05$). Reproduced and modified from [458] under a Creative Commons BY license.

Supernatant cytokine profiling also identified factors with diminished secretion levels leading to the discovery of a decline in insulin-like growth factor-binding protein 3 (IGFBP3), osteopontin (secreted phosphoprotein 1, SPP1) and thrombospondin 1 (THBS1) secretion (Figure 2.18A). Still, only IGFBP3 and SPP1 decrease reached a level of statistical

significance. Transcript level determination of these three candidates revealed reduced expression levels (Figure 2.18B), albeit *IGFBP3* levels did not decline significantly, *SPP1* levels were only significantly diminished 6 h after ATP treatment and *THBS1* levels were significantly decreased at both time points reinforcing the proposition of a time-dependent regulation of ATP-induced events.

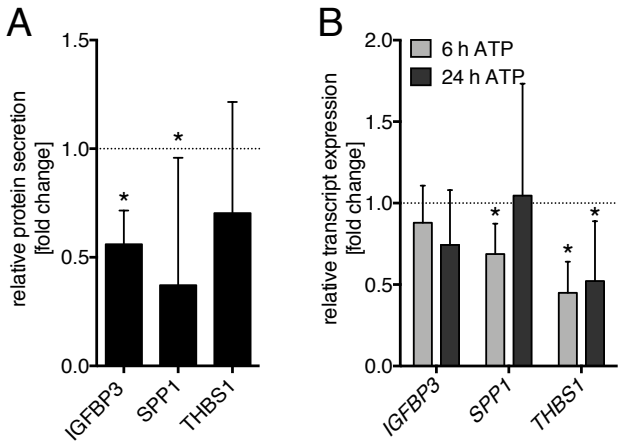

Figure 2.18 Influence of ATP treatment on ECM-associated protein secretion in HTPCs.
A. Secreted IGFBP3, SPP1 and THBS1 protein levels decreased in ATP-treated supernatants after 48 h of incubation (n = 4), albeit only IGFBP3 and SPP1 levels diminished significantly. **B.** Transcript levels of *IGFBP3* did not decline significantly in response to ATP treatment, *SPP1* transcript levels solely after 6 h of ATP treatment and *THBS1* transcript levels at 6 h and 24 h after treatment. HTPCs from eight patients were analyzed except for *SPP1* at 24 h (n = 6). Data represent geometric means + 95% confidence interval relative to controls. Asterisks denote statistical significance (one-sample *t*-test, $p < 0.05$). Reproduced and modified from [458] under a Creative Commons BY license.

Besides secreted proteins, whole cell lysates of HTPCs that were treated with ATP for 48 h, were analyzed by mass spectrometry. In total, 3533 proteins were identified and quantified (false discovery rate < 1%; complete list provided in the Supplementary Dataset 1 of [458]). 83 of these proteins were affected in abundance (p-value < 0.05; log2-fold change > |0.6|), comprising 38 proteins of decreased and 45 proteins of increased abundance. By interaction annotation, clustering of proteins with decreased abundance became evident (Figure 2.19A; PPI enrichment p-value $2.61e^{-11}$). Significant functional enrichment of KEGG pathways and GO terms related to ECM-cell interaction, ECM organization and collagen metabolism was observed. The complete lists of candidates and enriched pathways are depicted in the Supplementary Dataset 1 of [458]. No functional clustering was found among proteins increased in abundance.

From the clustering proteins of decreased abundance, *COL1A1*, *COL1A2*, *COL3A1*, *COL4A2*, *COL6A2* and *LOX* were chosen for transcript analysis in response to ATP (Figure 2.19B). Levels of all six selected transcripts were significantly diminished 6 h after ATP treatment, but recovered control levels 24 h after treatment. These findings support the idea of a time-dependent regulation of ATP-induced ECM molecule decrease.

In summary, ATP principally affected two sets of factors in HTPCs. On one side, smooth muscle cell characteristic markers, ECM molecules and ECM-associated factor generally declined in abundance. On the other side, pro-inflammatory cytokines and chemokines

became up-regulated by ATP. Thus, ATP appears to act as danger molecule on HTPCs evoking pro-inflammatory gene expression, meanwhile shifting the HTPC phenotype from producing and secreting ECM factors to pro-inflammatory factors.

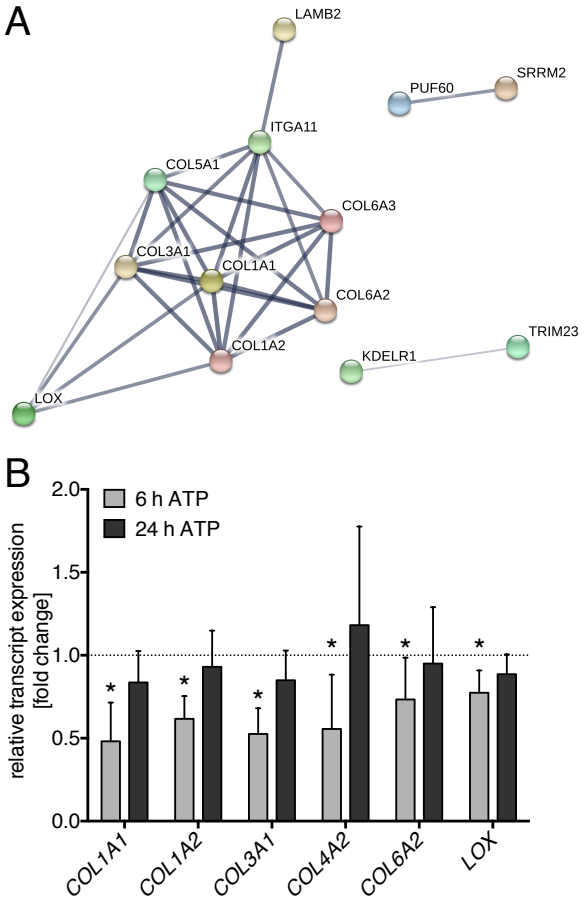

Figure 2.19 Regulation of ECM components by ATP treatment of HTPCs.

A. ATP-treated HTPC lysates (n = 6, 48 h) were analyzed by MS/MS and in abundance decreased proteins were identified. Interaction annotation uncovered enrichment of in abundance decreased proteins for KEGG pathways and GO terms related to ECM organization and collagen metabolism. The cluster of interaction between the enriched proteins was visualized via STRING analysis tool[469]. **B.** Of the in abundance decreased interacting proteins *COL1A1*, *COL1A2*, *COL3A1*, *COL4A2*, *COL6A2* and *LOX* were selected for transcript analysis. After 6 h of ATP treatment all transcript levels were significantly reduced, but restored at 24 h post ATP stimulation. HTPCs from eight patients were analyzed. Data represent geometric means + 95% confidence interval relative to controls. Asterisks denote statistical significance (one-sample *t*-test, $p < 0.05$). Reproduced and modified from [458] under a Creative Commons BY license.

2.3 NLRP3 – an inflammatory sensor in the testis?

The NLRP3 molecule is an intracellular sensor of danger to the cell[470,471]. ATP-gated purinergic receptors P2RX4 and P2RX7 are activators of NLRP3[290,309,334], which assembles together with the adapter molecule ASC and the effector molecule pro-caspase 1 to form the NLRP3 inflammasome[323]. Inflammasome signaling includes maturation and release of IL1 family cytokines[317,470]. Thus, this pathway provides one of many possible signaling mechanisms for ATP-mediated effects discovered in HTPCs. Hence, NLRP3 expression in

the testis was characterized regarding putative inflammatory events. In this context, the *AROM*$^{+}$ mouse was again employed as a systemic model of sterile inflammation in the testis.

2.3.1 NLRP3 expression in human and mouse testes

Since testicular NLRP3 has scarcely been described, NLRP3 expression in human and mouse testes was characterized. Immunohistochemical staining of testicular sections revealed expression in Sertoli cells of both species (Figure 2.20). Staining of Sertoli cells primarily ranged from the basal lamina to the lumen of the seminiferous tubules. Interestingly, NLRP3 positive staining of Sertoli cells was not restricted to adult, matured seminiferous tubules, but already discovered in Sertoli cells of the new-born mouse. In addition, interstitial tissue appeared to be stained in the adult mouse. In human, distinct staining of peritubular cells was observed, yet staining was less intense than in Sertoli cells and heterogeneously distributed among sectors of the seminiferous tubular wall.

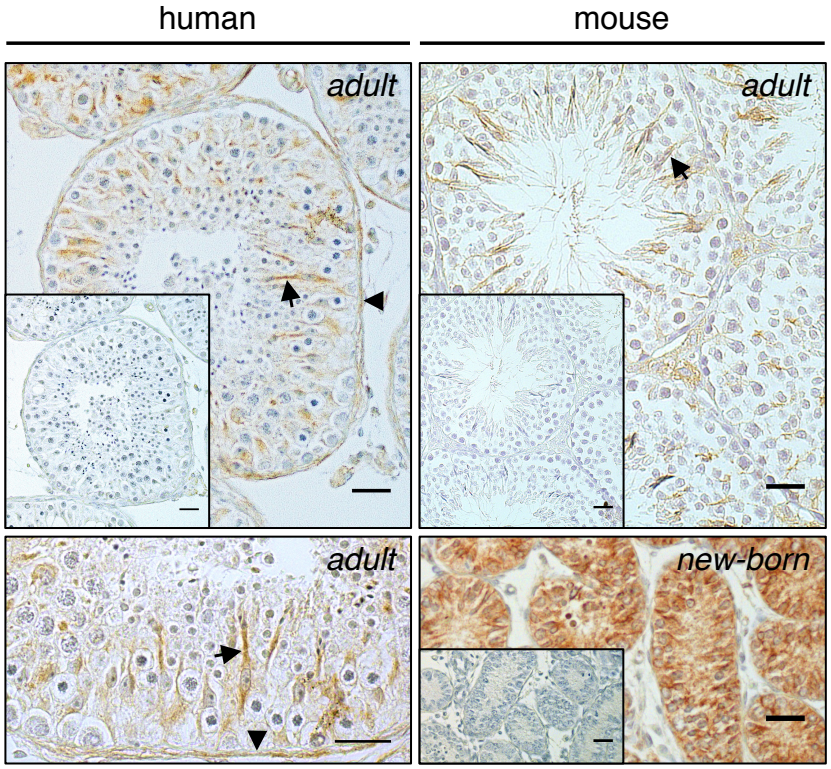

Figure 2.20 Expression of NLRP3 in somatic cells of human and mouse testis.
Immunohistochemical staining indicating NLRP3 expression in representative testicular sections of adult human (left panel) and adult and new-born mouse (right panel). Sertoli cell staining (examples indicated by arrows) was detected in all sections. In human, peritubular cells were immunopositive as well (examples indicated by arrowheads). In mouse, interstitial areas were stained. Insets: Negative controls consisting of primary antibody omission in consecutive sections. Bars = 25 µm.). Reproduced and modified from [472] with permission from BioScientifica Ltd. in the format Republish in a thesis/dissertation via Copyright Clearance Center.

Qualitative transcript evaluation confirmed *NLRP3* expression in whole human and mouse testis as well as in cultured human peritubular cells (Figure 2.21). Hence, it can be stated that NLRP3 is expressed in somatic cells of the testis.

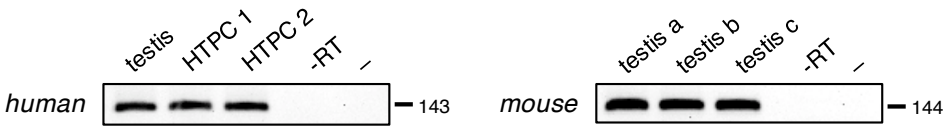

Figure 2.21 Qualitative *NLRP3* transcript expression in human and mouse testis.
NLRP3 transcripts were present in whole human testis and in HTPCs (two individual patients shown; left panel). In mouse, *Nlrp3* transcripts were detected in WT testes (three individuals shown; right panel). Figure shows RT-PCR reaction fragments visualized on agarose gels. Negative controls consisted of non-reverse transcribed RNA as template (-RT) and a non-template reaction (–). Amplicon lengths are indicated to the right of the corresponding fragments.

2.3.2 NLRP3 expression in mixed atrophy patients

NLRP3 as a mediator of inflammatory events may play a part in idiopathic male infertility provoked by sterile inflammatory processes in the testis. To explore this possibility, mixed atrophy samples were investigated to the advantage of examining seminiferous tubules of normal development residing next to tubules of impaired germ cell development (Figure 2.22).

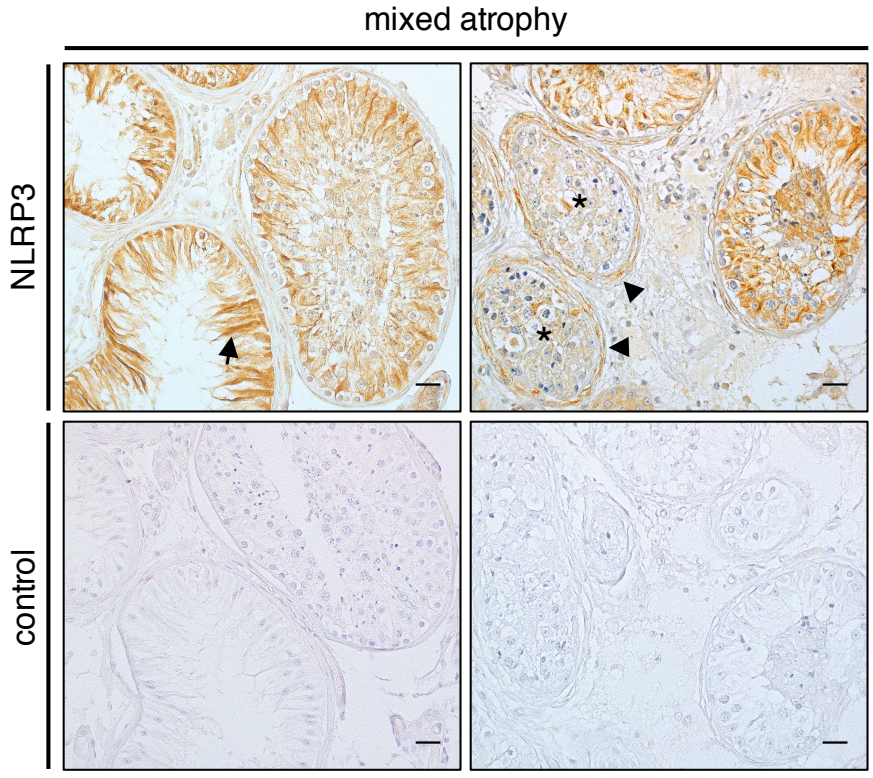

Figure 2.22 NLRP3 expression in human testes exhibiting mixed atrophy pathology.
Immunohistochemical staining indicating NLRP3 expression (upper panel) in human testicular sections derived from mixed atrophy patients revealed intense Sertoli cell staining (arrow) in seminiferous tubules exhibiting impairment of the germ cell lineage (left upper panel). In degenerated tubules (asterisks) in another mixed atrophy sample (upper right panel) Sertoli cell staining was completely missing while the tubular wall (arrowheads) was intensely stained. Controls (lower panel) consisted of primary antibody omission in consecutive sections. Staining was performed for n = 3 mixed atrophy patients. Bar = 25 µm. Reproduced and modified from [472] with permission from BioScientifica Ltd. in the format Republish in a thesis/dissertation via Copyright Clearance Center.

As described, staining implying NLRP3 expression was mostly found in Sertoli and peritubular cells. Sertoli cells in tubules displaying disturbed germ cell lineage development stained prominently for NLRP3, while peritubular cells of these tubules exhibited rather faint staining. In contrast, in tubules containing spermatogenic impairment, peritubular cells stained intensely, especially in thickened sectors of the seminiferous tubular wall, whereas distinct staining of Sertoli cells was entirely lacking. These results point to a probable link of the observed NLRP3 expression pattern with events associated with tubular degeneration and disturbed spermatogenesis, which are phenotypic characteristics in male subfertile patients.

2.3.3 NLRP3 regulation in a mouse model of sterile inflammation

Again, the *AROM*$^+$ mouse line was used as a systemic model of chronic sterile inflammation and male infertility, to investigate the putative connection of inflammatory processes and NLRP3 expression in the testis. Histologic morphology of the WT male testicular sections was inconspicuous at the examined age of 2.5 and ten months, respectively.

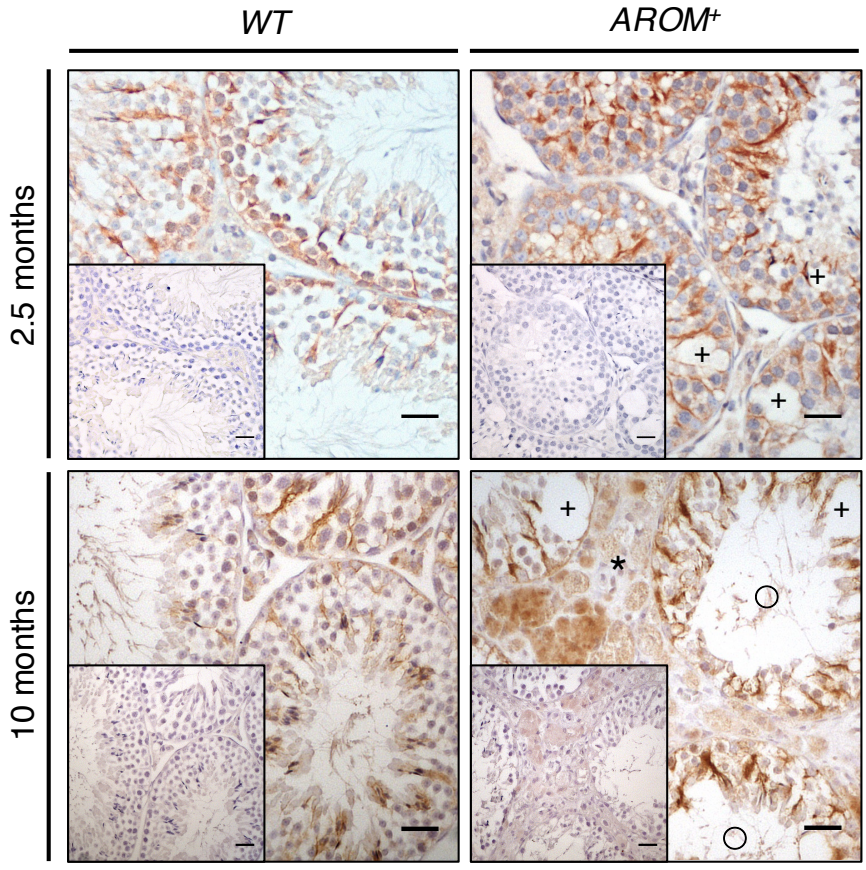

Figure 2.23 NLRP3 expression in the testis of WT and *AROM*$^+$ mice.
Immunohistochemical staining indicating NLRP3 expression in testicular sections of 2.5 and ten months old WT and *AROM*$^+$ mice. WT phenotypes were considered normal, in *AROM*$^+$ sections germ cell vacuolization (crosses) was evident, followed by tubular degeneration (circles) and increased abundance of interstitial tissue (asterisk) (ten months only). Staining was primarily observed in Sertoli cells, but also in the interstitial tissue of ten months old *AROM*$^+$ mice. Insets: Negative controls consisting of primary antibody omission in consecutive sections. Bars = 25 µm. Reproduced and modified from [472] with permission from BioScientifica Ltd. in the format Republish in a thesis/dissertation via Copyright Clearance Center.

In 2.5 months old *AROM*$^+$ mice, phenotypic alterations were already emerging in terms of germ cell vacuolization, whereas at ten months of age, disturbed tubular structure with partial depletion of germ cell lineage cells and interstitial cell conglomerates dominated the phenotypic picture (Figure 2.23).

Staining for NLRP3 expression was prevalently observed in Sertoli cell at all stages. A noticeable difference of staining location and intensity between *AROM*$^+$ and WT animals was not recognized at 2.5 months, but became obvious at ten months of age. In addition to Sertoli cells, prominent staining in the interstitial region, presumably consisting of a combination of hypertrophic macrophages and Leydig cells, was detected. Thus, the altered staining pattern for NLRP3 expression with progressing severity of the testicular phenotype implies a link between *AROM*$^+$ overexpression and NLRP3 presence.

Concomitantly, changes in *Nlrp3* expression were quantified by assessing testicular *Nlrp3* transcript levels in *AROM*$^+$ compared to WT mice at two, five and ten months of age (Figure 2.24). *Nlrp3* transcript levels were elevated in all three age groups, albeit the difference to WT levels was statistically significant only in five and ten months old animals. Remarkably, comparison of relative transcript expression between *AROM*$^+$ mice of different age groups revealed increasing *Nlrp3* levels, supporting the notion of impaired testicular function in the *AROM*$^+$ phenotype coinciding with elevated *Nlrp3* expression and inflammatory events.

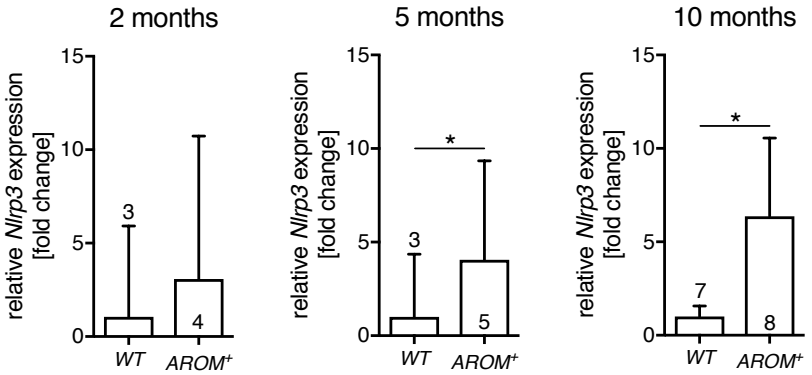

Figure 2.24 Elevated *Nlrp3* transcript expression in testes of *AROM*$^+$ mice.

Nlrp3 transcript levels were increased in two, five and ten months old *AROM*$^+$ mice compared to WT littermates. Notably, relative *Nlrp3* transcript levels of *AROM*$^+$ mice increased with age. Transcript levels are depicted normalized to WT control levels. Numbers of animals analyzed are denoted in the graphs. Data represent geometric means + 95% confidence interval. Asterisks denote statistical significance (unpaired *t*-test, $p < 0.05$). Reproduced and modified from [472] with permission from BioScientifica Ltd. in the format Republish in a thesis/dissertation via Copyright Clearance Center.

To verify a relation between ascending *Nlrp3* expression levels and the *AROM*$^+$ phenotype, four weeks old mice treated with an aromatase inhibitor (AI) and a placebo control, respectively, for six weeks were analyzed. *Nlrp3* transcript levels in the testis were significantly elevated in *AROM*$^+$ (±AI) mice compared to WT (±AI) mice (Figure 2.25). Importantly, AI treatment in *AROM*$^+$ mice significantly reduced *Nlrp3* transcript levels, although the initial basal levels of the WT could not be restored completely. In contrast, AI

treatment did not exhibit an effect in WT mice regarding *Nlrp3* levels. Therefore, AI treatment reversed increased *Nlrp3* expression evoked by aromatase overexpression.

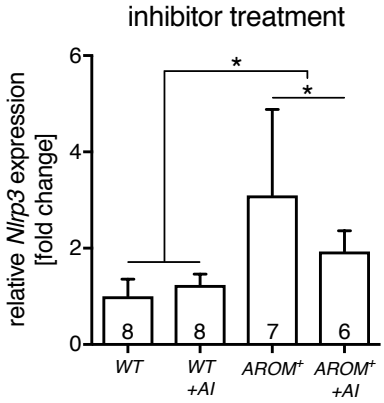

Figure 2.25 Comparison of *Nlrp3* transcript levels in testes of 2.5 months old *AROM*$^+$ mice treated with an aromatase inhibitor (AI).

Nlrp3 transcript levels were evaluated according to genotype of 2.5 months old WT and *AROM*$^+$ mice treated with AI and placebo for six weeks, respectively. Transcript levels are depicted normalized to WT control levels. Numbers of animals analyzed are denoted in the graphs. Data represent geometric means + 95% confidence interval. Asterisks denote statistical significance (ANOVA with Tukey's post-test, $p < 0.05$). Reproduced and modified from [472] with permission from BioScientifica Ltd. in the format Republish in a thesis/dissertation via Copyright Clearance Center.

In conclusion, NLRP3 expression by somatic cells of the testis in human and mouse appeared to be altered in subfertile and infertile pathologies. In the human, NLRP3 was differentially expressed in morphologically altered tubules. In the *AROM*$^+$ mouse phenotypic changes associated with chronic inflammation and infertility were accompanied by increased *Nlrp3* expression levels, that were due to aromatase overexpression.

3 Discussion

3.1 Deficiency of biglycan does not rescue from an inflammatory environment

Long-standing work from Schäfer and colleagues established the ECM molecule biglycan (BGN) as an autonomous trigger of sterile inflammation, primarily in mouse models of hepatic and renal diseases[127,180]. Its mechanism of joint signaling through TLR2 and 4 and P2RX4 and 7 activation was elucidated, thereby implicating biglycan in NLRP3 inflammasome activation and cytokine production and release[169,188].

In this work, initial experiments on human testicular sections showed association of biglycan with fibrotic remodeling of the tubular wall, supported by the fact, that biglycan is a known contributor to the ECM of the tubular wall[129] and vastly produced by cultured peritubular cells[101]. Additionally, I observed an increase of *Bgn* as well as *Tlr2*, *Tlr4*, *P2rx4* and *P2rx7* in the testes of *AROM*$^{+}$ mice compared to WT mice, which implied augmented abundance of biglycan and presumable target receptors in an inflammatory context. Thus, these primary findings indicated a putative role of biglycan in contributing to an inflammatory environment in the testis. This hypothesis was further supported by the study from Mayer *et al*., confirming the connection of testicular biglycan with tubular fibrosis and reporting signaling of biglycan through TLR2 leading to an increment of the pro-inflammatory factors IL6, CCL2 and PTX3 in human testicular peritubular cells (HTPCs)[95].
Based on these conclusions, introducing the *Bgn* knock-out into the *AROM*$^{+}$ mouse would attenuate or even counteract the chronic inflammatory phenotype observed in the testis of this mouse line. Contrasting to this assumption, *Bgn* deficiency did not substantially affect the testicular phenotype of *AROM*$^{+}$ mice in terms of weights, testicular morphology, steroid levels or transcription profile in both examined age groups. Significant changes between *AROM*$^{+}$ and *AROM*$^{+}$ *Bgn*$^{-/0}$ genotypes were noticed solely in transcription levels analyses of *Tlr2*, *Tlr4* and *P2rx7* in four months old mice. Transcript levels of *Tlr2*, *Tlr4* and *P2rx7* were found to be enhanced by the *Bgn* knock-out, an effect that could not be recapitulated at ten months of age. However, the cytokine transcript levels associated with TLR and P2X receptor signaling remained unaltered in both, four and ten months old mice, contrary to the reported increase in HTPCs[95]. This prompts the notion that biglycan probably has a different means of action in the mouse compared to the human testis and might modulate receptor expression at a certain age without affecting inflammatory signaling.

Very little is known about biglycan expression in the murine testis. Estradiol has been identified as an inducer of biglycan expression the mouse skin[473] and in human peritubular cells[95]. Studies of the developing mouse gonads implicated expression in the basement membrane as well as in interstitial cells[474,475], but the overall amount of biglycan has not been investigated. Immunohistochemical staining of testicular sections yielded different results in the mouse and human specimens examined. While in human samples, the tubular wall and parts of the interstitial tissue stained prominently (Figure 2.1), mouse samples exhibited faint to no staining at all (not shown). Different antibodies were tested, but staining

in the mouse proved to be difficult and therefore, reliable results could not be produced. Other than antibody failure, biglycan levels might be considerably lower in the mouse compared to the human testis.
It is further unexplored, if or how sequestered biglycan regains its soluble state in the testis, that is compulsory for biglycan actions on TLRs and P2X receptors[127,169,188]. Thus, bioavailability of biglycan or its fragments might be low in the murine testis and therefore not a key element in testicular inflammation. *De novo* synthesis is the second factor influencing bioavailability of biglycan, putatively carried out by infiltrating macrophages[144,145,165]. This correlates with the co-occurrence of macrophages and elevated biglycan transcript levels in the *AROM*$^+$ testes. Yet, in this scenario biglycan production is more likely a downstream effect of the initial inflammatory signaling events that evoke macrophage infiltration, than their putative cause.

While the sole *Bgn* knock-out did not exhibit differences in all parameters examined, including testicular morphology and inflammatory gene expression compared to WT, a phenotype in other systems has been well-documented, particularly in bone and connective tissue formation and homeostasis[127,151,476]. Several knock-out studies evaluated biglycan deficiency in combination with the knock-out of another proteoglycan[150,154,156,477,478] and were able to show synergistic phenotypic defects in case of a double knock-out, thereby implying a compensating effect between biglycan and the other proteoglycan. This has especially been shown for decorin, the sister molecule of biglycan[148,447,448,479]. In the human testis, decorin abundance has been linked to male infertility[62,98] and levels were shown to be increased in the testes of *AROM*$^+$ mice[98]. Subsequently, decorin transcript levels were significantly elevated in *AROM*$^+$ and *AROM*$^+$ *Bgn*$^{-/0}$ mouse testes, yet a compensating effect in the *AROM*$^+$ *Bgn*$^{-/0}$ mice in response to the biglycan knock-out could not be observed.

It has to be noted that the inflammatory phenotype of *AROM*$^+$ mice in the mixed background (FVB/N and C57BL6) seemed less pronounced than in the original mouse line (FVB/N background)[111-113]. *AROM*$^+$ mice exhibited fewer cases of cryptorchidism and testis weights were not significantly reduced compared to the original study[112]. The *AROM*$^+$ hallmark, the decrease in intratesticular testosterone levels[111,112], could not be recapitulated, although estradiol levels were strongly elevated. At four months of age testicular morphology in the *AROM*$^+$-containing genotypes was altered regarding the accumulation of interstitial tissue, but germ cell vacuolization and disturbed tubular epithelial structures were not detected before ten months of age. This again contrasts with the previous findings[112,113], where these phenotypic changes were visible already at the age of four months. The hypothesis of a lower inflammatory degree is further supported by the comparison of *Cd68* and *Tnfa* transcript expression. Both were significantly elevated in *AROM*$^+$ testes, *Cd68* indicating an increased abundance of macrophages, *Tnfa* as a marker of inflammatory events, yet fold changes between WT and *AROM*$^+$ mice were smaller than in the original report[111]. Morphological evaluation together with assessment of germ cell lineage and spermatogonial stem cell markers *Ddx4* and *Fgfr3* transcript levels did not imply disturbed spermatogenesis in the *AROM*$^+$ testes of four months old mice at all. Decreased levels of *Ddx4* and *Fgfr3* in ten

months old *AROM*$^+$ mice, albeit not significantly compared to WT, along with partial disruption of the tubular epithelium suggest spermatogenic failure to some, but not full extent. These findings could point to either a later onset of infertility characteristics or an alleviated phenotype in comparison with the original *AROM*$^+$ transgenic line. However, it has to be stated that a vast degree of heterogeneity between individual mice was observed, particularly in histological and transcript level evaluation. The underlying causes for the phenotypical differences between original and the backcrossed *AROM*$^+$ mice cannot readily be elucidated. It can only be speculated that the mixture of background may play a part. Recently, *AROM*$^+$ mice in a C57BL6 background were described to display a lower rate of cryptorchidism but an almost similar testicular phenotype[480,481].

In the *AROM*$^+$ transgenic line, inflammation-associated male infertility is provoked by a hormonal imbalance between estradiol and testosterone. The underlying molecular mechanisms of how estradiol causes this phenotype have begun to emerge only recently. Estradiol signaling through estrogen receptor α was reported to cause Leydig cell hyperplasia, activate macrophages[482] and subsequently promote Leydig cell engulfment by activated macrophages[480]. Since excess estradiol increases with age in the *AROM*$^+$ mice[111,480], these findings may explain why phenotypic alterations like abundance of Leydig cell-macrophage conglomerates and presence of inflammatory signaling factors aggravate with increasing age. As a result, loss of spermatogenesis-supporting Leydig cells advances with age leading to infertility[483]. Still, the origin of increasing estradiol levels with age remains unclear and further mechanisms participating to the development of the inflammatory phenotype have yet to be clarified.
Thus, results obtained from the *AROM*$^+$ mice certainly provide valuable insight of mechanisms in a sterile inflammatory milieu, but it has to be acknowledged that despite the phenotypic similarities of the impaired testes, there are differences between the mouse and the human regarding testicular structure and immune cell population, which have to be taken into account here.

Altogether, closer investigation is definitely necessary to determine the role of biglycan in the testis. Knowledge of testicular expression sites and bioavailability, for instance, will contribute to assessing, if biglycan is cause or effect of inflammatory processes in the testis. While *in vitro* results in HTPCs and murine immune cells and *in vivo* results in murine models suggest biglycan as cause, the failure of the biglycan knock-out strategy to counter the inflammatory testicular phenotype in the *AROM*$^+$ infertility mouse model indicates otherwise and hints at a more diverse function.

3.2 ATP contributes to testicular inflammation dependent on purinergic signaling

Extracellular ATP acts as physiological activator of purinergic signaling in the testis. In the healthy testis, ATP can be released by Sertoli cells[464] or apoptotic cells[280], whereas the number of ATP-liberating macrophages[45] and mast cells[47,66] is elevated under

pathophysiologic conditions. Thus, ATP signaling is supposed to be amplified under these conditions.
Analysis of HTPCs revealed their vast repertoire of purinergic receptors as putative ATP targets. Yet, P2RX4 and P2RX7 were determined prime candidates for ATP-mediated signaling, since their *in vivo* expression in peritubular cells could be related to thickened sectors of the tubular wall (Figure 2.12) and thus, infertility-associated fibrotic remodeling. These findings correspond to several *in vivo* studies reporting P2RX4- as well as P2RX7-mediated fibrosis in various organs, including lung[32,457], kidney[484], liver[485] or heart[486].
Functionality assessment of purinergic receptors in collaboration with the Spehr group at RWTH Aachen University revealed the prevalent action of P2RX4 in HTPCs, but joint assembly and activation of P2RX4 with P2RX7 could not be completely excluded. At this point, further investigation is needed to dissect the exact contributions of individual P2RX isoforms, their possible functional interactions or heterotrimer formation and subsequent involvement in downstream signaling.
ATP was found to orchestrate a series of altered transcript and secretion levels in HTPCs. Negative feedback on *P2RX4* and *P2RX7* transcript levels proposes self-limiting actions of ATP and provides evidence, that despite contrary results of functionality assessment, P2RX4 and P2RX7 could both be involved in ATP signal mediation in HTPCs. Several studies already suggested a functional regulation of P2RX7 by P2RX4[314-316].

The ATP actions discovered in HTPCs essentially promote regulation of two subsets of factors. Inflammatory cytokines and chemokines became elevated, while smooth muscle cell characteristics and ECM factors declined in expression.
Among the pro-inflammatory factors positively altered in expression by ATP, especially CCL2, IL6 and IL33 abundance have been associated with fostering fibrosis[31] and IL1β is a prominent promotor of collagen deposition[32,487]. The monocyte chemoattractant CCL2 and the cytokine IL6 have previously been identified in HTPCs[96,101] and implicated in inflammatory signaling following TLR activation[95]. IL6 can be produced through P2RX4 signaling in pro-inflammatory environments[308,488], but it is induced via P2RX7 as well[489-492]. CCL2 expression, however, has thus far extensively been linked to P2RX7 activation[491-494]. Yet, IL6 and CCL2 transcript levels were merely elevated approximately two-fold and secretion levels were hardly affected by ATP. In contrast, transcript levels of monocyte chemoattractant and sister molecule to CCL2, CCL7, vigorously increased after 24 h of ATP treatment and its secretion levels rose threefold compared to untreated controls. This finding is consistent to *in vitro* experiments in murine mast cells, where this effect was attributed to P2RX7[492]. The second factor with increased transcript and secretion levels, CXCL5, is prevalently acting as a chemoattractant recruiting neutrophils[495], but can be a ligand at the same receptor, CC chemokine receptor 2, as CCL2 and CCL7[496] and may thus exert mutual effects. P2RX4-dependent production and secretion of CXCL5 was very recently discovered by another group and seems to be a unique feature of P2RX4 since it has not been related to any other P2X receptor including P2RX7[497]. IL1β and IL33 both belong to the IL1 family of pro-inflammatory cytokines. Both were increased in transcript levels by ATP treatment, albeit IL33 considerably less than IL1β. IL33 is constitutively expressed in smooth muscle

cells[498,499] and although IL33 production through the ATP/P2RX7 axis has previously been determined in mast cells[500], the direct link to P2RX4 is still missing. IL33 and P2RX4 have both independently been implicated in neuropathic pain[501-504], which could emerge as the sought connection between them. IL1β as the prototypical pro-inflammatory cytokine has been associated with P2RX4[308,309] as well as P2RX7 signaling[305,334,377,505], separately or in combination[314-316,488]. Elucidating the underlying mechanisms of P2X receptor-dependent IL1β induction identified NLRP3 inflammasome activation as one putative pathway. ATP is able to trigger both, the P2RX4/NLRP3 axis[309,310] or the P2RX7/NLRP3 axis[305,377,505,506] in different environments and conditions. In addition, an NLRP3 inflammasome-independent mechanism of IL1β release has been described[507]. However, IL33 and IL1β could not be detected in the supernatant of ATP-treated HTPCs suggesting either that release required a certain, missing stimulus or that released amounts were still below detection limit. In this context, future investigations regarding the exact ATP signaling pathways will be crucial. Pivotal questions, that need to be addressed are a possible interplay of purinergic receptors in cytokine synthesis and the potential self-regulation of cytokine induction. Immediate responses of HTPCs to ATP revealed functional prevalence of P2RX4. Yet, several studies suggested P2RX4 actions controlling P2RX7 signaling[314-316], which could still indicate an involvement of both receptor isoforms and would not have been detected in the immediate time course of the Ca^{2+} transients monitored for assessing purinergic functionality. Distinguishing their roles in ATP-mediated signaling in HTPCs could simultaneously reveal mechanisms of cytokine induction since time-dependent regulation and differing expression amounts indicate involvement of more than one signaling pathway. Initiation of cytokine production, however, could not only be assigned to P2RX signaling, but also be influenced by cytokines themselves. *IL1B* and *IL6* transcript levels were increased shortly after ATP treatment of HTPCs. IL1β, for instance, holds the ability to trigger CCL2 and IL6 induction[508], but also prompts CCL7[509] or CXCL12[510] synthesis. In turn, IL6 can initiate CCL2 or CXCL5 production[511-514]. Hence, some of the observed alterations in transcript levels could simply be a by-product of ATP-induced IL1β or IL6 signaling giving a probable explanation for their time-dependence and different extent.

Smooth muscle cell factors and ECM synthesis are regarded as defining characteristics of the peritubular cell type[67,83,101,515]. Loss of contractile markers in HTPCs has been shown to connect to subfertile phenotypes[100]. Since ATP signaling in HTPCs is to mimic responses under pathologic conditions, the observed decline of smooth-muscle cell markers in response to ATP agrees with the proposed correlation with subfertile pathologies In line with the decrease of smooth muscle cell hallmarks is the link of P2RX4 to reduced smooth muscle actin expression in airway remodeling[457]. Additionally, P2RX4 was reported to influence actin cytoskeletal reorganization[516,517] and has been negatively related to smooth muscle actin as well as collagen production in kidney disease[518].
Collagens are at the core of ECM formation, while the other down-regulated ECM components IGFBP3, osteopontin and thrombospondin 1 do not primarily provide ECM structure but rather operate in the regulation of matrix-matrix and cell-matrix interactions.

IGFBP3 is known as an important modulator of IGF bioavailability in serum and tissues, but is expressed by smooth muscle cells as well[519]. In smooth muscle cells, it has been shown to prompt collagen production[520] and in turn, can be bound by collagen[521]. In reverse conclusion, decline in IGFBP3 levels could negatively impact collagen expression. IGFBP3 is further a direct binding partner to osteopontin and thrombospondin 1[522]. Osteopontin and thrombospondin 1 both, are matricellular proteins involved in cell-matrix communication and regulation of cellular functions[523,524]. Osteopontin, which is also expressed by smooth muscle cells[525], can be induced via P2RX4 signaling in stress conditions[526]. Moreover, osteopontin is an inducer of pro-inflammatory cytokine expression and mediator of inflammation[527], collagen deposition[528] and fibrosis[529,530]. These findings clearly contrast to the detected decrease in osteopontin after ATP treatment. However, most reports indicating pro-inflammatory osteopontin function were performed in immune cells, whereas studies conducted in human testis are not available. The diverse osteopontin expression pattern identified in the testes of other species indicates a complex regulation and function in spermatogenesis[531-534] and may thus point to an altogether different role of osteopontin in peritubular cells, which has yet to be uncovered. Thrombospondin 1, on the contrary, interacts not only with collagens[535], but is able to induce collagen deposition[536]. Lack of thrombospondin 1 leads to lung inflammation[524,537,538]. These results are perfectly in line with thrombospondin 1 decline simultaneously to collagen decrease and inflammatory factor induction in ATP-treated HTPCs.
Both, smooth muscle cell factors like smooth muscle actin and ECM molecules like collagens, lysyl oxidase or thrombospondin 1 are commonly up-regulated in tissue fibrosis[31]. ECM abundance is further associated with fibrotic tubule remodeling and has thus been described to be augmented in subfertile phenotypes[38]. Since up-regulated ECM production and secretion could not be found in ATP-treated HTPCs, it can only be deduced that in this case the *in vitro* results do not completely reflect the *in vivo* situation in infertile patients. In this respect, it can only be hypothesized that ATP signaling does not take part in fibrogenesis via ECM secretion and smooth muscle actin regulation in pathologic conditions. Still, fibrosis is a result of long-term inflammation[539] and therefore, the examined time range might not be sufficient to detect changes in ECM production. Further, cooperativity of peritubular cells with Sertoli cells has been described in regard to ECM synthesis[78] and might thus argue for the difference of *in vitro* and *in vivo* results.

The transiently affected factors, CXCL12 and GDNF are of special nature. Both have previously been identified to be secreted by HTPCs[101,102] and *in vivo* crucially contribute to spermatogonial stem cell maintenance[104,106,107]. CXCL12 and ATP have previously been suggested to synergistically guide stem cell recruitment[540]. Yet, the impact of ATP on their transcription level was short-lived and marginal (below twofold) and the secretion level of CXCL12 was found to remain unaltered by ATP.

On transcript level, time dependence of expression after ATP treatment was observed. In a shorter mode of action, ATP treatment induced immediate regulation of smooth muscle cell characteristics (*ACTA2*, *CNN1*), stem cell niche regulatory factors (*CXCL12*, *GDNF*), ECM

secretive properties (*COLs*, *LOX*, *SPP1*, *THBS1*) and a first wave of pro-inflammatory factors (*IL1B*, *IL6*, *CCL2*). Subsequently, the effect ceased except for *ACTA2*, *CNN1* and *IL1B* transcript levels, while a second wave of pro-inflammatory cytokines and chemokines (*IL33*, *CCL7*, *CXCL5*) was established, that obviously required prolonged ATP stimulation. The effects detected on transcript level basis were not necessarily reflected in cell lysates and accumulated amounts of protein in the supernatant. This may point to a discrepancy in the dynamics of transcript and protein synthesis that could not be mirrored in the experimental set-up. These differences could be due to transcript regulation, for instance via degradation, before translation. In case of cell lysate analysis, the mass spectrometric approach was designed to cover the maximum possible range of proteins. Hence, small proteins like cytokines and chemokines were hardly detected. In the supernatant, proteins corresponding to transcripts with highly altered relative levels remained below detection limit of the profiling assay or did apparently not become secreted more abundantly.

In conclusion, ATP acts as danger molecule in the testis by creating an inflammatory environment dependent on purinergic signaling through cytokine and chemokine production in HTPCs. Since ATP signaling exhibits a negative effect on contractile and ECM secreting properties of HTPCs, a direct connection to fibrogenesis as seen in subfertile pathologies could not be proven. With respect to basal receptor expression and transcript and secreted protein evaluation, variability of results is likely due to variation of HTPC donors. Donors cannot be recruited controlling factors such as age, genetic background and most importantly lifestyle and health status, which most certainly account for variation in HTPC responses to treatment. Yet, inflammation is a critical factor in infertility and further investigation will unravel underlying mechanisms to a greater extent.

Putative relevance of ATP break-down by ectonucleotidases into its metabolites ADP, AMP and adenosine is another point to be considered in future experiments. Ectonucleotidases CD39, which catalyzes ATP degradation to ADP/AMP[541], and CD73, which generates adenosine from AMP[542], are readily expressed in immune cells[275] including macrophages[543,544] and mast cells[545,546]. In addition, expression in the murine testis has been identified comprising peritubular cells as well as interstitial macrophages[547,548]. ATP metabolites ADP and adenosine are activators of the P2Y receptors and the P1 receptors, respectively[549]. Hence, ATP degradation could not only cease the observed ATP effects, but lead to pro-inflammatory signaling via P2RYs or anti-inflammatory signaling via P1 receptors[275]. Consequently, expression of ectonucleotidases in HTPCs, course of putative ATP degradation and (joint) activation and functional contribution of all purinergic receptors need to be assessed.

However, cytokines promote inflammation and are thus eminent in infertility. Cytokines are not only able to recruit immune cells to the testis, which amplify the immune response to a danger signal such as ATP[26]. They have been implicated in breaching the blood-testis barrier, inhibition of steroidogenesis, impairment of sperm integrity and germ cell apoptosis[27,30]. Consequently, cytokine levels, especially in the semen, have already been proposed as indicators of testicular health[550]. ATP-mediated cytokine production could thus be monitored as a first sign of testicular inflammation associated with infertility.

3.3 The NLRP3 inflammasome specifies a putative signaling pathway in testicular inflammation

Signaling via the NLRP3 inflammasome is a highly feasible mechanism in P2X receptor-mediated cytokine induction. In this work, the sensor component of the NLRP3 inflammasome, NLRP3, was discovered to be expressed in somatic cells of the testis of both, human and mouse.

In human samples, presence of NLRP3 was validated in Sertoli cells and peritubular cells by immunohistochemistry and transcript expression. Although an earlier study failed to detect NLRP3 expression in the testis[551], these results are in line with a more recent transcript analysis in the human testis[437]. Cooperativity between Sertoli cells and peritubular cells is well-established[78,79] and both substantially contribute to the blood-testis barrier[15,552]. Further, Sertoli cells as well as peritubular cells have been described to exhibit immunoregulatory properties[95,553], which may provide a link to the immune factor NLRP3. Samples from mixed atrophy (MA) patients were examined for the benefit of analyzing seminiferous tubules with normal and disturbed morphology in the same section. I found that NLRP3 abundance in MA samples was connected to Sertoli cells in germ cell-depleted tubules and peritubular cells in fibrotically thickened walls of degenerated tubules lacking Sertoli cells and spermatogenesis. These findings provided evidence for a putative association of testicular NLRP3 expression with subfertile pathologies. The NLRP3 inflammasome pathway has previously been described to be involved in collagen deposition and the development of fibrosis in various organs, whereas inhibition of NLRP3 reduced fibrogenesis[554-557]. Further inflammasome-independent NLRP3 is able to contribute to collagen production and fibrosis as evidenced in (cardiac) myofibroblasts[445]. Thus, NLRP3 could directly contribute to fibrotically thickened walls of seminiferous tubules, where it is pronouncedly expressed in MA patients and might provide a putative target for therapeutic interference to alleviate the MA phenotype.

In the mouse, I detected NLRP3 expression predominantly confined to Sertoli cells, being present already in the immature testes of new-born animals as well as in the adult mouse. NLRP3 expression in peritubular cells, unlike in the human, could not be confirmed. Yet, the possibility cannot readily be excluded since the peritubular layer in mouse is much slimmer than in human[515] and staining might therefore not be detectable using immunohistochemistry. These results correspond to a previous study of NLRP3 expression in primary immature Sertoli cells and an adult Sertoli cell line of the mouse. This report further encompassed NLRP3 inflammasome functionality *in vitro*, including IL1β production and thereby implicated the NLRP3 inflammasome in the development of inflammation-associated infertility[558].
In the inflammation-associated infertile *AROM*$^{+}$ mouse, testicular NLRP3 expression was found to be elevated and increased levels corresponded to the severity of the disease. Augmented NLRP3 expression in *AROM*$^{+}$ testes was reversed by aromatase inhibitor

treatment although WT levels were not entirely reestablished. These findings indicate NLRP3 elevation as a downstream effect of the hormonal imbalances due to aromatase overexpression that also lead to the inflammatory *AROM*$^+$ phenotype. Hence, NLRP3 expression in the mouse testis could participate in mechanisms fostering testicular inflammation.

In another sterile inflammation and infertility-related mouse model caused though testicular ischemia/reperfusion injury by testicular torsion[438], a state that can result in infertility if not treated appropriately[559,560], inhibition of NLRP3 signaling ameliorated testicular damage regarding disturbed morphology as well as pro-inflammatory interleukin production. Interference with P2RX7 activation resulted in the same phenotype, implying that the P2RX7/NLRP3 axis drives testicular inflammation under sterile conditions. NLRP3 activation has been reported in sterile injury of brain or lung as well[561,562] and similarly to the testicular study, endogenous ATP as danger signal elicited inflammation via P2RX7/NLRP3 signaling by directing neutrophils to the site of sterile hepatic injury[286]. These reports render an involvement of NLRP3 in sterile testicular inflammation in the *AROM*$^+$ line a very likely scenario. Yet, mechanistic action of NLRP3 in the *AROM*$^+$ testis remains to be unraveled.
This mechanistic ignorance applies to the human testis as well. Although expression of NLRP3 in peritubular cells was established *in vivo* and *in vitro*, I did not observe an increase of *NLRP3* transcript levels in ATP-treated compared to untreated HTPCs (not shown). Still, *IL1B* transcript levels were vigorously enhanced (Figure 2.16). This elicits the question, if ATP treatment is insufficient for NLRP3 activation or if *IL1B* elevation is mediated independently of the NLRP3 inflammasome in HTPCs. According to the generally accepted hypothesis stating that two independent hits of danger are necessary for NLRP3 inflammasome assembly, sole ATP treatment cannot suffice for NLRP3 inflammasome activation. Yet, there are reports of one-step inflammasome activation by stimuli that engage in ATP release simultaneously to the priming process[289,563-565]. ATP then provides the second hit by autocrine or paracrine signaling. Even though the possibility of ATP-triggered ATP release und thus, ATP acting as first and second hit, exists[566-569], ATP has neither been reported as priming stimulus nor as lone activator of the NLRP3 inflammasome. This argues for an inflammasome-independent mechanism of IL1β induction in ATP-treated HTPCs. ATP evoking production of IL1β in an NLRP3 inflammasome-independent manner has already been observed in cells of the myeloid lineage[507,570], but mechanistic steps still need to be resolved. Since *IL1B* transcription, but not IL1β secretion, was triggered in HTPCs, ATP may be solely involved in transcriptional activation in HTPCs. Nevertheless, adding the required priming stimulus before ATP treatment could alter the proposed mechanism completely in favor of an NLRP3-dependent event. Therefore, ATP actions regarding the molecular impact in HTPCs remain to be determined.

Prominent NLRP3 expression in subfertile, inflammatory conditions relates to Muckle-Wells syndrome (MWS), where constitutively active NLRP3 signaling provides an autoinflammatory milieu due to increased IL1β signaling throughout the body[323,402].

Subfertility is an issue reported in MWS patients[412,571]. Very few data are available and overall systematic assessment of subfertility cases is missing, but patients displayed oligozoospermia (reduced sperm count) due to decreased sperm concentration or low semen volume or suffered from azoospermia (no sperm count)[412]. Although the mechanism leading to infertility in MWS has not been clarified, excess IL1β production has been suggested[411,412], since IL1β has been shown to affect steroid synthesis and is associated with sperm pathology[27,572-574]. Treatment with IL1β inhibitors did improve clinical disease symptoms but had marginal effects regarding sperm counts[412,575]. The results led to the hypothesis that impairment of spermatogenesis in MWS patients may manifest and progress with age and that effective intervention may be achieved by earlier treatment, for instance before puberty[575]. Though, IL1 is considered critical to sperm maturation, at least in rodents, so that an optimal time window for treatment with IL1β inhibitors must be determined carefully to avoid unwanted side-effects[411].
However, case studies have to be expanded and systematic investigation is needed to provide insight to mechanistic details. A direct correlation of the gain-of-function mutations in the *NLRP3* gene to subfertility remains to be confirmed. Still, excess NLRP3 signaling appears to be associated with subfertile phenotypes as discovered in testicular sections of MA patients.

NLRP3 in the testis could further promote inflammasome-independent actions. A variety of alternative NLRP3 functions has been described, in particular in non-immune cells. In some cases, NLRP3 actions are of inflammatory nature[434,440], while especially in epithelial cells NLRP3 is involved in non-inflammatory processes. Maintenance of epithelial barriers has been suggested[441,442] and NLRP3 activity in murine Sertoli cells implicated NLRP3 in the regulation of claudins, which are critical components to the tight junctions participating to the blood-testis barrier. Hence, NLRP3 has been proposed to contribute to formation and maintenance of the blood-testis barrier[439]. Yet, the blood-testis barrier is established in parallel to spermatogenesis at the onset of puberty[576], whereas NLRP3 was constitutively expressed at different stages of sexual development in the mouse, i.e. before and after onset of sexual maturity. Together with the increased NLRP3 expression associated with inflammation and/or subfertility in mouse and human, this finding argues for two distinct roles of NLRP3 in the testis.
NLRP3 was constantly present in Sertoli cells throughout developmental stages and expression was independent of an inflammation-related phenotype, which indicates a non-inflammatory and therefore most likely inflammasome-independent function in the healthy testis. It is tempting to speculate on a non-inflammatory role of NLRP3 in testicular immunoregulation or testicular homeostasis, but there is currently no evidence suggesting either. However, under certain circumstances, which might be evoked by hormonal imbalances or release of endogenous DAMPs, the NLRP3 inflammasome in the testis could be activated and participate to inflammatory events via IL1β secretion and pro-fibrotic collagen deposition that eventually promote subfertile or infertile pathologies.

The results altogether confirm NLRP3 expression in somatic testicular cells of mouse and human and indicate involvement in non-inflammatory as well as inflammatory processes putatively leading to subfertile phenotypes. Despite promising initial observations, the investigation of NLRP3 actions in the testis has to be extended. It remains to be determined, if NLRP3 forms a functional inflammasome with ASC and caspase 1 that yields cytosolic ASC specks and induces IL1β release as well as pyroptotic cell death or if NLRP3 can contribute to testicular inflammation in an inflammasome-independent manner. HTPCs could be employed as an *in vitro* model to study these questions in terms of molecular mechanisms, the $AROM^{+}$ mouse line could serve as a model to place the discovered mechanistic actions into a systemic inflammatory and subfertile context. Regardless the efforts in elucidating testicular NLRP3 function, NLRP3 activation and signaling can solely provide one possible option in generating a cytokine and chemokine response in the testis and alternative pathways need to be considered as well.

4 Material and Methods

4.1 Material

4.1.1 Testicular tissue material

Human testicular tissue samples for immunohistochemistry and explant culture of HTPCs were obtained via collaborations with Prof. Dr. J.U. Schwarzer (Andrology Center, Munich, Germany) and Prof. Dr. F.-M. Köhn (Andrologicum, Munich, Germany). Samples for HTPC culture and immunohistochemistry stemmed from patients undergoing surgery to obtain tissue for TESE (testicular sperm extraction) or reconstructive surgery of the vas deferens. Thus, samples were derived from patients exhibiting normal spermatogenesis as well as patients suffering sub- or infertility symptoms. All patients granted informed consent for the scientific use of the material and the local ethical committee (Ethikkommission, TUM School of Medicine, Technical University of Munich, Munich, Germany, project number 5158/11 in terms of DFG MA 1080/23-1) approved the study. Experiments were performed in compliance with all relevant guidelines and regulations.

4.1.2 cDNA

cDNA	**Manufacturer**
Human testis	Primerdesign, Cambridge, UK
Human testis	Daniel Aigner, Anatomy III – Cell Biology, BMC, LMU, Munich, Germany

4.1.3 Cell culture media and supplements

Medium/Supplement	**Manufacturer**
CASYclean	Omni Life Sciences, Bremen, Germany
CASYton	Omni Life Sciences, Bremen, Germany
Dimethyl sulfoxide (DMSO)	Sigma-Aldrich, St. Louis, MO, USA
DMEM, high glucose	Gibco, Paisley, UK
DMEM, high glucose, no glutamine, no phenol red	Gibco, Paisley, UK
Dulbecco's PBS	Gibco, Paisley, UK
Fetal bovine serum (FBS)	Capricorn Scientific, Ebsdorfergrund, Germany
Glutamine (200 mM)	Gibco, Paisley, UK
Penicillin/streptomycin	Biochrom, Berlin, Germany
Trypsin/EDTA	Biochrom, Berlin, Germany

4.1.4 Antibodies

Antibody	**Dilution**	**Manufacturer**
Biotinylated goat anti mouse secondary antibody	IHC: 1:500	Jackson Immunosearch Laboratories, Newmarket, UK

Biotinylated goat anti rabbit secondary antibody	IHC: 1:500	Jackson Immunosearch Laboratories, Newmarket, UK
Monoclonal mouse anti-Mast Cell Tryptase antibody (M70529)	IHC: 1:300	Dako, Carpinteria, CA, USA
Monoclonal rabbit anti-P2RX7 IgG (GTX62830)	WB: 1:500	GeneTex/Biozol, Eching, Germany
Mouse IgG from serum	IHC: 1:5000, 1:10000	Sigma-Aldrich, St. Louis, MO, USA
Peroxidase (POX) conjugated goat anti rabbit secondary antibody	WB: 1:5000, 1:10000	Jackson Immunosearch Laboratories, Newmarket, UK
Polyclonal rabbit anti-BGN IgG (HPA003157)	IHC 1:500	Sigma-Aldrich, St. Louis, MO, USA
Polyclonal rabbit anti-NLRP3 IgG (R30750)	IHC: 1:500, 1:1000	NSJ Bioreagents, San Diego, CA, USA
Polyclonal rabbit anti-P2RX4 IgG (HPA039494)	IHC: 1:50 WB: 1:100	Atlas Antibodies, Stockholm, Sweden
Blocking peptide PrEST Antigen P2RX4	20x of antibody	Atlas Antibodies, Stockholm, Sweden
Polyclonal rabbit anti-P2RX7 IgG (HPA042013)	IHC: 1:50	Atlas Antibodies, Stockholm, Sweden
Rabbit IgG	IHC: 1:5000, 1:10000	Chemicon/ EMD Millipore, Temecula, CA, USA

4.1.5 Oligonucleotide primer

Gene	Reference ID	Nucleotide sequences	Amplicon size	Annealing temperature
Bgn	NM_007542.4	5′-GAC AAC CGT ATC CGC AAA GT-3′ 5′-CAA AGG CTC CTG GTT CAA AG-3′	115 bp	60°C
Ccl2	NM_011333.3	5’-GGC TCA GCC AGA TGC AGT TAA-3’ 5’-CCA GCC TAC TCA TTG GGA TCA-3’	80 bp	60°C
Cd68	NM_001291058.1	5′-CCA GCT GTT CAC CTT GAC CT-3′ 5′-AGA GGG GCT GGT AGG TTG AT-3′	208 bp	60°C
Cyp17a1	NM_007809.3	5′-CAA GCC AAG ATG AAT GCA GA-3′ 5′-AGG ATT GTG CAC CAG GAA AG-3′	165 bp	59°C
Dcn	NM_001190451.1	5′-TGA GCT TCA ACA GCA TCA CC-3′ 5′-AAG TCA TTT TGC CCA ACT GC-3′	181 bp	60°C
Ddx4	NM_001145885.1	5′-CCA AGC GAG GTG GCT GCC AAG ATG-3′ 5′-AGA ACC AAA AAG GCC ACC ACC ACG-3′	170 bp	60°C
Fgfr3	NM_008010.5	5′-ATG ACG AAG ATG GGG AGG ACG-3′ 5′-CAG CGG AAG CGG ACA GTG TT-3′	118 bp	58°C
Hprt	NM_013556.2	5′-CTG GTG AAA AGG ACC TCT CGA A-3′ 5′-CTG AAG TCA TCA TTA TAG TCA AGG GCA T-3′	110 bp	60°C
Il1b	NM_008361.3	5′-TGA AGT TGA CGG ACC CCA AA-3′ 5′-TGA TGT GCT GCT GCG AGA TT-3′	101 bp	60°C
Il6	NM_031168.1	5′-GTT CTC TGG GAA ATC GTG GAA A-3′ 5′-AAG TGC ATC ATC GTT GTT CAT ACA-3′	78 bp	60°C
Nlrp3	NM_145827.3	5′-TCT CCA CAA TTC TGA CCC ACA-3′	144 bp	60°C

		5′-ACA TTT CAC CCA ACT GTA GGC-3′		
P2rx4	NM_011026.2	5′-GAC CAA CAC TTC TCA GCT TGG-3′ 5′-GTG ACG ATC ATG TTG GTC ATG-3′	105 bp	60°C
P2rx7	NM_011027.3	5′-TTA TGG CAC CGT CAA GTG G-3′ 5′-TCT CCG TCA CCT CTG CTA TG-3′	146 bp	60°C
Ppia	NM_008907.1	5′-CATCCTAAAGCATACAGGTCCTG-3′ 5′-TCCATGGCTTCCACAATG-3′	165 bp	60°C
Ptx3	NM_008987.3	5′-TAG TGT TGG TGG TGG GTG GA-3′ 5′-CAT GCT CCC CTG CTC TGA AC-3′	110 bp	60°C
Rpl19	NM_009078.2	5′-CTG AAG GTC AAA GGG AAT GTG-3′ 5′-GGA CAG AGT CTT GAT GAT CTC-3′	195 bp	60°C
Tlr2	NM_011905.3	5′-CTC CCA CTT CAG GCT CTT TG-3′ 5′-TTA TCT TGC GCA GTT TGC AG-3′	110 bp	60°C
Tlr4	NM_021297.2	5′-GGA CTG GGT GAG AAA TGA GC-3′ 5′-AGC CTT CCT GGA TGA TGT TG-3′	125 bp	60°C
Tnfa	NM_013693.3	5’-CAC AGA AAG CAT GAT CCG CG-3’ 5’-TGA TGA GAG GGA GGC CAT TTG-3’	209 bp	59°C

Gene	**Reference ID**	**Nucleotide sequences**	**Amplicon size**	**Annealing temperature**
ACTA2	NM_001613.2	5’-ACA ATG AGC TTC GTG TTG CC-3’ 5’-GAG TCA TTT TCT CCC GGT TGG-3’	90 bp	59°C
CCL2	NM_002982.3	5’-CAG CCA GAT GCA ATC AAT GCC-3’ 5’-TGG AAT CCT GAA CCC ACT TCT-3’	190 bp	58°C
CCL7	NM_006273.3	5′-TGG AGA GCT ACA GAA GGA CCA-3′ 5′-GTG GGG TCA GCA CAG ATC TC-3′	94 bp	58°C
CNN1	NM_001299.5	5′-CGA AGA CGA AAG GAA ACA AGG T-3′ 5′-GCT TGG GGT CGT AGA GGT G-3′	186 bp	62°C
COL1A1	NM_000088.3	5′-AAG AGG AAG GCC AAG TCG AG-3′ 5′-CAC ACG TCT CGG TCA TGG TA-3′	91 bp	60°C
COL1A2	NM_000089.3	5′-CCG GAG ATA GAG GAC CAC GT-3′ 5′-CAG CAA AGT TCC CAC CGA GA-3′	132 bp	60°C
COL3A1	NM_000090.3	5′-GGT GGT TTT CAG TTT AGC TAC GG-3′ 5′-TGA TGT TCT GGG AAG CTC GG-3′	106 bp	59°C
COL4A2	NM_001846.3	5′-AAG GAA TCA TGG GCT TTC CT-3′ 5′-CTC TGG CAC CTT TTG CTA GG-3′	204 bp	60°C
COL6A2	NM_001849.3	5′-GTC ATG AAA CAC GAA GCC TAC G-3′ 5′-CAC CCT TCT GTC CAC GGT AG-3′	97 bp	59°C
CXCL12	NM_000609.6	5′-TCA GCC TGA GCT ACA GAT GC-3′ 5′-CTT TAG CTT CGG GTC AAT GC-3′	161 bp	60°C
CXCL5	NM_002994.4	5′-CAG CGC TCT CTT GAC CAC TA-3′ 5′-GAA CTC CTT GCG TGG TCT GT-3′	194 bp	60°C
GDNF	NM_000514.3	5′-GCA GAC CCA TCG CCT TTG AT-3′ 5′-ATC CAC ACC TTT TAG CGG AAT G-3′	93 bp	60°C
HPRT	NM_000194.2	5′-CCT GGC GTC GTG ATT AGT GA-3′ 5′-GGC CTC CCA TCT CCT TCA TC-3′	163 bp	60°C
IGFBP3	NM_001013398.1	5’-ACA GCC AGC GCT ACA AAG TT-3’ 5’-CTA CGG CAG GGA CCA TAT TC-3’	100 bp	59°C
IL1B	NM_000576.2	5′-CTT GGT GAT GTC TGG TCC ATA TG-3′ 5′-GGC CAC AGG TAT TTT GTC ATT AC-3′	127 bp	60°C
IL33	NM_001199641.1	5′-AGG TGA CGG TGT TGA TGG TAA-3′	142 bp	60°C

		5′-AAG GAC AAA GAA GGC CTG GT-3′		
IL6	NM_000600.4	5′-AAC CTG AAC CTT CCA AAG ATG G-3′ 5′-TCT GGC TTG TTC CTC ACT ACT-3′	159 bp	60°C
LOX	NM_001317073.1	5′-CAC ACA CAC AGG GAT TGA GTC-3′ 5′-AGT CAG ATT CAG GAA CCA GGT-3′	147 bp	60°C
NLRP3	NM_004895.4	5′-GTG TTT CGA ATC CCA CTG TG-3’ 5′-TCT GCT TCT CAC GTA CTT TCT G-3’	143 bp	59°C
P2RX1	NM_002558.3	5′-CTG GGA TGT GGC TGA CTA CG-3′ 5′-AAG TTC TCG GCC TCT CGG A-3′	303 bp	60°C
P2RX2	NM_001282164.1	5′-GCC TCT GTC AGC CAA TTT CTG-3′ 5′-TCT CCA CGA TAA AGC CCA GC-3′	196 bp	60°C
P2RX3	NM_002559.3	5′-TCC CCA GGC TAC AAC TTC AG-3′ 5′-TTG AAC TTG CCA GCA TTC CC-3′	128 bp	60°C
P2RX4	NM_001256796.1	5′-AGA TGC GAC CAC TGT GTG TA-3′ 5′-GTT GAG ACT CCG TTG CTG TG-3′	78 bp	60°C
P2RX5	NM_175080.2	5′-GTC AGA AGG GGA ACG GAT CT-3′ 5′-GCA ATT CAC GTG CTC CTG T-3′	64 bp	60°C
P2RX6	NM_005446.3	5′-TGA GAT CTG GAG TTG GTG CC-3′ 5′-ATT GTG GTT CAT AGC GGC AG-3′	188 bp	60°C
P2RX7	NM_002562.5	5′-TGT CCC ATT TTC CGA CTA GG-3′ 5′-CCA ACG GTC TAG GTT GCA GT-3′	120 bp	60°C
P2RY1	NM_002563.4	5′-AGT TTT ACT ACC TGC CGG CT-3′ 5′-CAG CAC GTA CAA GAA GTC GG-3′	158 bp	60°C
P2RY2	NM_176072.2	5′-ATC AAT GGC ACC TGG GAT GG-3′ 5′-ACG CAT TCC AGG TCT TGA GG-3′	169 bp	60°C
P2RY4	NM_002565.3	5′-CGT GCC CAA CCT GTT CTT TG-3′ 5′-GCA AAC AAG AGT GAC CAG GC-3′	157 bp	60°C
P2RY6	NM_176797.2	5′-CCG CGA GAAC TTC AAG CAA C-3′ 5′-AAG GGC CAG TGA TCA CCT TG-3′	222 bp	60°C
P2RY11	NM_001198690.1	5′-GCG GCC TAC AGA GCG TAT AG-3′ 5′-GCA CAT AGG AGC TGG CGT AG-3′	190 bp	60°C
P2RY12	NM_022788.4	5′-GCA GCC GAG AGA CAA GAA TG-3′ 5′-GGG GAC TTT ACC TAC ACC CC-3′	196 bp	60°C
P2RY13	NM_176894.2	5′-ACT GCC GCC ATA AGA AGA CA-3′ 5′-GCA CCG CTC AGA TCT GTT GA-3′	105 bp	60°C
P2RY14	NM_001081455.1	5′-AAA CGC TCA CTG GGC AAA AC-3′ 5′-GAG GCT GTG TGG AGG TTG AA-3′	120 bp	60°C
RPL19	NM_000981.3	5′-AGG CAC ATG GGC ATA GGT AA-3′ 5′-CCA TGA GAA TCC GCT TGT TT-3′	199 bp	60°C
SPP1	NM_001040058.1	5′-TTT TCA CTC CAG TTG TCC CC-3′ 5′-TAC TGG ATG TCA GGT CTG CG-3′	109 bp	59°C
THBS1	NM_003246.3	5′-AGT CGT CTC TGC AAC AAC CC-3′ 5′-AGC TAG TAC ACT TCA CGC CG-3′	148 bp	60°C

All oligonucleotides, including the random 15mer oligonucleotides for cDNA synthesis, were synthesized by Metabion (Planegg, Germany).

4.1.6 Chemicals

Chemical	Manufacturer
2′(3′)-O-(4-Benzoylbenzoyl)adenosine 5′-triphosphate (BzATP)	Sigma-Aldrich, St. Louis, MO, USA
3-[1-[[(3'-Nitro[1,1'-biphenyl]-4-yl)oxy]methyl]-3-(4-pyridinyl)propyl]-2,4-thiazolidinedione (AZ11645373)	Tocris, Bio-Techne, Wiesbaden-Nordenstadt, Germany
Acetic acid	Merck, Darmstadt, Germany
Acrylamide	AppliChem, Darmstadt, Germany
Adenosine triphosphate (ATP)	Sigma-Aldrich, St. Louis, MO, USA
Agarose	Biozym, Hessisch Oldendorf, Germany
Albumin standard	Pierce, Thermo Fischer Scientific, Waltham, MA, USA
Ammonium persulfate (APS)	Merck, Darmstadt, Germany
Boric acid	Roth, Karlsruhe, Germany
Bovine serum albumin (BSA)	Sigma-Aldrich, St. Louis, MO, USA
Bromophenol blue	Serva, Heidelberg, Germany
Citric acid monohydrate	Roth, Karlsruhe, Germany
dNTPs (dATP/dCTP/dGTP/dTTP)	Qiagen, Hilden, Germany
EDTA	Roth, Karlsruhe, Germany
Entellan	Merck, Darmstadt, Germany
Ethanol, absolute	AppliChem, Darmstadt, Germany
Ethanol/Walkol	Waldeck, Münster, Germany
Finrozole	Vetcare, Helsinki, Finland
Fluo4-AM	Molecular Probes, Eugene, OR, Germany
Fluoforte	Enzo Life Sciences, Lausen, Switzerland
Formaldehyde (37%), acid-free	Roth, Karlsruhe, Germany
Glycerol	Merck, Darmstadt, Germany
Glycine	AppliChem, Darmstadt, Germany
H_2O_2 (30%)	Sigma-Aldrich, St. Louis, MO, USA
Glycoblue Coprecipitant	Invitrogen, Life Technologies, Carlsbad, CA, USA
Hemalum solution acid	Roth, Karlsruhe, Germany
Hydrochloric acid	Roth, Karlsruhe, Germany
Isopropanol	Roth, Karlsruhe, Germany
Methanol	Roth, Karlsruhe, Germany
MidoriGreen Advance DNA Stain	Nippon Genetics, Düren, Germany
Milk powder	Vitalia, Bruckmühl, Germany
N,N,N’,N’-Tetramethylethylenediamine (TEMED)	Bio-Rad, Hercules, CA, USA
Normal goat serum	Sigma-Aldrich, St. Louis, MO, USA
Normal mouse serum	Dianova, Hamburg, Germany
Normal rabbit serum	Chemicon/ EMD Millipore, Temecula, CA, USA
Nuclease eliminator	Amresco, Solon, OH, USA
Nuclease free water	Ambion, Austin, TX, USA

PBS Dulbecco	Biochrom, Berlin, Germany
pH calibration standard pH 4/7/10	Roth, Karlsruhe, Germany
Picric acid	AppliChem, Darmstadt, Germany
Piperazine-N,N′-bis(2-ethanesulfonic acid) (PIPES)	Roth, Karlsruhe, Germany
Ponceau S	Sigma-Aldrich, St. Louis, MO, USA
Protease and Phosphatase Inhibitor Tablets	Pierce, Thermo Fischer Scientific, Waltham, MA, USA
RNase free water	Qiagen, Hilden, Germany
RNasin Plus	Promega, Madison, WI, USA
Sodium acetate (NaAc)	Roth, Karlsruhe, Germany
Sodium chloride (NaCl)	Roth, Karlsruhe, Germany
Sodium deoxycholate, DOC	Roth, Karlsruhe, Germany
Sodium dodecyl sulfate (SDS)	Roth, Karlsruhe, Germany
Sodium(II) citrate dihydrate	Roth, Karlsruhe, Germany
Sucrose	Merck, Darmstadt, Germany
Tris	Roth, Karlsruhe, Germany
TRIsure	Bioline reagents Ltd., London, UK
Triton X 100	Roth, Karlsruhe, Germany
Tween 20	Roth, Karlsruhe, Germany
Xylol	Roth, Karlsruhe, Germany
β-Mercaptoethanol	Sigma-Aldrich, St. Louis, MO, USA

4.1.7 Buffers and solutions

Buffer	**Composition**
100x Ponceau S	2% (w/v) Ponceau S 1% (v/v) Acetic acid
10x Laemmli buffer	0.25 M Tris 1.92 M Glycine 1% (w/v) SDS
10x TBE	0.9 M Tris 0.9 M Boric acid 0.2 M EDTA pH 8.0
10x Transfer buffer	0.25 M Tris 1.92 M Glycine pH 8.3
1x Transfer buffer	10% (v/v) 10x Transfer buffer 10% (v/v) methanol
20x TBST	2 M NaCl 0.08 M Tris 1% (v/v) Tween 20 pH 7.5
4x Separating gel buffer	1.5 M Tris 0.01 M EDTA 0.4% (w/v) SDS

	pH 8.8
4x Stacking gel buffer	0.5 M Tris 0.01 M EDTA 0.4% (w/v) SDS pH 6.8
APS (10%)	10% (w/v) APS in ddH_2O
Bouin's solution	0.9% (v/v) Picric acid 9% (v/v) Formaldehyde 5% (v/v) Acetic acid
Bromophenol blue	0.1 M Tris 24% (v/v) Glycerol 5% (w/v) SDS Traces of Bromophenol blue pH 6.8
Citrate buffer	1.8 mM Citric acid 8.2 mM Sodium(II) citrate pH 6.0
NPE buffer	0.15 M NaCl 10 mM PIPES 1 mM EDTA pH 7.2
PBS	9.55 g PBS Dulbecco in 1 L dH_2O pH 7.5
Protease and Phosphatase inhibitor cocktail	1 Inhibitor tablet in 10 mL Sample buffer
RIPA buffer	0.15 M NaCl 50 mM Tris 0.5% (w/v) Sodium deoxycholate 0.1% (w/v) SDS 1% (v/v) Triton X 100 pH 8.0
Sample buffer for protein lysates	62.5 mM Tris 0.3 M Sucrose 2% (w/v) SDS pH 6.8
Tris/HCl (50 mM)	50 mM Tris 40 mM HCl pH 7.6

4.1.8 Kits, molecular-weight size markers and assays

Kit	**Manufacturer**
BCA Protein Assay Kit	Pierce, Thermo Scientific, Rockford, IL, USA
DC Protein Assay Kit	Bio-Rad, Hercules, CA, USA
DNase I Amplification Grade Kit	Invitrogen, Life Technologies, Carlsbad, CA, USA
GeneRuler Low Range DNA Ladder	Thermo Scientific, Rockford, IL, USA

LDH Cytotoxicity Assay Kit	Pierce, Thermo Scientific, Rockford, IL, USA
Loading dye (6x)	Thermo Scientific, Rockford, IL, USA
PageRuler Plus Prestained Protein Ladder	Thermo Scientific, Rockford, IL, USA
Protease and Phosphatase Inhibitor Tablets	Pierce, Thermo Scientific, Rockford, IL, USA
Proteome Profiler Human XL Cytokine Array Kit	R&D Systems, Minneapolis, MN, USA
QuantiFast SYBR Green PCR Kit	Qiagen, Hilden, Germany
RNeasy Plus Micro Kit	Qiagen, Hilden, Germany
SensiFAST cDNA Synthesis Kit	Bioline reagents Ltd., London, UK
SIGMA*FAST* 3,3'-Diaminobenzidine (DAB) tablets	Sigma-Aldrich, St Louis, MO, USA
SuperScript II Reverse Transcriptase Kit	Invitrogen, Life Technologies, Carlsbad, CA, USA
SuperSignal West Femto Maximum Sensitivity Substrate	Pierce, Thermo Scientific, Rockford, IL, USA
Vectastain ABC Kit	Vector Laboratories, Burlingame, CA, USA
Wizard SV Gel and PCR Clean-Up System	Promega, Madison, WI, USA

4.1.9 Equipment

Equipment	**Manufacturer**
-20°C freezer	Liebherr, Bulle, Switzerland
-80°C freezer Herafreeze HFU	Thermo Fisher Scientific, Rockford, IL, USA
4°C fridge	Liebherr, Bulle, Switzerland
Analytical balance DualRange XS 205	Mettler-Toledo, Greifensee, Switzerland
Bio-Rad gel Doc XR$^+$	Bio-Rad, Hercules, CA, USA
Camera 18.2 Color Mosaik	Visitron Systems, Puchheim, Germany
Camera ProgRes MF cool	Jenoptik, Jena, Germany
CASY TT Cell Counter and Analyser System	Schärfe System, Reutlingen, Germany
Centrifuge 5418	Eppendorf, Hamburg, Germany
Centrifuge Microfuge 1-14	Sigma, Osterode am Harz, Germany
Centrifuge Multifuge X3	Heraeus, Hanau, Germany
Chemi Smart 5000	PeqLab, Erlangen, Germany
CoolCell Cell Freezing Container	BioCision, San Rafael, CA, USA
Cooling centrifuge Biofuge Fresco	Heraeus, Hanau, Germany
Drying oven	Heraeus, Hanau, Germany
Electric stirrer Multipoint HP15	Variomag, Daytona Beach, FL, USA
FastGene GelPic LED Box	Nippon Genetics, Düren, Germany
Gel chambers, gel combs, gel slides	Bio-Rad, Hercules, CA, USA
Glass plates, combs, casting stand	Bio-Rad, Hercules, CA, USA
ibidi Gas Incubation System	ibidi, Planegg, Germany
ibidi Heating System	ibidi, Planegg, Germany
Ice maker Scotsman MF46	Scotsman Ice Systems, Ipswich, UK
IKA magnetic stirrer RCT	IKA-Werke, Staufen, Germany
IKA microtiter shaker MTS4	IKA-Werke, Staufen, Germany
IKA minishaker MS 2	IKA-Werke, Staufen, Germany
Incubation/Inactivation water bath 1003	GFL, Burgwedel, Germany

Incubator Galaxy 170 S	New Brunswick/Eppendorf, Hamburg, Germany
Leica DM2500 microscope	Leica Microsystems, Wetzlar, Germany
Leica DMC2900 CMOS Sensor camera	Leica Microsystems, Wetzlar, Germany
Leica DMIL LED	Leica Microsystems, Wetzlar, Germany
Light Cycler 96 System	Roche, Basel, Switzerland
Membrane vacuum pump N86KN.18	KNF Neuberger, Freiburg, Germany
Membrane vacuum pump PC 3004 vario	Vacuubrand, Wertheim, Germany
Microplate Reader Fluostar Optima	BMG Labtech, Ortenberg, Germany
Microtome Leica SM2000R	Leica Microsystems, Wetzlar, Germany
Microwave M690	Miele, Gütersloh, Germany
Microwave Tender Cooker	Nordic Ware, Minneapolis, MN, USA
Mini-PROTEAN3 Cell System	Bio-Rad, Hercules, CA, USA
Multichannel pipette 20-200 µL	Rainin, Greifensee, Switzerland
Multipipette Plus	Eppendorf, Hamburg, Germany
Nanodrop 2000c Spectrophotometer	Thermo Scientific, Rockford, IL, USA
Peristaltic pump	Chromapor, Duisburg, Germany
pH meter FE20/EL20	Mettler-Toledo, Greifensee, Switzerland
Pipette 5000 µL	Gilson, Middleton, WI, USA
Pipettes 2/10/20/100/200/1000 µL	Eppendorf, Hamburg, Germany
Pipetus	Hirschmann Laborgeräte, Eberstadt, Germany
Power Pac 300	Bio-Rad, Hercules, CA, USA
Precision Balance BP 310 S	Sartorius, Göttingen, Germany
Shaker Duomax 1030/2030	Heidolph, Schwabach, Germany
Sprout minicentrifuge	Biozym, Hessisch Oldendorf, Germany
Sterile workbench FlowSafe B-[MaxPro]²-160	Berner, Elmshorn, Germany
Sub Cell GT Agarose Gel System	Bio-Rad, Hercules, CA, USA
Thermocycler PTC 200	Bio-Rad, Hercules, CA, USA
TissueLyser LT	Qiagen, Hilden, Germany
Ultra Turrax T25	IKA-Werke, Staufen, Germany
Ultrasound processor 50H	Hielscher Ultrasonics, Teltow, Germany
VacuuHandControl VHCpro	Vacuubrand, Wertheim, Germany
Vortex Genie 2	Scientific Industries, Bohemia, NY, USA
Zeiss Z1 Axio Observer	Carl Zeiss Microscopy, Jena, Germany
Zeiss Axioplan 2	Carl Zeiss Microscopy, Jena, Germany
Zeiss Axiovert 135	Carl Zeiss Microscopy, Jena, Germany
Zeiss Axiovert 200M	Carl Zeiss Microscopy, Jena, Germany
Zeiss Colibri.2 System	Carl Zeiss Microscopy, Jena, Germany
Zeiss LSM 5 Laser Module	Carl Zeiss Microscopy, Jena, Germany

4.1.10 Consumables

Consumable	**Manufacturer**
0.9 mm needle Sterican	B. Braun, Melsungen, Germany
10 mL syringe Luer solo	B. Braun, Melsungen, Germany
24/48/96 Well Culture Plate	Nunc, Thermo Scientific, Rockford, IL, USA
BZO Seal Film	Biozym, Hessisch Oldendorf, Germany

CASY cups	Omni Life Sciences, Bremen Germany
Cell scraper	Kisker, Steinfurt, Germany
Combitips advanced 2.5/5 mL	Eppendorf, Hamburg, Germany
Cryotube vials (2 mL)	Thermo Scientific, Rockford, IL, USA
Disposable scalpel stainless steel	Teqler, Netmed, Wasserbillig, Luxembourg
Filter pipette tips (10/20/200/1250 µL)	StarLab, Hamburg, Germany
Nitrocellulose membrane	Machery & Nagel, Düren, Germany
Parafilm	American National Can, Chicago, IL, USA
Pasteur-plast pipettes	Ratiolab, Dreieich, Germany
PCR 96 Well TW-MT plate white	Biozym, Hessisch Oldendorf, Germany
PD tips 0.5 mL	Brand, Wertheim, Germany
Perfusor tube Luer lock	B. Braun, Melsungen, Germany
Pipette tips (10/ 200/1000/5000 µL)	Biozym, Hessisch Oldendorf, Germany
Reaction tubes (0.2/0.5/1.5/2.0 mL)	Sarstedt, Nürnbrecht, Germany
Reagent Reservoirs (25 mL)	VWR, Darmstadt, Germany
Sempercare nitrile gloves	Semperit, Vienna, Austria
Serological pipettes (1/5/10/25/50 mL)	Sarstedt, Nürnbrecht, Germany
Soy-free natural ingredient food pellets	Special Diets Services, Witham, UK
Syringe filter Filtropur S 0.2 µm	Sarstedt, Nürnbrecht, Germany
Superfrost Plus Microscope Slides	Menzel Gläser, Braunschweig, Germany
TC Dish 35/60	Sarstedt, Nürnbrecht, Germany
Tubes (13 mL)	Sarstedt, Nürnbrecht, Germany
Tubes (15 mL, 50 mL)	Greiner Bio-One, Frickenhausen, Germany
Urine cups	Sarstedt, Nürnbrecht, Germany
Whatman gel blot paper GB003	Whatman, GE Healthcare, Maidstone, UK
µ-Dish (35 mm ∅, glass bottom)	ibidi, Planegg, Germany

4.1.11 Software and web-based tools

Software	**Origin**
AIM v.4.2	Carl Zeiss Microscopy, Jena, Germany
Basic Local Alignment Search Tool (BLAST)	http://blast.ncbi.nlm.nih.gov/
ChemiCapt v.11.10	Vilber Lourmat, Marne-la-Vallée, France
Fiji – ImageJ v.2.0.0	https://fiji.sc/
FinchTV v.1.5.0	Geospiza Inc., PerkinElmer, Seattle, WA, USA
Graphpad Prism v.6.0	GraphPad Software Inc., San Diego, CA, USA
ImageLab v.5.2.1	Bio-Rad, Hercules, CA, USA
LAS v.4.6	Leica Microsystems, Wetzlar, Germany
LAS X v.1.9	Leica Microsystems, Wetzlar, Germany
Nanodrop 2000/2000c v.1.4.2	Thermo Scientific, Rockford, IL, USA
PHANTAST plugin for Fiji	https://github.com/nicjac/PHANTAST-FIJI/releases
Primer3 v.4.0.0	http://primer3.ut.ee/
ProgRes CapturePro v.2.9.0.1	Jenoptik, Jena, Germany
SerialCloner v.2.6.1	http://serialbasics.free.fr/Serial_Cloner
SPOT advanced software v.4.6	SPOT Imaging Solutions, Sterling Heights, MI, USA

STRING v.10.0	http://string-db.org
SWISS-MODEL	https://swissmodel.expasy.org/
ZEN v.2	Carl Zeiss Microscopy, Jena, Germany

4.2 Methods

4.2.1 Mouse model generation and analyses

Mouse models were generated in collaboration with the Institute of Biomedicine and Turku Center for Disease Modeling at the University of Turku, Finland. All animals were bred and housed in specific pathogen-free conditions with automatic light control (twelve hours light, twelve hours darkness) and temperature (21 ± 1°C) in specified pathogen-free conditions at the Central Animal Laboratory of the University of Turku under a license by the Finnish Animal Ethics Committee also complying to the institutional animal care policies of the University of Turku. Littermates were housed together in the same cage, one to six animals per cage. The mice had unrestricted access to soy-free natural ingredient food pellets and tap water.

The *AROM*$^+$ transgenic mouse was employed as a systemic model of male infertility. This mouse line expresses human P450 aromatase under control of the ubiquitin C promoter[111-113]. Testes from two, three and five months old animals of this mouse line and age-matching wild type (WT) animals were used for immunohistochemistry and qRT-PCR studies. To link discovered changes between *AROM*$^+$ and WT mice to the aromatase overexpression, four weeks old age-matched *AROM*$^+$ and WT mice were divided in two subgroups and treated with the aromatase inhibitor (AI) Finrozole (daily with dose of 10 mg per kg of body weight by gavage in 0.2 ml of vehicle) and a placebo as control for six weeks, respectively (Aguilar-Pimentel *et al.*, unpublished). Testes from these 2.5 months old mice were used for immunohistochemistry and qRT-PCR experiments.

To assess the impact of biglycan (*Bgn,* located on the X chromosome) deficiency in *AROM*$^+$ mice, the *AROM*$^+$ mouse line (FVB/N background) was bred to a *Bgn* knock-out line (*Bgn*$^{-/0}$, obtained from Dr. Marian Young, NIH NIDCR, Bethesda, MD, USA; C57BL6 background) for two generations to obtain F2 males of all desired genotypes. The exact breeding scheme is displayed in Figure 4.1.

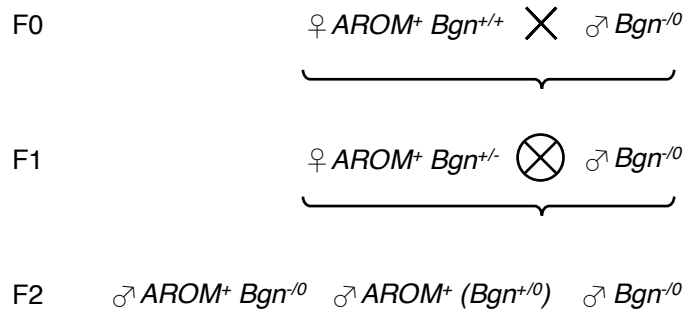

Figure 4.1 Breeding scheme for *AROM*$^+$ x *Bgn*$^{-/0}$

In the F0 generation female *AROM*$^+$ mice (FVB/N background) were bred to male *Bgn*$^{-/0}$ mice (C57BL6 background). From this crossing's offspring (F1 generation) female *AROM*$^+$ *Bgn*$^{+/-}$ mice were bred to male *Bgn*$^{-/0}$ mice to obtain equal numbers for the four genotypes to be investigated in male offspring (F2 generation): *AROM*$^+$ *Bgn*$^{-/0}$, *AROM*$^+$ (*Bgn*$^{+/0}$), *Bgn*$^{-/0}$ and *WT* (*Bgn*$^{+/0}$).

Mice were genotyped by PCR with primer pairs for wild type (WT) (forward 5'-CAG GAA CAT TGA CCA TG-3' and reverse 5'-GAA AGG ACA CAT GGC ACT GAA G-3') and mutated allele (forward as in WT and reverse 5'-TGG ATG TGG AAT GTG TGC GAG G-3') at the University of Turku. Male F2 offspring was subdivided into four groups by genotype and analyzed at four and ten months of age. Animals were weighed before euthanasia, then testes were collected. Testicular weights were determined additionally. One testicle was frozen in liquid nitrogen for RNA and protein isolation, the other testicle was fixed in Bouin's solution. Of the ten months old offspring, testicular steroid levels were determined at the Sahlgrenska Academy, Centre for Bone and Arthritis Research, University of Gothenburg using the gas chromatography tandem mass spectrometry method[577]. Therefore, testicular protein was isolated and measured using the BCA Protein Assay Kit at the University of Turku. Comparable steroid levels were calculated by total steroid mass per tissue mass analyzed.

As means of quantifying altered testicular structure and morphology, mean seminiferous tubule diameters were determined for individual animals. Length of longitudinal and perpendicular axis of each tubular cross section were measured and the diameter calculated by dividing their sum by two. For each mouse tubular diameters were averaged. Body weights and testis weights per body weights as well as tubular diameters of different genotypes were compared using a one-way ANOVA with Tukey's post-test to correct for multiple comparisons (statistical significance $p < 0.05$).

4.2.2 Immunohistochemistry

Tissue samples from human or mouse testis were fixed in Bouin's solution for 24 h, then transferred to 70% EtOH. EtOH was changed daily until the solution remained colorless. Samples were embedded in paraffin, sectioned at a layer thickness of 5 µm and mounted on glass slides. Sections were de-paraffinized by 2x xylol and an EtOH series (2x 100%, 90%, 80%, 70%, 3 min each) and rehydrated in PBS (10 min). Demasking of antigens was performed by boiling the sections in citrate buffer followed by a slow cool-down. All further incubation steps before DAB staining were performed in a humid chamber. Sections were washed with PBS (2x for 5 min), then the endogenous peroxidase activity was inhibited using 3% hydrogen peroxide / 9% methanol in PBS for 30 min. Sections were washed with PBS (3x for 5 min), then incubated with 5% or 10% normal goat serum in PBS for 30 min to block unspecific antibody binding. Primary antibody diluted in 5% or 10% normal goat serum in PBS applied over night at 4°C. Sections were washed with PBS (3x for 5 min), then the secondary antibody diluted in 5% or 10% normal goat serum in PBS was applied for 2 h. Subsequently, sections were treated with an avidin-biotin-peroxidase complex (ABC reagent)[578] for 2 h before washing with PBS (3x for 5 min). Sections were incubated with Tris/HCl for 10 min. Staining was performed by applying the chromogen DAB for 10 min at most. The reaction was stopped in dH_2O and sections were counterstained in a hematoxylin solution, then washed in tap H_2O. Sections were de-hydrated in an ascending EtOH series (70%, 80%, 90%, 2x 100%, 3 min each) and xylol (2x for 5 min). Sections were mounted using entellan and dried over night.

Negative controls consisted of pre-adsorbed primary antibody or host-specific non-immune serum (1:5000, 1:10000) diluted in 5% or 10% normal goat serum in PBS instead of primary antibody or primary antibody was omitted completely. For pre-adsorption control, diluted primary antibody was incubated with a 20-fold excess concentration of complementary blocking peptide for 2-4 h in a shaker (300 rpm, 20°C). The mixture was centrifuged for 10 min at 13,000 rpm and the supernatant was used instead of primary antibody.

4.2.3 Peritubular cell culture

HTPCs were obtained by explant culture of human testicular tissue samples as described previously[67,96]. Briefly, testicular tissue samples stemming from patients (28-56 years old) undergoing reconstructive surgery of the vas deferens were dissected and placed under plasma drops in culture until outgrowth of HTPCs occurred. Patients granted written informed consent and the ethical committee (Ethikkommission, Technische Universität München, Fakultät für Medizin, München, project number 5158/11) approved the scientific use of the cells. HTPCs were screened for presence of smooth muscle-cell specific markers and absence of markers from possibly contaminating cells as well as mycoplasma before use or cryopreservation. In this thesis only cryopreserved cells in passages 5-16 were used.

4.2.3.1 Cell cultivation

Cells were cultivated at 37°C, 5% (v/v) CO_2 and 95% humidity. The culture medium (DMEM, high glucose including 10% FBS and 1% penicillin/streptomycin) was replaced every other day. If confluent, HTPCs were subcultivated. For this purpose, cells were washed with PBS and incubated with 1 mL Trypsin-EDTA for 4 min at 37°C. The reaction was stopped by applying at least an equal amount of culture medium and HTPCs were pelleted at 700 rpm for 3 min. The pellet was divided onto culture dishes in a 1:3 ratio for mere expansion purposes or used for cell count determination and defined cell seeding for experiments.

4.2.3.2 Thawing and freezing of cells

Cryopreserved HTPCs were thawed in a water bath (37°C) and immediately resuspended in pre-warmed culture medium. Cells were centrifuged at 700 rpm for 3 min. The cell pellet was resuspended in culture medium and transferred to a P60 cell culture dish.
For cryopreservation HTPCs were trypsinized as described. The pellet was resuspended in 1 mL culture medium containing 10% DMSO and transferred to a cryo vial. The vial was cooled down slowly to -80°C over night in a cell freezing container and subsequently transferred to liquid nitrogen for long-term storage.

4.2.3.3 Cell count determination and seeding

If confluent, the cell count was determined by using an automated cell counting and analyzing device, CASY. A trypsinized HTPC pellet was resuspended in 1 mL PBS, diluted 1:500 in 10 mL CASYton and measured by CASY in three cycles of 400 µL sample volume each. The diameter range for viable cells was set from 14 µm to 50 µm. The determined

concentration of viable cells was used to seed equal cell numbers into the appropriate culture vessels for experiments. Approximate cell numbers are depicted in Table 4.1.

Table 4.1 Approximate total cell numbers seeded per culture vessels depending on the method

Culture vessel	Method	Number of cells seeded
35 mm ∅ µ-dish	Ca^{2+} imaging	50000
35 mm ∅ µ-dish	Live cell imaging	40000
60 mm ∅ culture dish	RNA/protein isolation	200000
96 well plate	LDH assay	5000

4.2.3.4 Treatment of HTPCs

For experiments in general, HTPCs were seeded in defined numbers and grown to approximately 90% confluence. 24 h prior treatment, cells were washed with PBS and deprived of FBS supplementation in the culture medium. Stimulation was performed in serum-free culture medium missing phenol red (DMEM, high glucose, no glutamine, no phenol red supplemented with 4 mM L-glutamine and 1% penicillin/streptomycin). As untreated controls, HTPCs were incubated in serum-free culture media only. If an agent for treatment was not soluble in culture medium, the solvent was added to the control experiment in equal concentration. Pilot studies for RNA and protein isolation were performed to determine optimal time periods for treatment depending on stimulating agent and type of experiment. For RNA isolation, 6 h and 24 h were chosen, respectively. 48 h were used for protein analyses and collection of supernatants. Agents and corresponding solvents used for experiments are shown in Table 4.2.

Table 4.2 Stimulating and blocking agents with corresponding solvents used in experiments

Agent	Solvent	Final concentration	Experiment
ATP	Serum-free culture medium	1 mM	RNA/protein isolation
AZ11645373	DMSO	0.5 µM	Ca^{2+} imaging
BzATP	PBS	100 µM	Ca^{2+} imaging

4.2.4 Functional assessment of peritubular cells

4.2.4.1 Live cell imaging

To monitor HTPC response to treating agents treated versus untreated cells were imaged in a heating and gas incubation system (37°C, 5% (v/v) CO_2, 95% relative humidity), which was set up on a transmitted light microscope. Cells were observed for up to 72 h, thereby taking a picture every 20 min to generate time-lapse series. Cell count and confluence were determined at 6 h, 24 h, 48 h and 72 h, respectively. Cells were counted manually using the Fiji cell counter plug-in[579]. Confluence was calculated using the Fiji plug-in PHANTAST[580]. Differences in cell numbers or confluence between treated and untreated HTPCs were examined by paired *t*-tests (two-tailed; statistical significance $p < 0.05$).

4.2.4.2 Cytotoxicity Assay

Chemical compound-mediated cytotoxicity was determined via lactate dehydrogenase (LDH) release from cells as sign of membrane disruption and therefore viability loss. The LDH Cytotoxicity Assay Kit was used according to the manufacturer's instructions. The colorimetric assay was performed in quadruplicates for each treatment and absorbance was measured at 492 nm and 690 nm, respectively. LDH activity was calculated by subtracting absorbance at 690 nm from absorbance at 492 nm. Cytotoxicity was determined via following formula (1).

$$\text{Cytotoxicity} = \frac{\text{Compound treated LDH activity} - \text{Basal LDH activity}}{\text{Maximum LDH activity} - \text{Basal LDH activity}} \quad (1)$$

Statistical analysis of cytotoxicity extent was determined using a one-sample *t*-test (statistical significance $p < 0.05$).

4.2.4.3 Imaging of intracellular calcium transients

Alterations of intracellular Ca^{2+} levels in response to extracellular stimuli were recorded in order to assess receptor presence and functionality. Therefore, HTPCs were loaded with a calcium-sensitive fluorescent dye, Fluo4 or Fluoforte, (5 µM) for 30 min under standard conditions (37°C, 5% (v/v) CO_2, 95% relative humidity). After dye removal, cells were transferred to the stage of on an inverted confocal microscope using a peristaltic pump with flexible tubes and needles to generate a set-up for applying and removing substances for a specified course of time. Typically, once a steady baseline was obtained, stimulating agent (100 µM BzATP) was applied for 30-60 s, then washed out over a period of several minutes, then applied again. In case, receptor activities were attempted to be blocked, the inhibitor (0.5 µM AZ11645373, Ca^{2+}-free culture medium) was already administered while dye loading and remained present until washout. As positive control 0.005% trypsin was used at the end of each experiment[64,67,68]. Fluorescent intensity (excitation wavelength 488 nm) was monitored with a long-pass filter (505 nm) at a cycle time of 1.97 s. Ca^{2+}-dependent fluorescent levels in each cell were evaluated individually by defining regions of interest. Baseline-corrected fluorescent intensities for regions of interest were displayed as a function of time.

4.2.5 Molecular biology methods

4.2.5.1 RNA isolation

Total RNA from HTPCs was isolated using the RNeasy Plus Micro Kit. Cells were harvested by removing the culture media and washing the culture dishes with PBS once. Then, cells were gently scraped from the surface in 350 µL RLT buffer supplemented with 1% β-Mercaptoethanol. At this point samples were either stored at -80°C or directly processed. RNA was extracted following the manufacturer's instructions and eluted in 20 µL nuclease-free H_2O.

Total RNA from mouse testes was isolated using TRIsure. A piece of frozen testicular tissue was homogenized with one stainless steel bead in 1 mL TRIsure for 1 min at 50 Hz. RNA

extraction was performed according to the manufacturer's protocol with the additional use of Glycoblue (1.5 µL per 500 µL aqueous phase) for better visualization of the RNA pellet. RNA concentration and quality were determined using a NanoDrop device. If necessary, RNA was purified by sodium acetate precipitation before cDNA synthesis. RNA was stored at -80°C.

4.2.5.2 RNA purification by precipitation

To remove contaminants from RNA with low quality, sodium acetate precipitation was performed. To this, RNA was precipitated by adding 10% (v/v) 3 M sodium acetate, 400% (v/v) EtOH (100%) and 1 µL of Glycoblue dye. The solution was mixed thoroughly, then frozen at -80°C o/n. Precipitate was pelleted by centrifugation (16000 rpm, 30 min, 4°C) and washed twice with ice-cold EtOH (80%) by removing the supernatant, adding 500 µL EtOH and centrifugation (16000 rpm, 10 min, 4°C). After discarding the supernatant and removing all residual fluid, the pellet was air-dried for approximately 10 min, then dissolved in 40 µL nuclease free H_2O.

4.2.5.3 cDNA synthesis

RNA isolated from HTPCs was transcribed using the SuperScript II Reverse Transcriptase Kit. 200 ng of RNA were pre-mixed with 0.8 µL random 15mer primers (100 µM) and filled up to 11.5 µL with nuclease free H_2O. In case qRT-PCR of low abundant mRNAs was the ultimate goal, 1 µg instead of 200 ng RNA was transcribed. The mix was incubated for 10 min at 70°C and for 5 min at 25°C. Then 7.5 µL nucleotide master mix consisting of 4 µL 5x First Strand Buffer, 2 µL 0.1 M DTT, 1 µL 10 mM dNTPs and 0.5 µL 40 U/µL RNasin were added. RNA and nucleotide mix were incubated for 10 min at 25°C and 2 min at 42°C. 1 µL SuperScript II Reverse Transcriptase (200 U/µL) was added and incubation was carried out for 50 min at 42°C, 15 min at 70°C and 10 min at 4°C. To exclude genomic DNA contamination, -RT control samples were generated by omitting the SuperScript II Reverse Transcriptase. Either, a corresponding control sample was generated for each individual sample or RNAs from samples with similar treatment were pooled and non-reverse transcribed together as one control sample.

RNA from mouse testes was treated with DNaseI to eliminate genomic DNA prior to cDNA synthesis. Therefore, the DNaseI, Amplification Grade Kit was used according to the manufacturer's instructions, albeit nuclease free H_2O was used instead of DEPC-H_2O. cDNA synthesis of 1 µg DNaseI-treated RNA was performed with the SensiFAST cDNA Synthesis Kit following the manufacturer's instructions, but with an extended transcription of 30 min instead of 15 min at 42°C. One -RT control sample was generated per genotype and age group.

cDNA was stored at -20°C.

4.2.5.4 Quantitative real-time PCR

Amplification of cDNA for quantification purposes was performed using the QuantiFast SYBR Green PCR Kit in a LightCycler 96 System. Primers (see section 4.1.5) were designed

using the Primer3 web-tool. Wherever possible, primer pairs were designed to span an exon-exon junction to exclude genomic DNA contamination. Initially, a temperature gradient qRT-PCR was performed to determine the optimal annealing temperature (T_a, see section 4.1.5) for each set of primers. Samples were analyzed in duplicates or triplicates with following reaction mix (Table 4.3) and cycler program (Table 4.4). Non-reverse transcribed RNA as template (-RT) and nuclease free H_2O as non-template (–) were included as control reactions in each experiment to exclude sample contamination.

Table 4.3 Reaction mix composition for qRT-PCR

Reagent	Volume [µL]
2x QuantiFast SYBR Green PCR Master Mix	6.25
Forward primer (3.33/5/10 µM)	1.125
Reverse primer (3.33/5/10 µM)	1.125
cDNA template (1-20 ng)	4

Table 4.4 Cycler program for qRT-PCR reaction

Step	Temperature [°C]	Time [s]
Initiation	95	300
Amplification (35-43x)		
Denaturation	95	10
Annealing/Extension	T_a	30
Melting curve (0.2°C/s)	65-97	160
Cool-down	37	30

Obtained C_q values were analyzed according to the $2^{-\Delta\Delta Cq}$ method[581] using endogenous reference genes. For HPTCs, pair-wise analysis of treated versus untreated sample C_q values was performed with normalization to *HPRT* and *RPL19* as reference genes. One-sample *t*-tests of $-\Delta\Delta C_q$ values revealed statistical significance ($p < 0.05$). Results of mouse testes lysates were normalized to the mean of the WT population using *Hprt*, *Ppia* and *Rpl19* as endogenous reference. Statistical analyses were obtained by unpaired *t*-tests (two-tailed) or one-way ANOVA with Tukey's post-test to correct for multiple comparisons of $-\Delta\Delta C_q$ values (statistical significance $p < 0.05$).

4.2.5.5 Agarose gel electrophoresis and DNA sequencing

qRT-PCR products were analyzed on a 2% agarose gel. Therefore, agarose was dissolved and boiled in 1x TBE buffer. The gel was cooled down and MidoriGreen Advance DNA Stain (final concentration 0.005%) was added before casting. After complete polymerization, the gel was run in 1x TBE buffer at 80 V for 30-45 min. DNA fragments were visualized using blue LED light and compared to the DNA ladder for correct amplicon length. For each set of primers used in amplification, a DNA fragment was isolated from the gel and purified using the Wizard SV Gel and PCR Clean-Up System according to the manufacturer's instructions. Purified amplicons were pre-mixed with forward primer (final concentration 2.5 µM) and sent for sequence analysis (GATC, Konstanz, Germany). Sequencing results were compared and verified using BLAST and SerialCloner.

4.2.6 Proteinbiochemical methods

4.2.6.1 Protein isolation

For protein isolation, cultured HTPCs (after stimulation) were harvested by washing them with PBS once and freezing them at -80°C until isolation. Isolation was performed on ice. Cells were scraped off the culture dish using 1.5 mL NPE buffer and transferred to a 2 mL-tube. Cells were pelleted by centrifugation (10000 rpm, 3 min, 4°C) and resuspended in 1.5 mL PBS. Centrifugation was repeated and the remaining pellet was dissolved in 100 µL protease and phosphatase inhibitor cocktail. Samples were cooled on ice for 30 min before cell lysis via ultrasound (10 times at cycle 0.5 and amplitude 40 in an ultra turrax).
Protein concentration was assessed via the DC Protein Assay Kit based on an improved Lowry assay[582,583] according to the Microplate Assay Protocol of the manufacturer. Absorption of samples at 690 nm was determined in duplicates after 30 min incubation using a dilution series of albumin (0.0-2.0 µg/µL) as calibrator.

4.2.6.2 SDS-Polyacrylamide gel electrophoresis

Protein samples were analyzed according to their molecular weight on a denaturing SDS-PAGE. First, proteins were concentrated in a 4.5% stacking gel at the dye front, then separated by a 12% separating gel. Gels were cast in reverse order using following protocol (Table 4.5).

Table 4.5 Reaction mix composition for separating and stacking gel

Reagent	Separating gel	Stacking gel
Acrylamide (30%)	5.2 mL	0.9 mL
4x Separating gel buffer	3.25 mL	–
4x Stacking gel buffer	–	1.5 mL
dH_2O	4.55 mL	3.55 mL
TEMED	26 µL	15 µL
APS (10%)	52 µL	30 µL

5-7 µg of protein were denatured by adding 10% (v/v) bromophenol blue and 10% (v/v) β-mercaptoethanol and incubating the mix at 95°C for 5 min. The gel was loaded with the samples and run in 1x Laemmli buffer at 90 V for 15 min followed by 120 V for 90 min.

4.2.6.3 Western Blot

To specifically detect the presence of individual proteins, Western blotting of proteins already separated by SDS-PAGE was performed. Proteins were transferred from acrylamide gel to a nitrocellulose membrane in a wet blotting system at 100 V for 75 min using 1x Transfer buffer. The membrane was stained with 1x Ponceau S to validate the protein transfer, then destained using 0.1% acetic acid. To reduce unspecific primary antibody binding, the membrane was incubated in 5% milk powder in 1x TBST for 60 min before applying the primary antibody in 1% milk powder in 1x TBST over night at 4°C. For pre-adsorption control, primary antibody in 1x TBST (2:1 of final concentration) was incubated with a 20-fold excess concentration of complementary blocking peptide for 2-3 h in a shaker (300 rpm, 20°C). The mixture was centrifuged for 10 min at 13,000 rpm. The supernatant

was diluted 1:2 with 2% milk powder in 1x TBST (final concentration 1% milk powder) and used instead of primary antibody. The membrane was washed 15 min with 1x TBST four times, then incubated with the corresponding peroxidase-conjugated secondary antibody in 1% milk powder in 1x TBST for 60 min. Again, the membrane was washed with 1x TBST for 15 min four times. Chemiluminescence was detected using the SuperSignal West Femto Maximum Sensitivity Substrate.

4.2.6.4 Supernatant profiling assay

To analyze regulation of 102 cytokines in whole HTPC supernatant simultaneously, the membrane-based sandwich immunoassay Proteome Profiler Human XL Cytokine Array Kit was used. Supernatants were harvested by centrifugation (8000 rpm, 3 min) and transferred to a new tube to remove any cell debris. 500 µL supernatant were either directly used in the assay or stored at -20°C. Total cell protein was isolated using RIPA buffer. Cells were washed with PBS once, then gently scratched off the surface using 1 mL PBS. Cells were pelleted by centrifuging (2000 rpm, 5 min, 4°C), then washed in 300 µL ice-cold PBS and pelleted again. Cells were lysed by resuspending thoroughly in 150 µL RIPA buffer. Samples were kept on ice for 30 min before sonication. Then, cell debris was removed by centrifugation (13000 rpm, 10 min, 4°C) and transferring the supernatant containing the proteins into a new tube. Protein concentration was determined with the DC Protein Assay Kit as described. The Proteome Profiler Human XL Cytokine Array Kit was used according to the manufacturer's instructions. Chemiluminescent signal intensity was detected and used for relative quantification of cytokines. Individual spot intensity on the membrane was analyzed using a Fiji Macro developed by Dr. Anna Klemm (Core Facility Bioimaging, Biomedical Center Munich, LMU). Means and of duplicate spots were determined, the mean density of the negative control spots was subtracted as blank. Values were corrected for whole lysate protein content and values from treated samples were normalized to the corresponding untreated sample to obtain relative cytokine levels. Relative cytokine levels in the supernatant of four patients were analysed for statistical significance ($p < 0.05$) via a one-sample *t*-tests of logarithmized values.

4.2.6.5 Mass spectrometry

ATP-treated and untreated HTPCs from six patients were harvested for mass spectrometric analysis. Therefore, the cells were trypsinized as described. After pelleting the cells once, the pellet was resuspended and centrifuged down (700 rpm, 3 min) again five times, three times in 1 mL serum-free culture medium and two times in 1 mL PBS, to remove all serum contaminants from the cells. Before the last centrifugation step a 20 µL sample was taken to ensure viability and approximately equal cell count and of paired samples by CASY measurement. After complete removal of any remaining supernatant, the obtained cell pellet was frozen at -80°C. Processing of ATP-treated versus control HTPC samples and mass spectrometric analyses (MS/MS) were performed by the Laboratory for Functional Genome Analysis (LAFUGA) at the LMU Gene Center. A candidate list of proteins affected in abundance by ATP was generated. Enrichment analysis of protein subsets with elevated or decreased abundance was performed with the STRING analysis tool using default options[469].

BIBLIOGRAPHY

1 Weinbauer, G. F., Luetjens, C. M., Simoni, M. & Nieschlag, E. in *Andrologie* (eds Eberhard Nieschlag, Hermann M. Behre, & Susan Nieschlag) Ch. Chapter 2, 15-61 (Springer Berlin Heidelberg, 2009).

2 Cooke, H. J. & Saunders, P. T. Mouse models of male infertility. *Nat Rev Genet* **3,** 790-801, (2002).

3 Clermont, Y. Spermatogenesis in man. A study of the spermatogonial population. *Fertil Steril* **17,** 705-721, (1966).

4 Clermont, Y. The cycle of the seminiferous epithelium in man. *Am J Anat* **112,** 35-51, (1963).

5 Neto, F. T., Bach, P. V., Najari, B. B., Li, P. S. & Goldstein, M. Spermatogenesis in humans and its affecting factors. *Semin Cell Dev Biol* **59,** 10-26, (2016).

6 Goossens, E. & Tournaye, H. Adult stem cells in the human testis. *Semin Reprod Med* **31,** 39-48, (2013).

7 Ehmcke, J. & Schlatt, S. A revised model for spermatogonial expansion in man: lessons from non-human primates. *Reproduction* **132,** 673-680, (2006).

8 O'Donnell, L., Nicholls, P. K., O'Bryan, M. K., McLachlan, R. I. & Stanton, P. G. Spermiation: The process of sperm release. *Spermatogenesis* **1,** 14-35, (2011).

9 Russell, L. D. in *Ultrastructure of Reproduction* (eds Jonathan Van Blerkom & Pietro M. Motta) Ch. Chapter 5, 46-66 (Springer US, 1984).

10 Hargrove, J. L., MacIndoe, J. H. & Ellis, L. C. Testicular contractile cells and sperm transport. *Fertil Steril* **28,** 1146-1157, (1977).

11 Ellis, L. C. & Nemetallah, B. R. in *Male Fertility and Its Regulation* (eds T. J. Lobl & E. S. E. Hafez) Ch. Chapter 27, 397-409 (Springer Netherlands, 1985).

12 Setchell, B. P., Voglmayr, J. K. & Waites, G. M. A blood-testis barrier restricting passage from blood into rete testis fluid but not into lymph. *J Physiol* **200,** 73-85, (1969).

13 Fijak, M. & Meinhardt, A. The testis in immune privilege. *Immunol Rev* **213,** 66-81, (2006).

14 Li, N., Wang, T. & Han, D. Structural, cellular and molecular aspects of immune privilege in the testis. *Front Immunol* **3,** 152, (2012).

15 Mital, P., Hinton, B. T. & Dufour, J. M. The Blood-Testis and Blood-Epididymis Barriers Are More than Just Their Tight Junctions. *Biol Reprod* **84,** 851-858, (2011).

16 Dym, M. & Fawcett, D. W. The blood-testis barrier in the rat and the physiological compartmentation of the seminiferous epithelium. *Biol Reprod* **3,** 308-326, (1970).

17 Fawcett, D. W., Leak, L. V. & Heidger, P. M., Jr. Electron microscopic observations on the structural components of the blood-testis barrier. *J Reprod Fertil Suppl* **10,** 105-122, (1970).

18 Setchell, B. P. The Functional Significance of the Blood-testis Barrier. *J Androl* **1,** 3-10, (1980).

19 Mruk, D. D. & Cheng, C. Y. The Mammalian Blood-Testis Barrier: Its Biology and Regulation. *Endocr Rev* **36,** 564-591, (2015).

20 Smith, L. B. & Walker, W. H. The regulation of spermatogenesis by androgens. *Semin Cell Dev Biol* **30,** 2-13, (2014).

21 Miller, W. L. & Auchus, R. J. The molecular biology, biochemistry, and physiology of human steroidogenesis and its disorders. *Endocr Rev* **32,** 81-151, (2011).

22 Svechnikov, K. *et al.* Origin, development and regulation of human Leydig cells. *Horm Res Paediatr* **73,** 93-101, (2010).

23 Chiba, K., Enatsu, N. & Fujisawa, M. Management of non-obstructive azoospermia. *Reprod Med Biol* **15,** 165-173, (2016).

24 Schuppe, H. C. *et al.* Chronic orchitis: a neglected cause of male infertility? *Andrologia* **40,** 84-91, (2008).

25 Rock, K. L., Latz, E., Ontiveros, F. & Kono, H. The sterile inflammatory response. *Annu Rev Immunol* **28,** 321-342, (2010).

26 Fraczek, M. & Kurpisz, M. Cytokines in the male reproductive tract and their role in infertility disorders. *Journal of Reproductive Immunology* **108,** 98-104, (2015).

27 Sarkar, O. *et al.* Impact of inflammation on male fertility. *Front Biosci (Elite Ed)* **3,** 89-95, (2011).

28 Mruk, D. D. & Cheng, C. Y. Sertoli-Sertoli and Sertoli-Germ Cell Interactions and Their Significance in Germ Cell Movement in the Seminiferous Epithelium during Spermatogenesis. *Endocr Rev* **25,** 747-806, (2004).

29 Li, M. W. *et al.* Tumor necrosis factor {alpha} reversibly disrupts the blood-testis barrier and impairs Sertoli-germ cell adhesion in the seminiferous epithelium of adult rat testes. *J Endocrinol* **190,** 313-329, (2006).

30 Jacobo, P., Guazzone, V. A., Theas, M. S. & Lustig, L. Testicular autoimmunity. *Autoimmun Rev* **10,** 201-204, (2011).

31 Lu, D. & Insel, P. A. Cellular mechanisms of tissue fibrosis. 6. Purinergic signaling and response in fibroblasts and tissue fibrosis. *Am J Physiol Cell Physiol* **306,** C779-788, (2014).

32 Kolb, M., Margetts, P. J., Anthony, D. C., Pitossi, F. & Gauldie, J. Transient expression of IL-1beta induces acute lung injury and chronic repair leading to pulmonary fibrosis. *J Clin Invest* **107,** 1529-1536, (2001).

33 Sigg, C. & Hedinger, C. Quantitative and ultrastructural study of germinal epithelium in testicular biopsies with "mixed atrophy". *Andrologia* **13,** 412-424, (1981).

34 Tsai, M. C., Cheng, Y. S., Lin, T. Y., Yang, W. H. & Lin, Y. M. Clinical characteristics and reproductive outcomes in infertile men with testicular early and late maturation arrest. *Urology* **80,** 826-832, (2012).

35 Ishikawa, T., Fujioka, H. & Fujisawa, M. Clinical and hormonal findings in testicular maturation arrest. *BJU Int* **94,** 1314-1316, (2004).

36 Heller, C. G., Maddock, W. O. & et al. The Sertoli cell. *J Clin Invest* **27,** 540, (1948).

37 McLachlan, R. I., Rajpert-De Meyts, E., Hoei-Hansen, C. E., de Kretser, D. M. & Skakkebaek, N. E. Histological evaluation of the human testis—approaches to optimizing the clinical value of the assessment: Mini Review. *Hum Reprod* **22,** 2-16, (2007).

38 de Kretser, D. M., Kerr, J. B. & Paulsen, C. A. The peritubular tissue in the normal and pathological human testis. An ultrastructural study. *Biol Reprod* **12,** 317-324, (1975).

39 Morita, Y. Histological investigation of testis in infertile man. II. Pathological problems. *Nagoya J Med Sci* **34,** 113-129, (1971).

40 Kisseleva, T. & Brenner, D. A. Mechanisms of fibrogenesis. *Exp Biol Med (Maywood)* **233,** 109-122, (2008).

41 Soderstrom, K. O. Tubular hyalinization in human testis. *Andrologia* **18,** 97-103, (1986).

42 Haider, S. G., Talati, J. & Servos, G. Ultrastructure of peritubular tissue in association with tubular hyalinization in human testis. *Tissue Cell* **31,** 90-98, (1999).

43 Schell, C. *et al.* 15-Deoxy-delta 12-14-prostaglandin-J2 induces hypertrophy and loss of contractility in human testicular peritubular cells: implications for human male fertility. *Endocrinology* **151,** 1257-1268, (2010).

44 Hussein, M. R. *et al.* Phenotypic characterization of the immune and mast cell infiltrates in the human testis shows normal and abnormal spermatogenesis. *Fertil Steril* **83,** 1447-1453, (2005).

45 Frungieri, M. B. *et al.* Number, distribution pattern, and identification of macrophages in the testes of infertile men. *Fertil Steril* **78,** 298-306, (2002).

46 Apa, D. D., Cayan, S., Polat, A. & Akbay, E. Mast cells and fibrosis on testicular biopsies in male infertility. *Arch Androl* **48,** 337-344, (2002).

47 Meineke, V., Frungieri, M. B., Jessberger, B., Vogt, H. & Mayerhofer, A. Human testicular mast cells contain tryptase: increased mast cell number and altered distribution in the testes of infertile men. *Fertil Steril* **74,** 239-244, (2000).

48 Pollanen, P. & Niemi, M. Immunohistochemical identification of macrophages, lymphoid cells and HLA antigens in the human testis. *Int J Androl* **10,** 37-42, (1987).

49 Agarwal, S., Choudhury, M. & Banerjee, A. Mast cells and idiopathic male infertility. *Int J Fertil* **32,** 283-286, (1987).

50 Schuppe, H.-C. & Meinhardt, A. in *Andrology for the Clinician* (eds Wolf-Bernhard Schill, Frank Comhaire, & Timothy B. Hargreave) 292-300 (Springer Berlin Heidelberg, 2006).

51 Kerr, J. B. Ultrastructure of the seminiferous epithelium and intertubular tissue of the human testis. *J Electron Microsc Tech* **19,** 215-240, (1991).

52 Hermo, L. & Lalli, M. Monocytes and mast cells in the limiting membrane of human seminiferous tubules. *Biol Reprod* **19,** 92-100, (1978).

53 Maseki, Y., Miyake, K., Mitsuya, H., Kitamura, H. & Yamada, K. Mastocytosis Occurring in the Testes From Patients With Idiopathic Male Infertility. *Fertil Steril* **36,** 814-817, (1981).

54 Jezek, D. *et al.* Mast cells in testicular biopsies of infertile men with 'mixed atrophy' of seminiferous tubules. *Andrologia* **31,** 203-210, (1999).

55 Hashimoto, J., Nagai, T., Takaba, H., Yamamoto, M. & Miyake, K. Increased mast cells in the limiting membrane of seminiferous tubules in testes of patients with idiopathic infertility. *Urol Int* **43,** 129-132, (1988).

56 Yamanaka, K. *et al.* Significance of human testicular mast cells and their subtypes in male infertility. *Hum Reprod* **15,** 1543-1547, (2000).

57 Welter, H. *et al.* Angiotensin II regulates testicular peritubular cell function via AT1 receptor: a specific situation in male infertility. *Mol Cell Endocrinol* **393,** 171-178, (2014).

58 Abe, Kurosawa, Ishikawa, Miyachi & Kido. Mast cell tryptase stimulates both human dermal fibroblast proliferation and type I collagen production. *Clinical & Experimental Allergy* **28,** 1509-1517, (1998).

59 Frungieri, M. B., Weidinger, S., Meineke, V., Kohn, F. M. & Mayerhofer, A. Proliferative action of mast-cell tryptase is mediated by PAR2, COX2, prostaglandins, and PPARgamma: possible relevance to human fibrotic disorders. *Proc Natl Acad Sci U S A* **99,** 15072-15077, (2002).

60 Cairns, J. A. & Walls, A. F. Mast cell tryptase stimulates the synthesis of type I collagen in human lung fibroblasts. *J Clin Invest* **99,** 1313-1321, (1997).

61 Gruber, B. L. *et al.* Human mast cells activate fibroblasts: tryptase is a fibrogenic factor stimulating collagen messenger ribonucleic acid synthesis and fibroblast chemotaxis. *J Immunol* **158,** 2310-2317, (1997).

62 Adam, M. *et al.* Mast cell tryptase stimulates production of decorin by human testicular peritubular cells: possible role of decorin in male infertility by interfering with growth factor signaling. *Hum Reprod* **26,** 2613-2625, (2011).

63 Akers, I. A. *et al.* Mast cell tryptase stimulates human lung fibroblast proliferation via protease-activated receptor-2. *Am J Physiol Lung Cell Mol Physiol* **278,** L193-201, (2000).

64 Frungieri, M. B., Albrecht, M., Raemsch, R. & Mayerhofer, A. The action of the mast cell product tryptase on cyclooxygenase-2 (COX2) and subsequent fibroblast proliferation involves activation of the extracellular signal-regulated kinase isoforms 1 and 2 (erk1/2). *Cell Signal* **17,** 525-533, (2005).

65 Iosub, R. *et al.* Development of testicular inflammation in the rat involves activation of proteinase-activated receptor-2. *J Pathol* **208,** 686-698, (2006).

66 Welter, H., Kohn, F. M. & Mayerhofer, A. Mast cells in human testicular biopsies from patients with mixed atrophy: increased numbers, heterogeneity, and expression of cyclooxygenase 2 and prostaglandin D2 synthase. *Fertil Steril* **96,** 309-313, (2011).

67 Albrecht, M., Ramsch, R., Kohn, F. M., Schwarzer, J. U. & Mayerhofer, A. Isolation and cultivation of human testicular peritubular cells: a new model for the investigation of fibrotic processes in the human testis and male infertility. *J Clin Endocrinol Metab* **91,** 1956-1960, (2006).

68 Windschuttl, S. *et al.* Are testicular mast cells involved in the regulation of germ cells in man? *Andrology* **2,** 615-622, (2014).

69 D'Andrea, M. R. *et al.* Characterization of protease-activated receptor-2 immunoreactivity in normal human tissues. *J Histochem Cytochem* **46,** 157-164, (1998).

70 Mayerhofer, A., Schell, C., Spinnler, K., Adam, M. & Welter, H. *Mast cells and their evolving role in the human testis*. (2013).

71 Haidl, G. *et al.* The role of mast cells in male infertility. *Expert Review of Clinical Immunology* **7,** 627-634, (2011).

72 Kern, S., Robertson, S. A., Mau, V. J. & Maddocks, S. Cytokine secretion by macrophages in the rat testis. *Biol Reprod* **53,** 1407-1416, (1995).

73 el-Demiry, M. I. *et al.* Lymphocyte sub-populations in the male genital tract. *Br J Urol* **57,** 769-774, (1985).

74 Suominen, J. & Soderstrom, K. O. Lymphocyte infiltration in human testicular biopsies. *Int J Androl* **5,** 461-466, (1982).

75 el-Demiry, M. I. *et al.* Immunocompetent cells in human testis in health and disease. *Fertil Steril* **48,** 470-479, (1987).

76 Bustos-Obregon, E. Ultrastructure and function of the lamina propria of mammalian seminiferous tubules. *Andrologia* **8,** 179-185, (1976).

77 Bustos-Obregon, E. & Holstein, A. F. On structural patterns of the lamina propria of human seminiferous tubules. *Z Zellforsch Mikrosk Anat* **141,** 413-425, (1973).

78 Skinner, M. K., Tung, P. S. & Fritz, I. B. Cooperativity between Sertoli cells and testicular peritubular cells in the production and deposition of extracellular matrix components. *J Cell Biol* **100,** 1941-1947, (1985).

79 Tung, P. S., Skinner, M. K. & Fritz, I. B. Cooperativity between Sertoli cells and peritubular myoid cells in the formation of the basal lamina in the seminiferous tubule. *Ann N Y Acad Sci* **438,** 435-446, (1984).

80 Skinner, M. K. & Fritz, I. B. Structural characterization of proteoglycans produced by testicular peritubular cells and Sertoli cells. *J Biol Chem* **260,** 11874-11883, (1985).

81 Tung, P. S. & Fritz, I. B. Characterization of rat testicular peritubular myoid cells in culture: alpha-smooth muscle isoactin is a specific differentiation marker. *Biol Reprod* **42,** 351-365, (1990).

82 Schlatt, S., Weinbauer, G. F., Arslan, M. & Nieschlag, E. Appearance of alpha-smooth muscle actin in peritubular cells of monkey testes is induced by androgens, modulated by follicle-stimulating hormone, and maintained after hormonal withdrawal. *J Androl* **14,** 340-350, (1993).

83 Volkmann, J. *et al.* Disturbed spermatogenesis associated with thickened lamina propria of seminiferous tubules is not caused by dedifferentiation of myofibroblasts. *Hum Reprod* **26,** 1450-1461, (2011).

84 Virtanen, I. *et al.* Peritubular myoid cells of human and rat testis are smooth muscle cells that contain desmin-type intermediate filaments. *Anat Rec* **215,** 10-20, (1986).

85 Anthony, C. T. & Skinner, M. K. Cytochemical and biochemical characterization of testicular peritubular myoid cells. *Biol Reprod* **40,** 811-823, (1989).

86 Ross, M. H. & Long, I. R. Contractile cells in human seminiferous tubules. *Science* **153,** 1271-1273, (1966).

87 Romano, F. *et al.* The contractile phenotype of peritubular smooth muscle cells is locally controlled: possible implications in male fertility. *Contraception* **72,** 294-297, (2005).

88 Davidoff, M. S., Breucker, H., Holstein, A. F. & Seidl, K. Cellular architecture of the lamina propria of human seminiferous tubules. *Cell Tissue Res* **262,** 253-261, (1990).

89 Skinner, M. K. & Fritz, I. B. Testicular peritubular cells secrete a protein under androgen control that modulates Sertoli cell functions. *Proc Natl Acad Sci U S A* **82,** 114-118, (1985).

90 Verhoeven, G., Hoeben, E. & De Gendt, K. Peritubular cell-Sertoli cell interactions: factors involved in PmodS activity. *Andrologia* **32,** 42-45, (2000).

91 Welsh, M. *et al.* Androgen receptor signalling in peritubular myoid cells is essential for normal differentiation and function of adult Leydig cells. *Int J Androl* **35,** 25-40, (2012).

92 Rebourcet, D. *et al.* Sertoli Cells Maintain Leydig Cell Number and Peritubular Myoid Cell Activity in the Adult Mouse Testis. *PLoS One* **9,** e105687, (2014).

93 Dym, M. The fine structure of the monkey (Macaca) Sertoli cell and its role in maintaining the blood-testis barrier. *Anat Rec* **175,** 639-656, (1973).

94 Mayerhofer, A. Human testicular peritubular cells: more than meets the eye. *Reproduction* **145,** R107-116, (2013).

95 Mayer, C. *et al.* Sterile inflammation as a factor in human male infertility: Involvement of Toll like receptor 2, biglycan and peritubular cells. *Sci Rep* **6,** 37128, (2016).

96 Schell, C. *et al.* Exploring human testicular peritubular cells: identification of secretory products and regulation by tumor necrosis factor-alpha. *Endocrinology* **149,** 1678-1686, (2008).

97 Spinnler, K., Frohlich, T., Arnold, G. J., Kunz, L. & Mayerhofer, A. Human tryptase cleaves pro-nerve growth factor (pro-NGF): hints of local, mast cell-dependent regulation of NGF/pro-NGF action. *J Biol Chem* **286,** 31707-31713, (2011).

98 Adam, M. *et al.* High levels of the extracellular matrix proteoglycan decorin are associated with inhibition of testicular function. *Int J Androl* **35,** 550-561, (2012).

99 Rey-Ares, V. *et al.* Prostaglandin E2 (PGE2) is a testicular peritubular cell-derived factor involved in human testicular homeostasis. *Mol Cell Endocrinol*, (2018).

100 Welter, H. *et al.* Partial loss of contractile marker proteins in human testicular peritubular cells in infertility patients. *Andrology* **1,** 318-324, (2013).

101 Flenkenthaler, F. *et al.* Secretome analysis of testicular peritubular cells: a window into the human testicular microenvironment and the spermatogonial stem cell niche in man. *J Proteome Res* **13,** 1259-1269, (2014).

102 Spinnler, K., Kohn, F. M., Schwarzer, U. & Mayerhofer, A. Glial cell line-derived neurotrophic factor is constitutively produced by human testicular peritubular cells and may contribute to the spermatogonial stem cell niche in man. *Hum Reprod* **25,** 2181-2187, (2010).

103 Meng, X. *et al.* Regulation of cell fate decision of undifferentiated spermatogonia by GDNF. *Science* **287,** 1489-1493, (2000).

104 Yang, Q. E., Kim, D., Kaucher, A., Oatley, M. J. & Oatley, J. M. CXCL12-CXCR4 signaling is required for the maintenance of mouse spermatogonial stem cells. *J Cell Sci* **126,** 1009-1020, (2013).

105 Westernstroer, B. *et al.* Developmental expression patterns of chemokines CXCL11, CXCL12 and their receptor CXCR7 in testes of common marmoset and human. *Cell Tissue Res* **361,** 885-898, (2015).

106 Chen, L. Y., Willis, W. D. & Eddy, E. M. Targeting the Gdnf Gene in peritubular myoid cells disrupts undifferentiated spermatogonial cell development. *Proc Natl Acad Sci U S A* **113,** 1829-1834, (2016).

107 Chen, L. Y., Brown, P. R., Willis, W. B. & Eddy, E. M. Peritubular myoid cells participate in male mouse spermatogonial stem cell maintenance. *Endocrinology* **155,** 4964-4974, (2014).

108 Windschuttl, S. *et al.* Human testicular peritubular cells secrete pigment epithelium-derived factor (PEDF), which may be responsible for the avascularity of the seminiferous tubules. *Sci Rep* **5,** 12820, (2015).

109 Landreh, L. *et al.* Human testicular peritubular cells host putative stem leydig cells with steroidogenic capacity. *J Clin Endocrinol Metab* **99,** E1227-1235, (2014).

110 Sandner, F. *et al.* Expression of the oestrogen receptor GPER by testicular peritubular cells is linked to sexual maturation and male fertility. *Andrology* **2,** 695-701, (2014).

111 Li, X. *et al.* Transgenic mice expressing p450 aromatase as a model for male infertility associated with chronic inflammation in the testis. *Endocrinology* **147,** 1271-1277, (2006).

112 Li, X. *et al.* Altered structure and function of reproductive organs in transgenic male mice overexpressing human aromatase. *Endocrinology* **142,** 2435-2442, (2001).

113 Li, X., Makela, S., Streng, T., Santti, R. & Poutanen, M. Phenotype characteristics of transgenic male mice expressing human aromatase under ubiquitin C promoter. *J Steroid Biochem Mol Biol* **86,** 469-476, (2003).

114 Simpson, E. R. *et al.* Aromatase cytochrome P450, the enzyme responsible for estrogen biosynthesis. *Endocr Rev* **15,** 342-355, (1994).

115 Mukai, K., Tsai, M., Saito, H. & Galli, S. J. Mast cells as sources of cytokines, chemokines, and growth factors. *Immunol Rev* **282,** 121-150, (2018).

116 Iozzo, R. V. & Murdoch, A. D. Proteoglycans of the extracellular environment: clues from the gene and protein side offer novel perspectives in molecular diversity and function. *Faseb j* **10,** 598-614, (1996).

117 Schaefer, L. & Iozzo, R. V. Biological functions of the small leucine-rich proteoglycans: from genetics to signal transduction. *J Biol Chem* **283,** 21305-21309, (2008).

118 Iozzo, R. V. & Schaefer, L. Proteoglycan form and function: A comprehensive nomenclature of proteoglycans. *Matrix Biol* **42,** 11-55, (2015).

119 McBride, O. W., Fisher, L. W. & Young, M. F. Localization of PGI (biglycan, BGN) and PGII (decorin, DCN, PG-40) genes on human chromosomes Xq13-qter and 12q, respectively. *Genomics* **6,** 219-225, (1990).

120 Fisher, L. W. *et al.* Human biglycan gene. Putative promoter, intron-exon junctions, and chromosomal localization. *J Biol Chem* **266,** 14371-14377, (1991).

121 Wegrowski, Y., Pillarisetti, J., Danielson, K. G., Suzuki, S. & Iozzo, R. V. The murine biglycan: complete cDNA cloning, genomic organization, promoter function, and expression. *Genomics* **30,** 8-17, (1995).
122 Fisher, L. W., Termine, J. D. & Young, M. F. Deduced protein sequence of bone small proteoglycan I (biglycan) shows homology with proteoglycan II (decorin) and several nonconnective tissue proteins in a variety of species. *J Biol Chem* **264,** 4571-4576, (1989).
123 Scott, P. G., Dodd, C. M., Bergmann, E. M., Sheehan, J. K. & Bishop, P. N. Crystal structure of the biglycan dimer and evidence that dimerization is essential for folding and stability of class I small leucine-rich repeat proteoglycans. *J Biol Chem* **281,** 13324-13332, (2006).
124 Matsushima, N., Ohyanagi, T., Tanaka, T. & Kretsinger, R. H. Super-motifs and evolution of tandem leucine-rich repeats within the small proteoglycans--biglycan, decorin, lumican, fibromodulin, PRELP, keratocan, osteoadherin, epiphycan, and osteoglycin. *Proteins* **38,** 210-225, (2000).
125 Choi, H. U. *et al.* Characterization of the dermatan sulfate proteoglycans, DS-PGI and DS-PGII, from bovine articular cartilage and skin isolated by octyl-sepharose chromatography. *J Biol Chem* **264,** 2876-2884, (1989).
126 Roughley, P. J. & White, R. J. Dermatan sulphate proteoglycans of human articular cartilage. The properties of dermatan sulphate proteoglycans I and II. *Biochem J* **262,** 823-827, (1989).
127 Nastase, M. V., Young, M. F. & Schaefer, L. Biglycan: a multivalent proteoglycan providing structure and signals. *J Histochem Cytochem* **60,** 963-975, (2012).
128 Bianco, P., Fisher, L. W., Young, M. F., Termine, J. D. & Robey, P. G. Expression and localization of the two small proteoglycans biglycan and decorin in developing human skeletal and non-skeletal tissues. *J Histochem Cytochem* **38,** 1549-1563, (1990).
129 Ungefroren, H., Ergun, S., Krull, N. B. & Holstein, A. F. Expression of the small proteoglycans biglycan and decorin in the adult human testis. *Biol Reprod* **52,** 1095-1105, (1995).
130 Scott, I. C. *et al.* Bone morphogenetic protein-1 processes probiglycan. *J Biol Chem* **275,** 30504-30511, (2000).
131 Iozzo, R. V. Matrix proteoglycans: from molecular design to cellular function. *Annu Rev Biochem* **67,** 609-652, (1998).
132 Schonherr, E. *et al.* Interaction of biglycan with type I collagen. *J Biol Chem* **270,** 2776-2783, (1995).
133 Douglas, T., Heinemann, S., Bierbaum, S., Scharnweber, D. & Worch, H. Fibrillogenesis of collagen types I, II, and III with small leucine-rich proteoglycans decorin and biglycan. *Biomacromolecules* **7,** 2388-2393, (2006).
134 Chen, S. & Birk, D. E. The regulatory roles of small leucine-rich proteoglycans in extracellular matrix assembly. *Febs j* **280,** 2120-2137, (2013).
135 Merline, R., Schaefer, R. M. & Schaefer, L. The matricellular functions of small leucine-rich proteoglycans (SLRPs). *J Cell Commun Signal* **3,** 323-335, (2009).
136 Hildebrand, A. *et al.* Interaction of the small interstitial proteoglycans biglycan, decorin and fibromodulin with transforming growth factor beta. *Biochem J* **302 (Pt 2),** 527-534, (1994).
137 Tufvesson, E. & Westergren-Thorsson, G. Tumour necrosis factor-alpha interacts with biglycan and decorin. *FEBS Lett* **530,** 124-128, (2002).
138 Chen, X. D., Fisher, L. W., Robey, P. G. & Young, M. F. The small leucine-rich proteoglycan biglycan modulates BMP-4-induced osteoblast differentiation. *Faseb j* **18,** 948-958, (2004).
139 Moreno, M. *et al.* Biglycan is a new extracellular component of the Chordin-BMP4 signaling pathway. *Embo j* **24,** 1397-1405, (2005).
140 Miguez, P. A., Terajima, M., Nagaoka, H., Mochida, Y. & Yamauchi, M. Role of glycosaminoglycans of biglycan in BMP-2 signaling. *Biochem Biophys Res Commun* **405,** 262-266, (2011).
141 Desnoyers, L., Arnott, D. & Pennica, D. WISP-1 binds to decorin and biglycan. *J Biol Chem* **276,** 47599-47607, (2001).
142 Inkson, C. A. *et al.* The potential functional interaction of biglycan and WISP-1 in controlling differentiation and proliferation of osteogenic cells. *Cells Tissues Organs* **189,** 153-157, (2009).

143 Berendsen, A. D. *et al.* Modulation of canonical Wnt signaling by the extracellular matrix component biglycan. *Proc Natl Acad Sci U S A* **108,** 17022-17027, (2011).

144 Schaefer, L. *et al.* Absence of decorin adversely influences tubulointerstitial fibrosis of the obstructed kidney by enhanced apoptosis and increased inflammatory reaction. *Am J Pathol* **160,** 1181-1191, (2002).

145 Schaefer, L. *et al.* Biglycan, a nitric oxide-regulated gene, affects adhesion, growth, and survival of mesangial cells. *J Biol Chem* **278,** 26227-26237, (2003).

146 Xu, T. *et al.* Targeted disruption of the biglycan gene leads to an osteoporosis-like phenotype in mice. *Nat Genet* **20,** 78-82, (1998).

147 Chen, X. D., Shi, S., Xu, T., Robey, P. G. & Young, M. F. Age-related osteoporosis in biglycan-deficient mice is related to defects in bone marrow stromal cells. *J Bone Miner Res* **17,** 331-340, (2002).

148 Corsi, A. *et al.* Phenotypic effects of biglycan deficiency are linked to collagen fibril abnormalities, are synergized by decorin deficiency, and mimic Ehlers-Danlos-like changes in bone and other connective tissues. *J Bone Miner Res* **17,** 1180-1189, (2002).

149 Chen, X. D., Allen, M. R., Bloomfield, S., Xu, T. & Young, M. Biglycan-deficient mice have delayed osteogenesis after marrow ablation. *Calcif Tissue Int* **72,** 577-582, (2003).

150 Kram, V., Kilts, T. M., Bhattacharyya, N., Li, L. & Young, M. F. Small leucine rich proteoglycans, a novel link to osteoclastogenesis. *Sci Rep* **7,** 12627, (2017).

151 Nikitovic, D. *et al.* The biology of small leucine-rich proteoglycans in bone pathophysiology. *J Biol Chem* **287,** 33926-33933, (2012).

152 Robinson, K. A. *et al.* Decorin and biglycan are necessary for maintaining collagen fibril structure, fiber realignment, and mechanical properties of mature tendons. *Matrix Biol* **64,** 81-93, (2017).

153 Bi, Y. *et al.* Identification of tendon stem/progenitor cells and the role of the extracellular matrix in their niche. *Nat Med* **13,** 1219-1227, (2007).

154 Ameye, L. *et al.* Abnormal collagen fibrils in tendons of biglycan/fibromodulin-deficient mice lead to gait impairment, ectopic ossification, and osteoarthritis. *Faseb j* **16,** 673-680, (2002).

155 Dourte, L. M. *et al.* Mechanical, compositional, and structural properties of the mouse patellar tendon with changes in biglycan gene expression. *J Orthop Res* **31,** 1430-1437, (2013).

156 Embree, M. C. *et al.* Biglycan and fibromodulin have essential roles in regulating chondrogenesis and extracellular matrix turnover in temporomandibular joint osteoarthritis. *Am J Pathol* **176,** 812-826, (2010).

157 Grandoch, M. *et al.* Loss of Biglycan Enhances Thrombin Generation in Apolipoprotein E-Deficient Mice: Implications for Inflammation and Atherosclerosis. *Arterioscler Thromb Vasc Biol* **36,** e41-50, (2016).

158 Heegaard, A. M. *et al.* Biglycan deficiency causes spontaneous aortic dissection and rupture in mice. *Circulation* **115,** 2731-2738, (2007).

159 Amenta, A. R. *et al.* Biglycan recruits utrophin to the sarcolemma and counters dystrophic pathology in mdx mice. *Proc Natl Acad Sci U S A* **108,** 762-767, (2011).

160 Rafii, M. S. *et al.* Biglycan binds to alpha- and gamma-sarcoglycan and regulates their expression during development. *J Cell Physiol* **209,** 439-447, (2006).

161 Mercado, M. L. *et al.* Biglycan regulates the expression and sarcolemmal localization of dystrobrevin, syntrophin, and nNOS. *Faseb j* **20,** 1724-1726, (2006).

162 Amenta, A. R. *et al.* Biglycan is an extracellular MuSK binding protein important for synapse stability. *J Neurosci* **32,** 2324-2334, (2012).

163 Nastase, M. V., Iozzo, R. V. & Schaefer, L. Key roles for the small leucine-rich proteoglycans in renal and pulmonary pathophysiology. *Biochim Biophys Acta* **1840,** 2460-2470, (2014).

164 Ciftciler, R. *et al.* The importance of serum biglycan levels as a fibrosis marker in patients with chronic hepatitis B. *J Clin Lab Anal* **31**, (2017).

165 Hsieh, L. T., Nastase, M. V., Zeng-Brouwers, J., Iozzo, R. V. & Schaefer, L. Soluble biglycan as a biomarker of inflammatory renal diseases. *Int J Biochem Cell Biol* **54,** 223-235, (2014).

166 Meyer, D. H., Krull, N., Dreher, K. L. & Gressner, A. M. Biglycan and decorin gene expression in normal and fibrotic rat liver: cellular localization and regulatory factors. *Hepatology* **16,** 204-216, (1992).

167 Kolb, M., Margetts, P. J., Sime, P. J. & Gauldie, J. Proteoglycans decorin and biglycan differentially modulate TGF-beta-mediated fibrotic responses in the lung. *Am J Physiol Lung Cell Mol Physiol* **280,** L1327-1334, (2001).

168 Pulskens, W. P. *et al.* TLR4 promotes fibrosis but attenuates tubular damage in progressive renal injury. *J Am Soc Nephrol* **21,** 1299-1308, (2010).

169 Schaefer, L. *et al.* The matrix component biglycan is proinflammatory and signals through Toll-like receptors 4 and 2 in macrophages. *J Clin Invest* **115,** 2223-2233, (2005).

170 Westermann, D. *et al.* Biglycan is required for adaptive remodeling after myocardial infarction. *Circulation* **117,** 1269-1276, (2008).

171 Melchior-Becker, A. *et al.* Deficiency of biglycan causes cardiac fibroblasts to differentiate into a myofibroblast phenotype. *J Biol Chem* **286,** 17365-17375, (2011).

172 Shimizu-Hirota, R. *et al.* Extracellular matrix glycoprotein biglycan enhances vascular smooth muscle cell proliferation and migration. *Circ Res* **94,** 1067-1074, (2004).

173 Weber, C. K. *et al.* Biglycan is overexpressed in pancreatic cancer and induces G1-arrest in pancreatic cancer cell lines. *Gastroenterology* **121,** 657-667, (2001).

174 Xing, X., Gu, X., Ma, T. & Ye, H. Biglycan up-regulated vascular endothelial growth factor (VEGF) expression and promoted angiogenesis in colon cancer. *Tumour Biol* **36,** 1773-1780, (2015).

175 Berendsen, A. D. *et al.* Biglycan modulates angiogenesis and bone formation during fracture healing. *Matrix Biol* **35,** 223-231, (2014).

176 Hu, L. *et al.* Biglycan stimulates VEGF expression in endothelial cells by activating the TLR signaling pathway. *Mol Oncol* **10,** 1473-1484, (2016).

177 Hu, L. *et al.* Biglycan enhances gastric cancer invasion by activating FAK signaling pathway. *Oncotarget* **5,** 1885-1896, (2014).

178 Yamamoto, K. *et al.* Biglycan is a specific marker and an autocrine angiogenic factor of tumour endothelial cells. *Br J Cancer* **106,** 1214-1223, (2012).

179 Gu, X. *et al.* Up-regulated biglycan expression correlates with the malignancy in human colorectal cancers. *Clin Exp Med* **12,** 195-199, (2012).

180 Schaefer, L., Tredup, C., Gubbiotti, M. A. & Iozzo, R. V. Proteoglycan neofunctions: regulation of inflammation and autophagy in cancer biology. *Febs j* **284,** 10-26, (2017).

181 Moreth, K. *et al.* Biglycan-triggered TLR-2- and TLR-4-signaling exacerbates the pathophysiology of ischemic acute kidney injury. *Matrix Biol* **35,** 143-151, (2014).

182 Schaefer, L. Complexity of danger: the diverse nature of damage-associated molecular patterns. *J Biol Chem* **289,** 35237-35245, (2014).

183 Iozzo, R. V. & Schaefer, L. Proteoglycans in health and disease: novel regulatory signaling mechanisms evoked by the small leucine-rich proteoglycans. *Febs j* **277,** 3864-3875, (2010).

184 Moreth, K. *et al.* The proteoglycan biglycan regulates expression of the B cell chemoattractant CXCL13 and aggravates murine lupus nephritis. *J Clin Invest* **120,** 4251-4272, (2010).

185 Zeng-Brouwers, J., Beckmann, J., Nastase, M. V., Iozzo, R. V. & Schaefer, L. De novo expression of circulating biglycan evokes an innate inflammatory tissue response via MyD88/TRIF pathways. *Matrix Biol* **35,** 132-142, (2014).

186 Nastase, M. V. *et al.* Biglycan, a novel trigger of Th1 and Th17 cell recruitment into the kidney. *Matrix Biol*, (2017).

187 Hsieh, L. T. *et al.* Biglycan- and Sphingosine Kinase-1 Signaling Crosstalk Regulates the Synthesis of Macrophage Chemoattractants. *Int J Mol Sci* **18**, (2017).

188 Babelova, A. *et al.* Biglycan, a danger signal that activates the NLRP3 inflammasome via toll-like and P2X receptors. *J Biol Chem* **284,** 24035-24048, (2009).

189 Hsieh, L. T. *et al.* Bimodal role of NADPH oxidases in the regulation of biglycan-triggered IL-1beta synthesis. *Matrix Biol* **49,** 61-81, (2016).

190 Burnstock, G. A basis for distinguishing two types of purinergic receptor. *Cell Membrane Receptors for Drugs and Hormones: A Multidisciplinary Approach***,** 107-118, (1978).

191 Abbracchio, M. P. & Burnstock, G. Purinoceptors: Are there families of P2X and P2Y purinoceptors? *Pharmacol Ther* **64,** 445-475, (1994).

192 Burnstock, G. & Kennedy, C. Is there a basis for distinguishing two types of P2-purinoceptor? *Gen Pharmacol* **16,** 433-440, (1985).

193 Yegutkin, G. G. Nucleotide- and nucleoside-converting ectoenzymes: Important modulators of purinergic signalling cascade. *Biochimica et Biophysica Acta (BBA) - Molecular Cell Research* **1783,** 673-694, (2008).
194 Baroja-Mazo, A., Barbera-Cremades, M. & Pelegrin, P. The participation of plasma membrane hemichannels to purinergic signaling. *Biochim Biophys Acta* **1828,** 79-93, (2013).
195 Zhou, Q. Y. *et al.* Molecular cloning and characterization of an adenosine receptor: the A3 adenosine receptor. *Proc Natl Acad Sci U S A* **89,** 7432-7436, (1992).
196 Libert, F. *et al.* Selective amplification and cloning of four new members of the G protein-coupled receptor family. *Science* **244,** 569-572, (1989).
197 Ralevic, V. & Burnstock, G. Receptors for purines and pyrimidines. *Pharmacol Rev* **50,** 413-492, (1998).
198 Abbracchio, M. P. *et al.* International Union of Pharmacology LVIII: update on the P2Y G protein-coupled nucleotide receptors: from molecular mechanisms and pathophysiology to therapy. *Pharmacol Rev* **58,** 281-341, (2006).
199 Van Kolen, K. & Slegers, H. Integration of P2Y receptor-activated signal transduction pathways in G protein-dependent signalling networks. *Purinergic Signal* **2,** 451-469, (2006).
200 White, P. J., Webb, T. E. & Boarder, M. R. Characterization of a Ca2+ response to both UTP and ATP at human P2Y11 receptors: evidence for agonist-specific signaling. *Mol Pharmacol* **63,** 1356-1363, (2003).
201 Qi, A. D., Kennedy, C., Harden, T. K. & Nicholas, R. A. Differential coupling of the human P2Y(11) receptor to phospholipase C and adenylyl cyclase. *Br J Pharmacol* **132,** 318-326, (2001).
202 Marteau, F. *et al.* Pharmacological characterization of the human P2Y13 receptor. *Mol Pharmacol* **64,** 104-112, (2003).
203 Boeynaems, J.-M. *et al.* P2Y receptors: New subtypes, new functions. *Drug Development Research* **59,** 30-35, (2003).
204 Palmer, R. K., Boyer, J. L., Schachter, J. B., Nicholas, R. A. & Harden, T. K. Agonist action of adenosine triphosphates at the human P2Y1 receptor. *Mol Pharmacol* **54,** 1118-1123, (1998).
205 Communi, D., Robaye, B. & Boeynaems, J. M. Pharmacological characterization of the human P2Y11 receptor. *Br J Pharmacol* **128,** 1199-1206, (1999).
206 Nicholas, R. A., Watt, W. C., Lazarowski, E. R., Li, Q. & Harden, K. Uridine nucleotide selectivity of three phospholipase C-activating P2 receptors: identification of a UDP-selective, a UTP-selective, and an ATP- and UTP-specific receptor. *Mol Pharmacol* **50,** 224-229, (1996).
207 Abbracchio, M. P. *et al.* Characterization of the UDP-glucose receptor (re-named here the P2Y14 receptor) adds diversity to the P2Y receptor family. *Trends Pharmacol Sci* **24,** 52-55, (2003).
208 Torres, G. E., Egan, T. M. & Voigt, M. M. Topological analysis of the ATP-gated ionotropic [correction of ionotrophic] P2X2 receptor subunit. *FEBS Lett* **425,** 19-23, (1998).
209 Newbolt, A. *et al.* Membrane topology of an ATP-gated ion channel (P2X receptor). *J Biol Chem* **273,** 15177-15182, (1998).
210 Valera, S. *et al.* A new class of ligand-gated ion channel defined by P2x receptor for extracellular ATP. *Nature* **371,** 516-519, (1994).
211 Brake, A. J., Wagenbach, M. J. & Julius, D. New structural motif for ligand-gated ion channels defined by an ionotropic ATP receptor. *Nature* **371,** 519-523, (1994).
212 Saul, A., Hausmann, R., Kless, A. & Nicke, A. Heteromeric assembly of P2X subunits. *Front Cell Neurosci* **7,** 250, (2013).
213 Barrera, N. P., Ormond, S. J., Henderson, R. M., Murrell-Lagnado, R. D. & Edwardson, J. M. Atomic force microscopy imaging demonstrates that P2X2 receptors are trimers but that P2X6 receptor subunits do not oligomerize. *J Biol Chem* **280,** 10759-10765, (2005).
214 Nicke, A. *et al.* P2X1 and P2X3 receptors form stable trimers: a novel structural motif of ligand-gated ion channels. *Embo j* **17,** 3016-3028, (1998).
215 Schneider, M. *et al.* Interaction of Purinergic P2X4 and P2X7 Receptor Subunits. *Front Pharmacol* **8,** 860, (2017).

216 Dubyak, G. R. Go it alone no more--P2X7 joins the society of heteromeric ATP-gated receptor channels. *Mol Pharmacol* **72,** 1402-1405, (2007).

217 Coddou, C., Yan, Z., Obsil, T., Huidobro-Toro, J. P. & Stojilkovic, S. S. Activation and regulation of purinergic P2X receptor channels. *Pharmacol Rev* **63,** 641-683, (2011).

218 Browne, L. E. & North, R. A. P2X receptor intermediate activation states have altered nucleotide selectivity. *J Neurosci* **33,** 14801-14808, (2013).

219 Bhargava, Y., Rettinger, J. & Mourot, A. Allosteric nature of P2X receptor activation probed by photoaffinity labelling. *Br J Pharmacol* **167,** 1301-1310, (2012).

220 Bean, B. P. ATP-activated channels in rat and bullfrog sensory neurons: concentration dependence and kinetics. *J Neurosci* **10,** 1-10, (1990).

221 Habermacher, C., Dunning, K., Chataigneau, T. & Grutter, T. Molecular structure and function of P2X receptors. *Neuropharmacology* **104,** 18-30, (2016).

222 Hattori, M. & Gouaux, E. Molecular mechanism of ATP binding and ion channel activation in P2X receptors. *Nature* **485,** 207-212, (2012).

223 Egan, T. M. & Khakh, B. S. Contribution of calcium ions to P2X channel responses. *J Neurosci* **24,** 3413-3420, (2004).

224 North, R. A. Molecular physiology of P2X receptors. *Physiol Rev* **82,** 1013-1067, (2002).

225 Evans, R. J. *et al.* Ionic permeability of, and divalent cation effects on, two ATP-gated cation channels (P2X receptors) expressed in mammalian cells. *J Physiol* **497 (Pt 2),** 413-422, (1996).

226 Compan, V. *et al.* P2X2 and P2X5 subunits define a new heteromeric receptor with P2X7-like properties. *J Neurosci* **32,** 4284-4296, (2012).

227 Virginio, C., MacKenzie, A., Rassendren, F. A., North, R. A. & Surprenant, A. Pore dilation of neuronal P2X receptor channels. *Nat Neurosci* **2,** 315-321, (1999).

228 Khakh, B. S., Bao, X. R., Labarca, C. & Lester, H. A. Neuronal P2X transmitter-gated cation channels change their ion selectivity in seconds. *Nat Neurosci* **2,** 322-330, (1999).

229 Wei, L., Caseley, E., Li, D. & Jiang, L. H. ATP-induced P2X Receptor-Dependent Large Pore Formation: How Much Do We Know? *Front Pharmacol* **7,** 5, (2016).

230 Pelegrin, P. Many ways to dilate the P2X7 receptor pore. *Br J Pharmacol* **163,** 908-911, (2011).

231 Dixon, A. K., Gubitz, A. K., Sirinathsinghji, D. J., Richardson, P. J. & Freeman, T. C. Tissue distribution of adenosine receptor mRNAs in the rat. *Br J Pharmacol* **118,** 1461-1468, (1996).

232 Conti, M. *et al.* Characterization and function of adenosine receptors in the testis. *Ann N Y Acad Sci* **564,** 39-47, (1989).

233 Burnett, L. A. *et al.* Testicular expression of Adora3i2 in Adora3 knockout mice reveals a role of mouse A3Ri2 and human A3Ri3 adenosine receptors in sperm. *J Biol Chem* **285,** 33662-33670, (2010).

234 Minelli, A. *et al.* Involvement of A1 adenosine receptors in the acquisition of fertilizing capacity. *J Androl* **25,** 286-292, (2004).

235 Adeoya-Osiguwa, S. A. & Fraser, L. R. Capacitation state-dependent changes in adenosine receptors and their regulation of adenylyl cyclase/cAMP. *Mol Reprod Dev* **63,** 245-255, (2002).

236 Bellezza, I. & Minelli, A. Adenosine in sperm physiology. *Mol Aspects Med* **55,** 102-109, (2017).

237 Bjorkgren, I. & Lishko, P. V. Purinergic signaling in testes revealed. *J Gen Physiol* **148,** 207-211, (2016).

238 Burnstock, G. Purinergic signalling in the reproductive system in health and disease. *Purinergic Signal* **10,** 157-187, (2014).

239 Fleck, D. *et al.* Distinct purinergic signaling pathways in prepubescent mouse spermatogonia. *J Gen Physiol* **148,** 253-271, (2016).

240 Glass, R., Bardini, M., Robson, T. & Burnstock, G. Expression of nucleotide P2X receptor subtypes during spermatogenesis in the adult rat testis. *Cells Tissues Organs* **169,** 377-387, (2001).

241 Navarro, B., Miki, K. & Clapham, D. E. ATP-activated P2X2 current in mouse spermatozoa. *Proc Natl Acad Sci U S A* **108,** 14342-14347, (2011).

242 Miller, M. R. *et al.* Unconventional endocannabinoid signaling governs sperm activation via the sex hormone progesterone. *Science* **352,** 555-559, (2016).
243 Lalevée, N., Rogier, C., Becq, F. & Joffre, M. Acute Effects of Adenosine Triphosphates, Cyclic 3′,5′-Adenosine Monophosphates, and Follicle-Stimulating Hormone on Cytosolic Calcium Level in Cultured Immature Rat Sertoli Cells. *Biol Reprod* **61,** 343-352, (1999).
244 Foresta, C., Rossato, M., Bordon, P. & Di Virgilio, F. Extracellular ATP activates different signalling pathways in rat Sertoli cells. *Biochem J* **311 (Pt 1),** 269-274, (1995).
245 Filippini, A. *et al.* Activation of inositol phospholipid turnover and calcium signaling in rat Sertoli cells by P2-purinergic receptors: modulation of follicle-stimulating hormone responses. *Endocrinology* **134,** 1537-1545, (1994).
246 Ko, W. H., Au, C. L. & Yip, C. Y. Multiple purinergic receptors lead to intracellular calcium increases in cultured rat Sertoli cells. *Life Sci* **72,** 1519-1535, (2003).
247 Veitinger, S. *et al.* Purinergic signalling mobilizes mitochondrial Ca(2)(+) in mouse Sertoli cells. *J Physiol* **589,** 5033-5055, (2011).
248 Antonio, L. S., Costa, R. R., Gomes, M. D. & Varanda, W. A. Mouse Leydig cells express multiple P2X receptor subunits. *Purinergic Signal* **5,** 277-287, (2009).
249 Poletto Chaves, L. A., Pontelli, E. P. & Varanda, W. A. P2X receptors in mouse Leydig cells. *Am J Physiol Cell Physiol* **290,** C1009-1017, (2006).
250 Verkhratsky, A. & Burnstock, G. Biology of purinergic signalling: its ancient evolutionary roots, its omnipresence and its multiple functional significance. *Bioessays* **36,** 697-705, (2014).
251 Burnstock, G. Purinergic nerves. *Pharmacol Rev* **24,** 509-581, (1972).
252 Burnstock, G., Campbell, G., Satchell, D. & Smythe, A. Evidence that adenosine triphosphate or a related nucleotide is the transmitter substance released by non-adrenergic inhibitory nerves in the gut. *Br J Pharmacol* **40,** 668-688, (1970).
253 Burnstock, G. Purinergic signalling and disorders of the central nervous system. *Nat Rev Drug Discov* **7,** 575-590, (2008).
254 Erlinge, D. & Burnstock, G. P2 receptors in cardiovascular regulation and disease. *Purinergic Signal* **4,** 1-20, (2008).
255 Burnstock, G. Local mechanisms of blood flow control by perivascular nerves and endothelium. *J Hypertens Suppl* **8,** S95-106, (1990).
256 Banks, F. C. *et al.* The purinergic component of human vas deferens contraction. *Fertil Steril* **85,** 932-939, (2006).
257 Fedan, J. S., Hogaboom, G. K., O'Donnell, J. P., Colby, J. & Westfall, D. P. Contribution by purines to the neurogenic response of the vas deferens of the guinea pig. *Eur J Pharmacol* **69,** 41-53, (1981).
258 Mulryan, K. *et al.* Reduced vas deferens contraction and male infertility in mice lacking P2X1 receptors. *Nature* **403,** 86-89, (2000).
259 Abbracchio, M. P. & Burnstock, G. Purinergic signalling: pathophysiological roles. *Jpn J Pharmacol* **78,** 113-145, (1998).
260 Burnstock, G. Short- and long-term (trophic) purinergic signalling. *Philos Trans R Soc Lond B Biol Sci* **371**, (2016).
261 Burnstock, G. & Verkhratsky, A. Long-term (trophic) purinergic signalling: purinoceptors control cell proliferation, differentiation and death. *Cell Death Dis* **1,** e9, (2010).
262 Burnstock, G. & Dale, N. Purinergic signalling during development and ageing. *Purinergic Signal* **11,** 277-305, (2015).
263 Pankratov, Y., Lalo, U., Krishtal, O. A. & Verkhratsky, A. P2X receptors and synaptic plasticity. *Neuroscience* **158,** 137-148, (2009).
264 Pankratov, Y. V., Lalo, U. V. & Krishtal, O. A. Role for P2X receptors in long-term potentiation. *J Neurosci* **22,** 8363-8369, (2002).
265 Orriss, I. R. *et al.* The regulation of osteoblast function and bone mineralisation by extracellular nucleotides: The role of p2x receptors. *Bone* **51,** 389-400, (2012).
266 Orriss, I. R., Burnstock, G. & Arnett, T. R. Purinergic signalling and bone remodelling. *Curr Opin Pharmacol* **10,** 322-330, (2010).
267 Burnstock, G. Purinergic Signalling: Therapeutic Developments. *Front Pharmacol* **8,** 661, (2017).

268 Ferrari, D., Vitiello, L., Idzko, M. & la Sala, A. Purinergic signaling in atherosclerosis. *Trends Mol Med* **21,** 184-192, (2015).

269 Kazemi, M. H. *et al.* Adenosine and adenosine receptors in the immunopathogenesis and treatment of cancer. *J Cell Physiol* **233,** 2032-2057, (2018).

270 Di Virgilio, F. & Adinolfi, E. Extracellular purines, purinergic receptors and tumor growth. *Oncogene* **36,** 293-303, (2017).

271 Burnstock, G. & Di Virgilio, F. Purinergic signalling and cancer. *Purinergic Signal* **9,** 491-540, (2013).

272 Ferrari, D. *et al.* Purinergic signaling in scarring. *Faseb j* **30,** 3-12, (2016).

273 van der Vliet, A. & Bove, P. F. Purinergic signaling in wound healing and airway remodeling. *Subcell Biochem* **55,** 139-157, (2011).

274 Cekic, C. & Linden, J. Purinergic regulation of the immune system. *Nat Rev Immunol* **16,** 177-192, (2016).

275 Antonioli, L., Pacher, P., Vizi, E. S. & Hasko, G. CD39 and CD73 in immunity and inflammation. *Trends Mol Med* **19,** 355-367, (2013).

276 Ryan, L. M., Rachow, J. W. & McCarty, D. J. Synovial fluid ATP: a potential substrate for the production of inorganic pyrophosphate. *J Rheumatol* **18,** 716-720, (1991).

277 Coade, S. B. & Pearson, J. D. Metabolism of adenine nucleotides in human blood. *Circ Res* **65,** 531-537, (1989).

278 Ontyd, J. & Schrader, J. Measurement of adenosine, inosine, and hypoxanthine in human plasma. *J Chromatogr* **307,** 404-409, (1984).

279 Lazarowski, E. R. Vesicular and conductive mechanisms of nucleotide release. *Purinergic Signal* **8,** 359-373, (2012).

280 Elliott, M. R. *et al.* Nucleotides released by apoptotic cells act as a find-me signal to promote phagocytic clearance. *Nature* **461,** 282-286, (2009).

281 Bours, M. J., Swennen, E. L., Di Virgilio, F., Cronstein, B. N. & Dagnelie, P. C. Adenosine 5'-triphosphate and adenosine as endogenous signaling molecules in immunity and inflammation. *Pharmacol Ther* **112,** 358-404, (2006).

282 Kronlage, M. *et al.* Autocrine purinergic receptor signaling is essential for macrophage chemotaxis. *Sci Signal* **3,** ra55, (2010).

283 Chen, Y. *et al.* ATP release guides neutrophil chemotaxis via P2Y2 and A3 receptors. *Science* **314,** 1792-1795, (2006).

284 Junger, W. G. Immune cell regulation by autocrine purinergic signalling. *Nat Rev Immunol* **11,** 201-212, (2011).

285 Di Virgilio, F. & Vuerich, M. Purinergic signaling in the immune system. *Auton Neurosci* **191,** 117-123, (2015).

286 McDonald, B. *et al.* Intravascular danger signals guide neutrophils to sites of sterile inflammation. *Science* **330,** 362-366, (2010).

287 Orioli, E., De Marchi, E., Giuliani, A. L. & Adinolfi, E. P2X7 Receptor Orchestrates Multiple Signalling Pathways Triggering Inflammation, Autophagy and Metabolic/Trophic Responses. *Curr Med Chem* **24,** 2261-2275, (2017).

288 Franceschini, A. *et al.* The P2X7 receptor directly interacts with the NLRP3 inflammasome scaffold protein. *Faseb j* **29,** 2450-2461, (2015).

289 Piccini, A. *et al.* ATP is released by monocytes stimulated with pathogen-sensing receptor ligands and induces IL-1beta and IL-18 secretion in an autocrine way. *Proc Natl Acad Sci U S A* **105,** 8067-8072, (2008).

290 Mariathasan, S. *et al.* Cryopyrin activates the inflammasome in response to toxins and ATP. *Nature* **440,** 228-232, (2006).

291 Ferrari, D. *et al.* The P2X7 receptor: a key player in IL-1 processing and release. *J Immunol* **176,** 3877-3883, (2006).

292 Liu, Y., Xiao, Y. & Li, Z. P2X7 receptor positively regulates MyD88-dependent NF-kappaB activation. *Cytokine* **55,** 229-236, (2011).

293 Korcok, J., Raimundo, L. N., Ke, H. Z., Sims, S. M. & Dixon, S. J. Extracellular nucleotides act through P2X7 receptors to activate NF-kappaB in osteoclasts. *J Bone Miner Res* **19,** 642-651, (2004).

294 Ferrari, D., Wesselborg, S., Bauer, M. K. A. & Schulze-Osthoff, K. Extracellular ATP Activates Transcription Factor NF-κB through the P2Z Purinoreceptor by Selectively Targeting NF-κB p65 (RelA). *J Cell Biol* **139,** 1635-1643, (1997).

295 Liu, T., Zhang, L., Joo, D. & Sun, S. C. NF-kappaB signaling in inflammation. *Signal Transduct Target Ther* **2,** 17023, (2017).

296 Yang, D., He, Y., Munoz-Planillo, R., Liu, Q. & Nunez, G. Caspase-11 Requires the Pannexin-1 Channel and the Purinergic P2X7 Pore to Mediate Pyroptosis and Endotoxic Shock. *Immunity* **43,** 923-932, (2015).

297 Ferrari, D. *et al.* P2Z purinoreceptor ligation induces activation of caspases with distinct roles in apoptotic and necrotic alterations of cell death. *FEBS Lett* **447,** 71-75, (1999).

298 Zanovello, P., Bronte, V., Rosato, A., Pizzo, P. & Di Virgilio, F. Responses of mouse lymphocytes to extracellular ATP. II. Extracellular ATP causes cell type-dependent lysis and DNA fragmentation. *J Immunol* **145,** 1545-1550, (1990).

299 Di Virgilio, F. *et al.* Cytolytic P2X purinoceptors. *Cell Death Differ* **5,** 191-199, (1998).

300 Di Virgilio, F., Bronte, V., Collavo, D. & Zanovello, P. Responses of mouse lymphocytes to extracellular adenosine 5'-triphosphate (ATP). Lymphocytes with cytotoxic activity are resistant to the permeabilizing effects of ATP. *J Immunol* **143,** 1955-1960, (1989).

301 Young, C. N. *et al.* A novel mechanism of autophagic cell death in dystrophic muscle regulated by P2RX7 receptor large-pore formation and HSP90. *Autophagy* **11,** 113-130, (2015).

302 Adinolfi, E. *et al.* Basal activation of the P2X7 ATP receptor elevates mitochondrial calcium and potential, increases cellular ATP levels, and promotes serum-independent growth. *Mol Biol Cell* **16,** 3260-3272, (2005).

303 Baricordi, O. R. *et al.* An ATP-activated channel is involved in mitogenic stimulation of human T lymphocytes. *Blood* **87,** 682-690, (1996).

304 Gentile, D., Natale, M., Lazzerini, P. E., Capecchi, P. L. & Laghi-Pasini, F. The role of P2X7 receptors in tissue fibrosis: a brief review. *Purinergic Signal* **11,** 435-440, (2015).

305 Riteau, N. *et al.* Extracellular ATP is a danger signal activating P2X7 receptor in lung inflammation and fibrosis. *Am J Respir Crit Care Med* **182,** 774-783, (2010).

306 Layhadi, J. A. & Fountain, S. J. P2X4 Receptor-Dependent Ca(2+) Influx in Model Human Monocytes and Macrophages. *Int J Mol Sci* **18**, (2017).

307 Woehrle, T. *et al.* Pannexin-1 hemichannel-mediated ATP release together with P2X1 and P2X4 receptors regulate T-cell activation at the immune synapse. *Blood* **116,** 3475-3484, (2010).

308 Li, F. *et al.* Inhibition of P2X4 suppresses joint inflammation and damage in collagen-induced arthritis. *Inflammation* **37,** 146-153, (2014).

309 Chen, K. *et al.* ATP-P2X4 signaling mediates NLRP3 inflammasome activation: a novel pathway of diabetic nephropathy. *Int J Biochem Cell Biol* **45,** 932-943, (2013).

310 de Rivero Vaccari, J. P. *et al.* P2X4 receptors influence inflammasome activation after spinal cord injury. *J Neurosci* **32,** 3058-3066, (2012).

311 Antonio, L. S. *et al.* P2X4 receptors interact with both P2X2 and P2X7 receptors in the form of homotrimers. *Br J Pharmacol* **163,** 1069-1077, (2011).

312 Casas-Pruneda, G., Reyes, J. P., Perez-Flores, G., Perez-Cornejo, P. & Arreola, J. Functional interactions between P2X4 and P2X7 receptors from mouse salivary epithelia. *J Physiol* **587,** 2887-2901, (2009).

313 Guo, C., Masin, M., Qureshi, O. S. & Murrell-Lagnado, R. D. Evidence for functional P2X4/P2X7 heteromeric receptors. *Mol Pharmacol* **72,** 1447-1456, (2007).

314 Sakaki, H. *et al.* P2X4 receptor regulates P2X7 receptor-dependent IL-1beta and IL-18 release in mouse bone marrow-derived dendritic cells. *Biochem Biophys Res Commun* **432,** 406-411, (2013).

315 Hung, S. C. *et al.* P2X4 assembles with P2X7 and pannexin-1 in gingival epithelial cells and modulates ATP-induced reactive oxygen species production and inflammasome activation. *PLoS One* **8,** e70210, (2013).

316 Kawano, A. *et al.* Regulation of P2X7-dependent inflammatory functions by P2X4 receptor in mouse macrophages. *Biochem Biophys Res Commun* **420,** 102-107, (2012).

317 Martinon, F., Burns, K. & Tschopp, J. The inflammasome: a molecular platform triggering activation of inflammatory caspases and processing of proIL-beta. *Mol Cell* **10,** 417-426, (2002).
318 Seong, S.-Y. & Matzinger, P. Hydrophobicity: an ancient damage-associated molecular pattern that initiates innate immune responses. *Nature Reviews Immunology* **4,** 469, (2004).
319 Matzinger, P. Tolerance, danger, and the extended family. *Annu Rev Immunol* **12,** 991-1045, (1994).
320 Janeway, C. A., Jr. Approaching the asymptote? Evolution and revolution in immunology. *Cold Spring Harb Symp Quant Biol* **54 Pt 1,** 1-13, (1989).
321 Latz, E., Xiao, T. S. & Stutz, A. Activation and regulation of the inflammasomes. *Nat Rev Immunol* **13,** 397-411, (2013).
322 Hoffman, H. M., Mueller, J. L., Broide, D. H., Wanderer, A. A. & Kolodner, R. D. Mutation of a new gene encoding a putative pyrin-like protein causes familial cold autoinflammatory syndrome and Muckle-Wells syndrome. *Nat Genet* **29,** 301-305, (2001).
323 Agostini, L. *et al.* NALP3 forms an IL-1beta-processing inflammasome with increased activity in Muckle-Wells autoinflammatory disorder. *Immunity* **20,** 319-325, (2004).
324 Bauernfeind, F. G. *et al.* Cutting edge: NF-kappaB activating pattern recognition and cytokine receptors license NLRP3 inflammasome activation by regulating NLRP3 expression. *J Immunol* **183,** 787-791, (2009).
325 Lawrence, T. The nuclear factor NF-kappaB pathway in inflammation. *Cold Spring Harb Perspect Biol* **1,** a001651, (2009).
326 Cogswell, J. P. *et al.* NF-kappa B regulates IL-1 beta transcription through a consensus NF-kappa B binding site and a nonconsensus CRE-like site. *J Immunol* **153,** 712-723, (1994).
327 Hiscott, J. *et al.* Characterization of a functional NF-kappa B site in the human interleukin 1 beta promoter: evidence for a positive autoregulatory loop. *Mol Cell Biol* **13,** 6231-6240, (1993).
328 Hoesel, B. & Schmid, J. A. The complexity of NF-kappaB signaling in inflammation and cancer. *Mol Cancer* **12,** 86, (2013).
329 Py, B. F., Kim, M. S., Vakifahmetoglu-Norberg, H. & Yuan, J. Deubiquitination of NLRP3 by BRCC3 critically regulates inflammasome activity. *Mol Cell* **49,** 331-338, (2013).
330 Juliana, C. *et al.* Non-transcriptional priming and deubiquitination regulate NLRP3 inflammasome activation. *J Biol Chem* **287,** 36617-36622, (2012).
331 Vanaja, S. K., Rathinam, V. A. & Fitzgerald, K. A. Mechanisms of inflammasome activation: recent advances and novel insights. *Trends Cell Biol* **25,** 308-315, (2015).
332 Martinon, F., Petrilli, V., Mayor, A., Tardivel, A. & Tschopp, J. Gout-associated uric acid crystals activate the NALP3 inflammasome. *Nature* **440,** 237-241, (2006).
333 Peeters, P. M., Perkins, T. N., Wouters, E. F., Mossman, B. T. & Reynaert, N. L. Silica induces NLRP3 inflammasome activation in human lung epithelial cells. *Part Fibre Toxicol* **10,** 3, (2013).
334 Ferrari, D. *et al.* Extracellular ATP triggers IL-1 beta release by activating the purinergic P2Z receptor of human macrophages. *J Immunol* **159,** 1451-1458, (1997).
335 Zhou, R., Yazdi, A. S., Menu, P. & Tschopp, J. A role for mitochondria in NLRP3 inflammasome activation. *Nature* **469,** 221-225, (2011).
336 Shimada, K. *et al.* Oxidized mitochondrial DNA activates the NLRP3 inflammasome during apoptosis. *Immunity* **36,** 401-414, (2012).
337 Murakami, T. *et al.* Critical role for calcium mobilization in activation of the NLRP3 inflammasome. *Proc Natl Acad Sci U S A* **109,** 11282-11287, (2012).
338 Lee, G. S. *et al.* The calcium-sensing receptor regulates the NLRP3 inflammasome through Ca2+ and cAMP. *Nature* **492,** 123-127, (2012).
339 Liston, A. & Masters, S. L. Homeostasis-altering molecular processes as mechanisms of inflammasome activation. *Nat Rev Immunol* **17,** 208-214, (2017).
340 Gaidt, M. M. & Hornung, V. The NLRP3 Inflammasome Renders Cell Death Pro-inflammatory. *J Mol Biol* **430,** 133-141, (2018).
341 Munoz-Planillo, R. *et al.* K(+) efflux is the common trigger of NLRP3 inflammasome activation by bacterial toxins and particulate matter. *Immunity* **38,** 1142-1153, (2013).

342 Shi, H. *et al.* NLRP3 activation and mitosis are mutually exclusive events coordinated by NEK7, a new inflammasome component. *Nat Immunol* **17,** 250-258, (2016).
343 Schmid-Burgk, J. L. *et al.* A Genome-wide CRISPR (Clustered Regularly Interspaced Short Palindromic Repeats) Screen Identifies NEK7 as an Essential Component of NLRP3 Inflammasome Activation. *J Biol Chem* **291,** 103-109, (2016).
344 He, Y., Zeng, M. Y., Yang, D., Motro, B. & Núñez, G. NEK7 is an essential mediator of NLRP3 activation downstream of potassium efflux. *Nature* **530,** 354, (2016).
345 Kim, J. K., Jin, H. S., Suh, H. W. & Jo, E. K. Negative regulators and their mechanisms in NLRP3 inflammasome activation and signaling. *Immunol Cell Biol* **95,** 584-592, (2017).
346 Broz, P. & Dixit, V. M. Inflammasomes: mechanism of assembly, regulation and signalling. *Nat Rev Immunol* **16,** 407-420, (2016).
347 Masumoto, J. *et al.* ASC, a novel 22-kDa protein, aggregates during apoptosis of human promyelocytic leukemia HL-60 cells. *J Biol Chem* **274,** 33835-33838, (1999).
348 Liepinsh, E. *et al.* The death-domain fold of the ASC PYRIN domain, presenting a basis for PYRIN/PYRIN recognition. *J Mol Biol* **332,** 1155-1163, (2003).
349 Richards, N. *et al.* Interaction between pyrin and the apoptotic speck protein (ASC) modulates ASC-induced apoptosis. *J Biol Chem* **276,** 39320-39329, (2001).
350 Srinivasula, S. M. *et al.* The PYRIN-CARD protein ASC is an activating adaptor for caspase-1. *J Biol Chem* **277,** 21119-21122, (2002).
351 Masumoto, J., Taniguchi, S. & Sagara, J. Pyrin N-terminal homology domain- and caspase recruitment domain-dependent oligomerization of ASC. *Biochem Biophys Res Commun* **280,** 652-655, (2001).
352 Lu, A. *et al.* Unified polymerization mechanism for the assembly of ASC-dependent inflammasomes. *Cell* **156,** 1193-1206, (2014).
353 Yang, X., Chang, H. Y. & Baltimore, D. Autoproteolytic activation of pro-caspases by oligomerization. *Mol Cell* **1,** 319-325, (1998).
354 Black, R. A. *et al.* Generation of biologically active interleukin-1 beta by proteolytic cleavage of the inactive precursor. *J Biol Chem* **263,** 9437-9442, (1988).
355 Gu, Y. *et al.* Activation of interferon-gamma inducing factor mediated by interleukin-1beta converting enzyme. *Science* **275,** 206-209, (1997).
356 Ghayur, T. *et al.* Caspase-1 processes IFN-gamma-inducing factor and regulates LPS-induced IFN-gamma production. *Nature* **386,** 619-623, (1997).
357 Howard, A. D. *et al.* IL-1-converting enzyme requires aspartic acid residues for processing of the IL-1 beta precursor at two distinct sites and does not cleave 31-kDa IL-1 alpha. *J Immunol* **147,** 2964-2969, (1991).
358 Shi, J. *et al.* Cleavage of GSDMD by inflammatory caspases determines pyroptotic cell death. *Nature* **526,** 660-665, (2015).
359 He, W. T. *et al.* Gasdermin D is an executor of pyroptosis and required for interleukin-1beta secretion. *Cell Res* **25,** 1285-1298, (2015).
360 Sborgi, L. *et al.* GSDMD membrane pore formation constitutes the mechanism of pyroptotic cell death. *Embo j* **35,** 1766-1778, (2016).
361 Liu, X. *et al.* Inflammasome-activated gasdermin D causes pyroptosis by forming membrane pores. *Nature* **535,** 153-158, (2016).
362 Shi, J. *et al.* Inflammatory caspases are innate immune receptors for intracellular LPS. *Nature* **514,** 187-192, (2014).
363 Kayagaki, N. *et al.* Noncanonical inflammasome activation by intracellular LPS independent of TLR4. *Science* **341,** 1246-1249, (2013).
364 Kayagaki, N. *et al.* Non-canonical inflammasome activation targets caspase-11. *Nature* **479,** 117-121, (2011).
365 Hagar, J. A., Powell, D. A., Aachoui, Y., Ernst, R. K. & Miao, E. A. Cytoplasmic LPS activates caspase-11: implications in TLR4-independent endotoxic shock. *Science* **341,** 1250-1253, (2013).
366 Schmid-Burgk, J. L. *et al.* Caspase-4 mediates non-canonical activation of the NLRP3 inflammasome in human myeloid cells. *Eur J Immunol* **45,** 2911-2917, (2015).
367 Case, C. L. *et al.* Caspase-11 stimulates rapid flagellin-independent pyroptosis in response to Legionella pneumophila. *Proc Natl Acad Sci U S A* **110,** 1851-1856, (2013).

368 Ruhl, S. & Broz, P. Caspase-11 activates a canonical NLRP3 inflammasome by promoting K(+) efflux. *Eur J Immunol* **45,** 2927-2936, (2015).

369 Baker, P. J. *et al.* NLRP3 inflammasome activation downstream of cytoplasmic LPS recognition by both caspase-4 and caspase-5. *Eur J Immunol* **45,** 2918-2926, (2015).

370 Kayagaki, N. *et al.* Caspase-11 cleaves gasdermin D for non-canonical inflammasome signalling. *Nature* **526,** 666-671, (2015).

371 Aglietti, R. A. *et al.* GsdmD p30 elicited by caspase-11 during pyroptosis forms pores in membranes. *Proc Natl Acad Sci U S A* **113,** 7858-7863, (2016).

372 He, Y., Hara, H. & Nunez, G. Mechanism and Regulation of NLRP3 Inflammasome Activation. *Trends Biochem Sci* **41,** 1012-1021, (2016).

373 Andrei, C. *et al.* Phospholipases C and A2 control lysosome-mediated IL-1 beta secretion: Implications for inflammatory processes. *Proc Natl Acad Sci U S A* **101,** 9745-9750, (2004).

374 Andrei, C. *et al.* The secretory route of the leaderless protein interleukin 1beta involves exocytosis of endolysosome-related vesicles. *Mol Biol Cell* **10,** 1463-1475, (1999).

375 Bianco, F. *et al.* Astrocyte-derived ATP induces vesicle shedding and IL-1 beta release from microglia. *J Immunol* **174,** 7268-7277, (2005).

376 MacKenzie, A. *et al.* Rapid secretion of interleukin-1beta by microvesicle shedding. *Immunity* **15,** 825-835, (2001).

377 Qu, Y., Franchi, L., Nunez, G. & Dubyak, G. R. Nonclassical IL-1 beta secretion stimulated by P2X7 receptors is dependent on inflammasome activation and correlated with exosome release in murine macrophages. *J Immunol* **179,** 1913-1925, (2007).

378 Brough, D. & Rothwell, N. J. Caspase-1-dependent processing of pro-interleukin-1beta is cytosolic and precedes cell death. *J Cell Sci* **120,** 772-781, (2007).

379 Martín-Sánchez, F. *et al.* Inflammasome-dependent IL-1β release depends upon membrane permeabilisation. *Cell Death And Differentiation* **23,** 1219, (2016).

380 Evavold, C. L. *et al.* The Pore-Forming Protein Gasdermin D Regulates Interleukin-1 Secretion from Living Macrophages. *Immunity* **48,** 35-44 e36, (2018).

381 Sims, J. E. & Smith, D. E. The IL-1 family: regulators of immunity. *Nat Rev Immunol* **10,** 89-102, (2010).

382 Tzeng, T. C. *et al.* A Fluorescent Reporter Mouse for Inflammasome Assembly Demonstrates an Important Role for Cell-Bound and Free ASC Specks during In Vivo Infection. *Cell Rep* **16,** 571-582, (2016).

383 Franklin, B. S. *et al.* The adaptor ASC has extracellular and 'prionoid' activities that propagate inflammation. *Nat Immunol* **15,** 727-737, (2014).

384 Baroja-Mazo, A. *et al.* The NLRP3 inflammasome is released as a particulate danger signal that amplifies the inflammatory response. *Nat Immunol* **15,** 738-748, (2014).

385 Franklin, B. S., Latz, E. & Schmidt, F. I. The intra- and extracellular functions of ASC specks. *Immunol Rev* **281,** 74-87, (2018).

386 Karasawa, T. & Takahashi, M. Role of NLRP3 Inflammasomes in Atherosclerosis. *J Atheroscler Thromb* **24,** 443-451, (2017).

387 Sheedy, F. J. *et al.* CD36 coordinates NLRP3 inflammasome activation by facilitating intracellular nucleation of soluble ligands into particulate ligands in sterile inflammation. *Nat Immunol* **14,** 812-820, (2013).

388 Duewell, P. *et al.* NLRP3 inflammasomes are required for atherogenesis and activated by cholesterol crystals. *Nature* **464,** 1357-1361, (2010).

389 Masters, S. L., Latz, E. & O'Neill, L. A. The inflammasome in atherosclerosis and type 2 diabetes. *Sci Transl Med* **3,** 81ps17, (2011).

390 Zhou, R., Tardivel, A., Thorens, B., Choi, I. & Tschopp, J. Thioredoxin-interacting protein links oxidative stress to inflammasome activation. *Nat Immunol* **11,** 136-140, (2010).

391 Maedler, K. *et al.* Glucose-induced beta cell production of IL-1beta contributes to glucotoxicity in human pancreatic islets. *J Clin Invest* **110,** 851-860, (2002).

392 Wen, H. *et al.* Fatty acid-induced NLRP3-ASC inflammasome activation interferes with insulin signaling. *Nat Immunol* **12,** 408-415, (2011).

393 Masters, S. L. *et al.* Activation of the NLRP3 inflammasome by islet amyloid polypeptide provides a mechanism for enhanced IL-1beta in type 2 diabetes. *Nat Immunol* **11,** 897-904, (2010).

394 Janson, J. *et al.* Spontaneous diabetes mellitus in transgenic mice expressing human islet amyloid polypeptide. *Proc Natl Acad Sci U S A* **93,** 7283-7288, (1996).
395 Vandanmagsar, B. *et al.* The NLRP3 inflammasome instigates obesity-induced inflammation and insulin resistance. *Nat Med* **17,** 179-188, (2011).
396 Guo, H., Callaway, J. B. & Ting, J. P. Inflammasomes: mechanism of action, role in disease, and therapeutics. *Nat Med* **21,** 677-687, (2015).
397 Robbins, G. R., Wen, H. & Ting, J. P. Inflammasomes and metabolic disorders: old genes in modern diseases. *Mol Cell* **54,** 297-308, (2014).
398 Heneka, M. T. *et al.* NLRP3 is activated in Alzheimer's disease and contributes to pathology in APP/PS1 mice. *Nature* **493,** 674-678, (2013).
399 Hook, V. Y., Kindy, M. & Hook, G. Inhibitors of cathepsin B improve memory and reduce beta-amyloid in transgenic Alzheimer disease mice expressing the wild-type, but not the Swedish mutant, beta-secretase site of the amyloid precursor protein. *J Biol Chem* **283,** 7745-7753, (2008).
400 Halle, A. *et al.* The NALP3 inflammasome is involved in the innate immune response to amyloid-beta. *Nat Immunol* **9,** 857-865, (2008).
401 Kingsbury, S. R., Conaghan, P. G. & McDermott, M. F. The role of the NLRP3 inflammasome in gout. *J Inflamm Res* **4,** 39-49, (2011).
402 Miyamae, T. Cryopyrin-associated periodic syndromes: diagnosis and management. *Paediatr Drugs* **14,** 109-117, (2012).
403 Touitou, I. *et al.* Infevers: an evolving mutation database for auto-inflammatory syndromes. *Hum Mutat* **24,** 194-198, (2004).
404 Hoffman, H. M. & Brydges, S. D. Genetic and molecular basis of inflammasome-mediated disease. *J Biol Chem* **286,** 10889-10896, (2011).
405 Feldmann, J. *et al.* Chronic Infantile Neurological Cutaneous and Articular Syndrome Is Caused by Mutations in CIAS1, a Gene Highly Expressed in Polymorphonuclear Cells and Chondrocytes. *The American Journal of Human Genetics* **71,** 198-203, (2002).
406 Muckle, T. J. & Wells, M. Urticaria, deafness, and amyloidosis: a new heredo-familial syndrome. *Q J Med* **31,** 235-248, (1962).
407 Muckle, T. J. The 'Muckle–Wells' syndrome. *British Journal of Dermatology* **100,** 87-92, (1979).
408 Aksentijevich, I. *et al.* The clinical continuum of cryopyrinopathies: novel CIAS1 mutations in North American patients and a new cryopyrin model. *Arthritis Rheum* **56,** 1273-1285, (2007).
409 Yu, J. R. & Leslie, K. S. Cryopyrin-associated periodic syndrome: an update on diagnosis and treatment response. *Curr Allergy Asthma Rep* **11,** 12-20, (2011).
410 Shinkai, K., McCalmont, T. H. & Leslie, K. S. Cryopyrin-associated periodic syndromes and autoinflammation. *Clin Exp Dermatol* **33,** 1-9, (2008).
411 Tran, T. A. Muckle-Wells syndrome: clinical perspectives. *Open Access Rheumatol* **9,** 123-129, (2017).
412 Tran, T. A. *et al.* Muckle-Wells syndrome and male hypofertility: a case series. *Semin Arthritis Rheum* **42,** 327-331, (2012).
413 Headley, A. P., Cordingley, F., Hawkins, P. N. & Riminton, D. S. Muckle-Wells cryopyrinopathy: complex phenotyping and response to therapy in a new multiplex kindred. *Inflammation* **37,** 396-401, (2014).
414 Rathinam, V. A. & Fitzgerald, K. A. Inflammasome Complexes: Emerging Mechanisms and Effector Functions. *Cell* **165,** 792-800, (2016).
415 Yu, J. *et al.* Inflammasome activation leads to Caspase-1-dependent mitochondrial damage and block of mitophagy. *Proc Natl Acad Sci U S A* **111,** 15514-15519, (2014).
416 Nakahira, K. *et al.* Autophagy proteins regulate innate immune responses by inhibiting the release of mitochondrial DNA mediated by the NALP3 inflammasome. *Nat Immunol* **12,** 222-230, (2011).
417 Sokolovska, A. *et al.* Activation of caspase-1 by the NLRP3 inflammasome regulates the NADPH oxidase NOX2 to control phagosome function. *Nat Immunol* **14,** 543-553, (2013).
418 Akhter, A. *et al.* Caspase-11 promotes the fusion of phagosomes harboring pathogenic bacteria with lysosomes by modulating actin polymerization. *Immunity* **37,** 35-47, (2012).

419 van Diepen, J. A. *et al.* Caspase-1 deficiency in mice reduces intestinal triglyceride absorption and hepatic triglyceride secretion. *J Lipid Res* **54,** 448-456, (2013).

420 Kotas, M. E. *et al.* Role of caspase-1 in regulation of triglyceride metabolism. *Proc Natl Acad Sci U S A* **110,** 4810-4815, (2013).

421 Guarda, G. *et al.* Differential Expression of NLRP3 among Hematopoietic Cells. *The Journal of Immunology* **186,** 2529, (2011).

422 Ali, M. F., Dasari, H., Van Keulen, V. P. & Carmona, E. M. Canonical Stimulation of the NLRP3 Inflammasome by Fungal Antigens Links Innate and Adaptive B-Lymphocyte Responses by Modulating IL-1beta and IgM Production. *Front Immunol* **8,** 1504, (2017).

423 Doitsh, G. *et al.* Cell death by pyroptosis drives CD4 T-cell depletion in HIV-1 infection. *Nature* **505,** 509-514, (2014).

424 Kumar, H. *et al.* Involvement of the NLRP3 inflammasome in innate and humoral adaptive immune responses to fungal beta-glucan. *J Immunol* **183,** 8061-8067, (2009).

425 Bruchard, M. *et al.* The receptor NLRP3 is a transcriptional regulator of TH2 differentiation. *Nat Immunol* **16,** 859-870, (2015).

426 Wang, C. *et al.* Chronic inflammation triggered by the NLRP3 inflammasome in myeloid cells promotes growth plate dysplasia by mesenchymal cells. *Sci Rep* **7,** 4880, (2017).

427 Bonar, S. L. *et al.* Constitutively activated NLRP3 inflammasome causes inflammation and abnormal skeletal development in mice. *PLoS One* **7,** e35979, (2012).

428 McCall, S. H. *et al.* Osteoblasts express NLRP3, a nucleotide-binding domain and leucine-rich repeat region containing receptor implicated in bacterially induced cell death. *J Bone Miner Res* **23,** 30-40, (2008).

429 Feldmann, J. *et al.* Chronic infantile neurological cutaneous and articular syndrome is caused by mutations in CIAS1, a gene highly expressed in polymorphonuclear cells and chondrocytes. *Am J Hum Genet* **71,** 198-203, (2002).

430 Sandanger, O. *et al.* The NLRP3 inflammasome is up-regulated in cardiac fibroblasts and mediates myocardial ischaemia-reperfusion injury. *Cardiovasc Res* **99,** 164-174, (2013).

431 Kawaguchi, M. *et al.* Inflammasome activation of cardiac fibroblasts is essential for myocardial ischemia/reperfusion injury. *Circulation* **123,** 594-604, (2011).

432 Wen, C. *et al.* Nalp3 inflammasome is activated and required for vascular smooth muscle cell calcification. *Int J Cardiol* **168,** 2242-2247, (2013).

433 Zhang, C. *et al.* Activation of Nod-like receptor protein 3 inflammasomes turns on podocyte injury and glomerular sclerosis in hyperhomocysteinemia. *Hypertension* **60,** 154-162, (2012).

434 Shigeoka, A. A. *et al.* An inflammasome-independent role for epithelial-expressed Nlrp3 in renal ischemia-reperfusion injury. *J Immunol* **185,** 6277-6285, (2010).

435 Hirota, J. A. *et al.* The airway epithelium nucleotide-binding domain and leucine-rich repeat protein 3 inflammasome is activated by urban particulate matter. *J Allergy Clin Immunol* **129,** 1116-1125 e1116, (2012).

436 Anderson, O. A., Finkelstein, A. & Shima, D. T. A2E induces IL-1ss production in retinal pigment epithelial cells via the NLRP3 inflammasome. *PLoS One* **8,** e67263, (2013).

437 Lech, M., Avila-Ferrufino, A., Skuginna, V., Susanti, H. E. & Anders, H. J. Quantitative expression of RIG-like helicase, NOD-like receptor and inflammasome-related mRNAs in humans and mice. *Int Immunol* **22,** 717-728, (2010).

438 Minutoli, L. *et al.* NLRP3 Inflammasome Involvement in the Organ Damage and Impaired Spermatogenesis Induced by Testicular Ischemia and Reperfusion in Mice. *J Pharmacol Exp Ther* **355,** 370-380, (2015).

439 Hayrabedyan, S. B., Zasheva, D. Y. & Todorova, K. O. NLRs Challenge Impacts Tight Junction Claudins In Sertoli Cells. *Folia Med (Plovdiv)* **57,** 43-48, (2015).

440 Mizushina, Y. *et al.* NLRP3 protein deficiency exacerbates hyperoxia-induced lethality through Stat3 protein signaling independent of interleukin-1beta. *J Biol Chem* **290,** 5065-5077, (2015).

441 Kostadinova, E. *et al.* NLRP3 protects alveolar barrier integrity by an inflammasome-independent increase of epithelial cell adherence. *Sci Rep* **6,** 30943, (2016).

442 Pulskens, W. P. *et al.* Nlrp3 prevents early renal interstitial edema and vascular permeability in unilateral ureteral obstruction. *PLoS One* **9,** e85775, (2014).

443 Wang, W. *et al.* Inflammasome-independent NLRP3 augments TGF-beta signaling in kidney epithelium. *J Immunol* **190,** 1239-1249, (2013).
444 Wang, H. *et al.* Inflammasome-independent NLRP3 is required for epithelial-mesenchymal transition in colon cancer cells. *Exp Cell Res* **342,** 184-192, (2016).
445 Bracey, N. A. *et al.* Mitochondrial NLRP3 protein induces reactive oxygen species to promote Smad protein signaling and fibrosis independent from the inflammasome. *J Biol Chem* **289,** 19571-19584, (2014).
446 Wynn, T. A. & Ramalingam, T. R. Mechanisms of fibrosis: therapeutic translation for fibrotic disease. *Nat Med* **18,** 1028-1040, (2012).
447 Zhang, G. *et al.* Genetic evidence for the coordinated regulation of collagen fibrillogenesis in the cornea by decorin and biglycan. *J Biol Chem* **284,** 8888-8897, (2009).
448 Wadhwa, S. *et al.* Impaired posterior frontal sutural fusion in the biglycan/decorin double deficient mice. *Bone* **40,** 861-866, (2007).
449 Castrillon, D. H., Quade, B. J., Wang, T. Y., Quigley, C. & Crum, C. P. The human VASA gene is specifically expressed in the germ cell lineage. *Proc Natl Acad Sci U S A* **97,** 9585-9590, (2000).
450 Fujiwara, Y. *et al.* Isolation of a DEAD-family protein gene that encodes a murine homolog of Drosophila vasa and its specific expression in germ cell lineage. *Proc Natl Acad Sci U S A* **91,** 12258-12262, (1994).
451 von Kopylow, K. *et al.* Screening for biomarkers of spermatogonia within the human testis: a whole genome approach. *Hum Reprod* **25,** 1104-1112, (2010).
452 Bridges, P. J. *et al.* Generation of Cyp17iCre transgenic mice and their application to conditionally delete estrogen receptor alpha (Esr1) from the ovary and testis. *Genesis* **46,** 499-505, (2008).
453 Zhang, P. *et al.* Developmental gonadal expression of the transcription factor SET and its target gene, P450c17 (17alpha-hydroxylase/c17,20 lyase). *DNA Cell Biol* **20,** 613-624, (2001).
454 Chistiakov, D. A., Killingsworth, M. C., Myasoedova, V. A., Orekhov, A. N. & Bobryshev, Y. V. CD68/macrosialin: not just a histochemical marker. *Lab Invest* **97,** 4-13, (2017).
455 Gicquel, T., Le Dare, B., Boichot, E. & Lagente, V. Purinergic receptors: new targets for the treatment of gout and fibrosis. *Fundam Clin Pharmacol* **31,** 136-146, (2017).
456 Burnstock, G. P2X ion channel receptors and inflammation. *Purinergic Signal* **12,** 59-67, (2016).
457 Chen, H. *et al.* Effect of P2X4R on airway inflammation and airway remodeling in allergic airway challenge in mice. *Mol Med Rep* **13,** 697-704, (2016).
458 Walenta, L. *et al.* ATP-mediated Events in Peritubular Cells Contribute to Sterile Testicular Inflammation. *Sci Rep* **8,** 1431, (2018).
459 He, M. L., Gonzalez-Iglesias, A. E. & Stojilkovic, S. S. Role of nucleotide P2 receptors in calcium signaling and prolactin release in pituitary lactotrophs. *J Biol Chem* **278,** 46270-46277, (2003).
460 Donnelly-Roberts, D. L., Namovic, M. T., Han, P. & Jarvis, M. F. Mammalian P2X7 receptor pharmacology: comparison of recombinant mouse, rat and human P2X7 receptors. *Br J Pharmacol* **157,** 1203-1214, (2009).
461 von Kugelgen, I. & Hoffmann, K. Pharmacology and structure of P2Y receptors. *Neuropharmacology* **104,** 50-61, (2016).
462 Stokes, L. *et al.* Characterization of a selective and potent antagonist of human P2X(7) receptors, AZ11645373. *Br J Pharmacol* **149,** 880-887, (2006).
463 Michel, A. D. *et al.* Mechanism of action of species-selective P2X(7) receptor antagonists. *Br J Pharmacol* **156,** 1312-1325, (2009).
464 Gelain, D. P., de Souza, L. F. & Bernard, E. A. Extracellular purines from cells of seminiferous tubules. *Mol Cell Biochem* **245,** 1-9, (2003).
465 Gelain, D. P. *et al.* Effects of follicle-stimulating hormone and vitamin A upon purinergic secretion by rat Sertoli cells. *Mol Cell Biochem* **278,** 185-194, (2005).
466 Wang, L. *et al.* ATP release from mast cells by physical stimulation: a putative early step in activation of acupuncture points. *Evid Based Complement Alternat Med* **2013,** 350949, (2013).

467 Osipchuk, Y. & Cahalan, M. Cell-to-cell spread of calcium signals mediated by ATP receptors in mast cells. *Nature* **359,** 241-244, (1992).

468 Trautmann, A. Extracellular ATP in the immune system: more than just a "danger signal". *Sci Signal* **2,** pe6, (2009).

469 Szklarczyk, D. *et al.* STRING v10: protein-protein interaction networks, integrated over the tree of life. *Nucleic Acids Res* **43,** D447-452, (2015).

470 Sharma, D. & Kanneganti, T. D. The cell biology of inflammasomes: Mechanisms of inflammasome activation and regulation. *J Cell Biol* **213,** 617-629, (2016).

471 Abderrazak, A. *et al.* NLRP3 inflammasome: from a danger signal sensor to a regulatory node of oxidative stress and inflammatory diseases. *Redox Biol* **4,** 296-307, (2015).

472 Walenta, L. *et al.* NLRP3 in Somatic Non-Immune Cells of Rodent and Primate Testes. *Reproduction*, (2018).

473 Rock, K. *et al.* Chronic UVB-irradiation actuates perpetuated dermal matrix remodeling in female mice: Protective role of estrogen. *Sci Rep* **6,** 30482, (2016).

474 Piprek, R. P., Kolasa, M., Podkowa, D., Kloc, M. & Kubiak, J. Z. Transcriptional profiling validates involvement of extracellular matrix and proteinases genes in mouse gonad development. *Mech Dev* **149,** 9-19, (2018).

475 Miqueloto, C. A. & Zorn, T. M. Characterization and distribution of hyaluronan and the proteoglycans decorin, biglycan and perlecan in the developing embryonic mouse gonad. *J Anat* **211,** 16-25, (2007).

476 Ni, G. X., Li, Z. & Zhou, Y. Z. The role of small leucine-rich proteoglycans in osteoarthritis pathogenesis. *Osteoarthritis Cartilage* **22,** 896-903, (2014).

477 Nuka, S. *et al.* Phenotypic characterization of epiphycan-deficient and epiphycan/biglycan double-deficient mice. *Osteoarthritis Cartilage* **18,** 88-96, (2010).

478 Kilts, T. *et al.* Potential roles for the small leucine-rich proteoglycans biglycan and fibromodulin in ectopic ossification of tendon induced by exercise and in modulating rotarod performance. *Scand J Med Sci Sports* **19,** 536-546, (2009).

479 Casar, J. C., McKechnie, B. A., Fallon, J. R., Young, M. F. & Brandan, E. Transient up-regulation of biglycan during skeletal muscle regeneration: delayed fiber growth along with decorin increase in biglycan-deficient mice. *Dev Biol* **268,** 358-371, (2004).

480 Yu, W. *et al.* Estrogen promotes Leydig cell engulfment by macrophages in male infertility. *J Clin Invest* **124,** 2709-2721, (2014).

481 Lin, W. *et al.* Molecular mechanisms of bladder outlet obstruction in transgenic male mice overexpressing aromatase (Cyp19a1). *Am J Pathol* **178,** 1233-1244, (2011).

482 Calippe, B. *et al.* 17Beta-estradiol promotes TLR4-triggered proinflammatory mediator production through direct estrogen receptor alpha signaling in macrophages in vivo. *J Immunol* **185,** 1169-1176, (2010).

483 Li, X., Li, H., Jia, L., Li, X. & Rahman, N. Oestrogen action and male fertility: experimental and clinical findings. *Cell Mol Life Sci* **72,** 3915-3930, (2015).

484 Solini, A. *et al.* Purinergic modulation of mesangial extracellular matrix production: role in diabetic and other glomerular diseases. *Kidney Int* **67,** 875-885, (2005).

485 Huang, C. *et al.* P2X7 blockade attenuates mouse liver fibrosis. *Mol Med Rep* **9,** 57-62, (2014).

486 Mezzaroma, E. *et al.* The inflammasome promotes adverse cardiac remodeling following acute myocardial infarction in the mouse. *Proc Natl Acad Sci U S A* **108,** 19725-19730, (2011).

487 Thomay, A. A. *et al.* Disruption of interleukin-1 signaling improves the quality of wound healing. *Am J Pathol* **174,** 2129-2136, (2009).

488 Sathanoori, R., Sward, K., Olde, B. & Erlinge, D. The ATP Receptors P2X7 and P2X4 Modulate High Glucose and Palmitate-Induced Inflammatory Responses in Endothelial Cells. *PLoS One* **10,** e0125111, (2015).

489 Solini, A., Chiozzi, P., Morelli, A., Fellin, R. & Di Virgilio, F. Human primary fibroblasts in vitro express a purinergic P2X7 receptor coupled to ion fluxes, microvesicle formation and IL-6 release. *J Cell Sci* **112 (Pt 3),** 297-305, (1999).

490 Xu, H. *et al.* High fatty acids modulate P2X(7) expression and IL-6 release via the p38 MAPK pathway in PC12 cells. *Brain Res Bull* **94,** 63-70, (2013).

491 Shieh, C. H., Heinrich, A., Serchov, T., van Calker, D. & Biber, K. P2X7-dependent, but differentially regulated release of IL-6, CCL2, and TNF-alpha in cultured mouse microglia. *Glia* **62,** 592-607, (2014).

492 Kurashima, Y. *et al.* Extracellular ATP mediates mast cell-dependent intestinal inflammation through P2X7 purinoceptors. *Nat Commun* **3,** 1034, (2012).

493 Panenka, W. *et al.* P2X7-like receptor activation in astrocytes increases chemokine monocyte chemoattractant protein-1 expression via mitogen-activated protein kinase. *J Neurosci* **21,** 7135-7142, (2001).

494 Braganhol, E. *et al.* Nucleotide receptors control IL-8/CXCL8 and MCP-1/CCL2 secretions as well as proliferation in human glioma cells. *Biochim Biophys Acta* **1852,** 120-130, (2015).

495 Le, Y., Zhou, Y., Iribarren, P. & Wang, J. Chemokines and chemokine receptors: their manifold roles in homeostasis and disease. *Cell Mol Immunol* **1,** 95-104, (2004).

496 Deshmane, S. L., Kremlev, S., Amini, S. & Sawaya, B. E. Monocyte chemoattractant protein-1 (MCP-1): an overview. *J Interferon Cytokine Res* **29,** 313-326, (2009).

497 Layhadi, J. A., Turner, J., Crossman, D. & Fountain, S. J. ATP Evokes Ca(2+) Responses and CXCL5 Secretion via P2X4 Receptor Activation in Human Monocyte-Derived Macrophages. *J Immunol* **200,** 1159-1168, (2018).

498 Prefontaine, D. *et al.* Increased expression of IL-33 in severe asthma: evidence of expression by airway smooth muscle cells. *J Immunol* **183,** 5094-5103, (2009).

499 Kaur, D. *et al.* IL-33 drives airway hyper-responsiveness through IL-13-mediated mast cell: airway smooth muscle crosstalk. *Allergy* **70,** 556-567, (2015).

500 Shimokawa, C. *et al.* Mast Cells Are Crucial for Induction of Group 2 Innate Lymphoid Cells and Clearance of Helminth Infections. *Immunity* **46,** 863-874 e864, (2017).

501 Zarpelon, A. C. *et al.* Spinal cord oligodendrocyte-derived alarmin IL-33 mediates neuropathic pain. *Faseb j* **30,** 54-65, (2016).

502 Machelska, H. & Celik, M. O. Recent advances in understanding neuropathic pain: glia, sex differences, and epigenetics. *F1000Res* **5,** 2743, (2016).

503 Liu, S. *et al.* Spinal IL-33/ST2 Signaling Contributes to Neuropathic Pain via Neuronal CaMKII-CREB and Astroglial JAK2-STAT3 Cascades in Mice. *Anesthesiology* **123,** 1154-1169, (2015).

504 Tsuda, M., Masuda, T., Tozaki-Saitoh, H. & Inoue, K. P2X4 receptors and neuropathic pain. *Front Cell Neurosci* **7,** 191, (2013).

505 Gicquel, T. *et al.* IL-1beta production is dependent on the activation of purinergic receptors and NLRP3 pathway in human macrophages. *Faseb j* **29,** 4162-4173, (2015).

506 Zhao, J. *et al.* P2X7 blockade attenuates murine lupus nephritis by inhibiting activation of the NLRP3/ASC/caspase 1 pathway. *Arthritis Rheum* **65,** 3176-3185, (2013).

507 Garcia, K. *et al.* ATP Induces IL-1beta Secretion in Neisseria gonorrhoeae-Infected Human Macrophages by a Mechanism Not Related to the NLRP3/ASC/Caspase-1 Axis. *Mediators Inflamm* **2016,** 1258504, (2016).

508 Weber, A., Wasiliew, P. & Kracht, M. Interleukin-1 (IL-1) pathway. *Sci Signal* **3,** cm1, (2010).

509 Polentarutti, N. *et al.* Expression of monocyte chemotactic protein-3 in human monocytes and endothelial cells. *Eur Cytokine Netw* **8,** 271-274, (1997).

510 Jung, Y. *et al.* Regulation of SDF-1 (CXCL12) production by osteoblasts; a possible mechanism for stem cell homing. *Bone* **38,** 497-508, (2006).

511 Scheller, J., Chalaris, A., Schmidt-Arras, D. & Rose-John, S. The pro- and anti-inflammatory properties of the cytokine interleukin-6. *Biochim Biophys Acta* **1813,** 878-888, (2011).

512 Jones, S. A. Directing transition from innate to acquired immunity: defining a role for IL-6. *J Immunol* **175,** 3463-3468, (2005).

513 McLoughlin, R. M. *et al.* Differential regulation of neutrophil-activating chemokines by IL-6 and its soluble receptor isoforms. *J Immunol* **172,** 5676-5683, (2004).

514 Romano, M. *et al.* Role of IL-6 and its soluble receptor in induction of chemokines and leukocyte recruitment. *Immunity* **6,** 315-325, (1997).

515 Maekawa, M., Kamimura, K. & Nagano, T. Peritubular myoid cells in the testis: their structure and function. *Arch Histol Cytol* **59,** 1-13, (1996).

516 Forst, A. L. *et al.* Podocyte Purinergic P2X4 Channels Are Mechanotransducers That Mediate Cytoskeletal Disorganization. *J Am Soc Nephrol* **27,** 848-862, (2016).
517 Pubill, D. *et al.* ATP induces intracellular calcium increases and actin cytoskeleton disaggregation via P2x receptors. *Cell Calcium* **29,** 299-309, (2001).
518 Kim, M. J. *et al.* Exaggerated renal fibrosis in P2X4 receptor-deficient mice following unilateral ureteric obstruction. *Nephrol Dial Transplant* **29,** 1350-1361, (2014).
519 Bushman, T. L. & Kuemmerle, J. F. IGFBP-3 and IGFBP-5 production by human intestinal muscle: reciprocal regulation by endogenous TGF-beta1. *Am J Physiol* **275,** G1282-1290, (1998).
520 Flynn, R. S. *et al.* Endogenous IGFBP-3 regulates excess collagen expression in intestinal smooth muscle cells of Crohn's disease strictures. *Inflamm Bowel Dis* **17,** 193-201, (2011).
521 Liu, B., Weinzimer, S. A., Gibson, T. B., Mascarenhas, D. & Cohen, P. Type Ialpha collagen is an IGFBP-3 binding protein. *Growth Horm IGF Res* **13,** 89-97, (2003).
522 Nam, T. J., Busby, W. H., Jr., Rees, C. & Clemmons, D. R. Thrombospondin and osteopontin bind to insulin-like growth factor (IGF)-binding protein-5 leading to an alteration in IGF-I-stimulated cell growth. *Endocrinology* **141,** 1100-1106, (2000).
523 Morris, A. H. & Kyriakides, T. R. Matricellular proteins and biomaterials. *Matrix Biol* **37,** 183-191, (2014).
524 Bornstein, P. & Sage, E. H. Matricellular proteins: extracellular modulators of cell function. *Curr Opin Cell Biol* **14,** 608-616, (2002).
525 Sodhi, C. P., Phadke, S. A., Batlle, D. & Sahai, A. Hypoxia stimulates osteopontin expression and proliferation of cultured vascular smooth muscle cells: potentiation by high glucose. *Diabetes* **50,** 1482-1490, (2001).
526 Ozaki, T. *et al.* The P2X4 receptor is required for neuroprotection via ischemic preconditioning. *Sci Rep* **6,** 25893, (2016).
527 Kahles, F., Findeisen, H. M. & Bruemmer, D. Osteopontin: A novel regulator at the cross roads of inflammation, obesity and diabetes. *Mol Metab* **3,** 384-393, (2014).
528 Trueblood, N. A. *et al.* Exaggerated left ventricular dilation and reduced collagen deposition after myocardial infarction in mice lacking osteopontin. *Circ Res* **88,** 1080-1087, (2001).
529 Zanotti, S. *et al.* Osteopontin is highly expressed in severely dystrophic muscle and seems to play a role in muscle regeneration and fibrosis. *Histopathology* **59,** 1215-1228, (2011).
530 Collins, A. R. *et al.* Osteopontin modulates angiotensin II-induced fibrosis in the intact murine heart. *J Am Coll Cardiol* **43,** 1698-1705, (2004).
531 Kim, S. & Shin, T. Immunohistochemical study of osteopontin in boar testis. *J Vet Sci* **8,** 107-110, (2007).
532 Luedtke, C. C. *et al.* Osteopontin expression and regulation in the testis, efferent ducts, and epididymis of rats during postnatal development through to adulthood. *Biol Reprod* **66,** 1437-1448, (2002).
533 Siiteri, J. E., Ensrud, K. M., Moore, A. & Hamilton, D. W. Identification of osteopontin (OPN) mRNA and protein in the rat testis and epididymis, and on sperm. *Mol Reprod Dev* **40,** 16-28, (1995).
534 Wilson, M. J., Liaw, L. & Koopman, P. Osteopontin and related SIBLING glycoprotein genes are expressed by Sertoli cells during mouse testis development. *Dev Dyn* **233,** 1488-1495, (2005).
535 Resovi, A., Pinessi, D., Chiorino, G. & Taraboletti, G. Current understanding of the thrombospondin-1 interactome. *Matrix Biol* **37,** 83-91, (2014).
536 Sweetwyne, M. T., Pallero, M. A., Lu, A., Van Duyn Graham, L. & Murphy-Ullrich, J. E. The calreticulin-binding sequence of thrombospondin 1 regulates collagen expression and organization during tissue remodeling. *Am J Pathol* **177,** 1710-1724, (2010).
537 Lawler, J. *et al.* Thrombospondin-1 is required for normal murine pulmonary homeostasis and its absence causes pneumonia. *J Clin Invest* **101,** 982-992, (1998).
538 Crawford, S. E. *et al.* Thrombospondin-1 is a major activator of TGF-beta1 in vivo. *Cell* **93,** 1159-1170, (1998).
539 Wynn, T. A. Cellular and molecular mechanisms of fibrosis. *J Pathol* **214,** 199-210, (2008).

540 Ferrari, D. *et al.* Purinergic stimulation of human mesenchymal stem cells potentiates their chemotactic response to CXCL12 and increases the homing capacity and production of proinflammatory cytokines. *Exp Hematol* **39,** 360-374, 374 e361-365, (2011).

541 Heine, P. *et al.* The C-terminal cysteine-rich region dictates specific catalytic properties in chimeras of the ectonucleotidases NTPDase1 and NTPDase2. *Eur J Biochem* **268,** 364-373, (2001).

542 Strater, N. Ecto-5'-nucleotidase: Structure function relationships. *Purinergic Signal* **2,** 343-350, (2006).

543 Zanin, R. F. *et al.* Differential macrophage activation alters the expression profile of NTPDase and ecto-5'-nucleotidase. *PLoS One* **7,** e31205, (2012).

544 Levesque, S. A., Kukulski, F., Enjyoji, K., Robson, S. C. & Sevigny, J. NTPDase1 governs P2X7-dependent functions in murine macrophages. *Eur J Immunol* **40,** 1473-1485, (2010).

545 Bulanova, E. & Bulfone-Paus, S. P2 receptor-mediated signaling in mast cell biology. *Purinergic Signal* **6,** 3-17, (2010).

546 Kuhny, M., Hochdorfer, T., Ayata, C. K., Idzko, M. & Huber, M. CD39 is a negative regulator of P2X7-mediated inflammatory cell death in mast cells. *Cell Commun Signal* **12,** 40, (2014).

547 Martin-Satue, M. *et al.* High expression and activity of ecto-5'-nucleotidase/CD73 in the male murine reproductive tract. *Histochem Cell Biol* **133,** 659-668, (2010).

548 Martin-Satue, M. *et al.* Localization of plasma membrane bound NTPDases in the murine reproductive tract. *Histochem Cell Biol* **131,** 615-628, (2009).

549 Yegutkin, G. G. Nucleotide- and nucleoside-converting ectoenzymes: Important modulators of purinergic signalling cascade. *Biochim Biophys Acta* **1783,** 673-694, (2008).

550 Pilatz, A. *et al.* [Seminal cytokines: is quantification useful in urogenital disorders?]. *Urologe A* **52,** 359-366, (2013).

551 Kummer, J. A. *et al.* Inflammasome components NALP 1 and 3 show distinct but separate expression profiles in human tissues suggesting a site-specific role in the inflammatory response. *J Histochem Cytochem* **55,** 443-452, (2007).

552 Franca, L. R., Hess, R. A., Dufour, J. M., Hofmann, M. C. & Griswold, M. D. The Sertoli cell: one hundred fifty years of beauty and plasticity. *Andrology* **4,** 189-212, (2016).

553 Kaur, G., Thompson, L. A. & Dufour, J. M. Sertoli cells--immunological sentinels of spermatogenesis. *Semin Cell Dev Biol* **30,** 36-44, (2014).

554 Lasithiotaki, I. *et al.* NLRP3 inflammasome expression in idiopathic pulmonary fibrosis and rheumatoid lung. *Eur Respir J* **47,** 910-918, (2016).

555 De Nardo, D., De Nardo, C. M. & Latz, E. New Insights into Mechanisms Controlling the NLRP3 Inflammasome and Its Role in Lung Disease. *Am J Pathol* **184,** 42-54, (2014).

556 Jiang, S. *et al.* Potentiation of hepatic stellate cell activation by extracellular ATP is dependent on P2X7R-mediated NLRP3 inflammasome activation. *Pharmacol Res* **117,** 82-93, (2017).

557 Artlett, C. M. The Role of the NLRP3 Inflammasome in Fibrosis. *Open Rheumatol J* **6,** 80-86, (2012).

558 Hayrabedyan, S. *et al.* Sertoli cells have a functional NALP3 inflammasome that can modulate autophagy and cytokine production. *Sci Rep* **6,** 18896, (2016).

559 Stern, J. A. *et al.* Long-term outcome following testicular ischemia in the rat. *J Androl* **11,** 390-395, (1990).

560 Cass, A. S. Torsion of the testis. *Postgrad Med* **87,** 69-70, 73-64, (1990).

561 Tian, X. *et al.* NLRP3 Inflammasome Mediates Dormant Neutrophil Recruitment following Sterile Lung Injury and Protects against Subsequent Bacterial Pneumonia in Mice. *Front Immunol* **8,** 1337, (2017).

562 Freeman, L. *et al.* NLR members NLRC4 and NLRP3 mediate sterile inflammasome activation in microglia and astrocytes. *J Exp Med* **214,** 1351-1370, (2017).

563 Amores-Iniesta, J. *et al.* Extracellular ATP Activates the NLRP3 Inflammasome and Is an Early Danger Signal of Skin Allograft Rejection. *Cell Rep* **21,** 3414-3426, (2017).

564 Gombault, A., Baron, L. & Couillin, I. ATP release and purinergic signaling in NLRP3 inflammasome activation. *Front Immunol* **3,** 414, (2012).

565 Ghiringhelli, F. *et al.* Activation of the NLRP3 inflammasome in dendritic cells induces IL-1beta-dependent adaptive immunity against tumors. *Nat Med* **15,** 1170-1178, (2009).

566 Hayoz, S., Jia, C. & Hegg, C. Mechanisms of constitutive and ATP-evoked ATP release in neonatal mouse olfactory epithelium. *BMC Neurosci* **13,** 53, (2012).
567 Anderson, C. M., Bergher, J. P. & Swanson, R. A. ATP-induced ATP release from astrocytes. *J Neurochem* **88,** 246-256, (2004).
568 Katsuragi, T. *et al.* Existence of ATP-evoked ATP release system in smooth muscles. *J Pharmacol Exp Ther* **259,** 513-518, (1991).
569 Praetorius, H. A. & Leipziger, J. ATP release from non-excitable cells. *Purinergic Signal* **5,** 433-446, (2009).
570 Cassel, S. L. *et al.* Inflammasome-independent IL-1beta mediates autoinflammatory disease in Pstpip2-deficient mice. *Proc Natl Acad Sci U S A* **111,** 1072-1077, (2014).
571 Leslie, K. S. *et al.* Phenotype, genotype, and sustained response to anakinra in 22 patients with autoinflammatory disease associated with CIAS-1/NALP3 mutations. *Arch Dermatol* **142,** 1591-1597, (2006).
572 Fraczek, M. & Kurpisz, M. Inflammatory mediators exert toxic effects of oxidative stress on human spermatozoa. *J Androl* **28,** 325-333, (2007).
573 Bentz, E. K. *et al.* A polymorphism of the interleukin-1 beta gene is associated with sperm pathology in humans. *Fertil Steril* **88,** 751-753, (2007).
574 Gruschwitz, M. S., Brezinschek, R. & Brezinschek, H. P. Cytokine levels in the seminal plasma of infertile males. *J Androl* **17,** 158-163, (1996).
575 Meinzer, U., Marie, I., Koné-Paut, I. & Tran, T.-A. Hypofertility in Muckle Wells syndrome and treatment with IL-1 targeting drugs. *Pediatric Rheumatology Online Journal* **9,** P14-P14, (2011).
576 Stanton, P. G. Regulation of the blood-testis barrier. *Semin Cell Dev Biol* **59,** 166-173, (2016).
577 Nilsson, M. E. *et al.* Measurement of a Comprehensive Sex Steroid Profile in Rodent Serum by High-Sensitive Gas Chromatography-Tandem Mass Spectrometry. *Endocrinology* **156,** 2492-2502, (2015).
578 Hsu, S. M., Raine, L. & Fanger, H. The use of antiavidin antibody and avidin-biotin-peroxidase complex in immunoperoxidase technics. *Am J Clin Pathol* **75,** 816-821, (1981).
579 Schindelin, J. *et al.* Fiji: an open-source platform for biological-image analysis. *Nat Methods* **9,** 676-682, (2012).
580 Jaccard, N. *et al.* Automated method for the rapid and precise estimation of adherent cell culture characteristics from phase contrast microscopy images. *Biotechnol Bioeng* **111,** 504-517, (2014).
581 Pfaffl, M. W. A new mathematical model for relative quantification in real-time RT-PCR. *Nucleic Acids Res* **29,** e45, (2001).
582 Lowry, O. H., Rosebrough, N. J., Farr, A. L. & Randall, R. J. Protein measurement with the Folin phenol reagent. *J Biol Chem* **193,** 265-275, (1951).
583 Peterson, G. L. Review of the Folin phenol protein quantitation method of Lowry, Rosebrough, Farr and Randall. *Anal Biochem* **100,** 201-220, (1979).
584 Rossi, S. P. *et al.* Alpha 1 adrenergic receptor-mediated inflammatory responses in human testicular peritubular cells. *Mol Cell Endocrinol*, (2018).
585 Kong, F. *et al.* Alpha1-Adrenergic Receptor Activation Stimulates Calcium Entry and Proliferation via TRPC6 Channels in Cultured Human Mesangial Cells. *Cellular Physiology and Biochemistry* **36,** 1928-1938, (2015).

Abbreviations

AC	Adenylate cyclase
ACTA	Actin, aortic smooth muscle
ADP	Adenosine 5’monophosphate
ADR	Adrenergic receptor
AI	Aromatase inhibitor
AMP	Adenosine 5’diphosphate
ANOVA	Analysis of variance
APS	Ammonium persulfate
AROM	Aromatase
ASC	Apoptosis associated speck-like protein containing a CARD
ATP	Adenosine 5’triphosphate
AZ11645373	3-[1-[[(3'-Nitro[1,1'-biphenyl]-4-yl)oxy]methyl]-3-(4-pyridinyl)propyl]-2,4-thiazolidinedione
BGN	Biglycan
BMP	Bone morphogenetic protein
bp	Base pair
BRCC3	BRCA1/BRCA2-containing complex subunit 3
BSA	Bovine serum albumin
BzATP	2′(3′)-O-(4-Benzoylbenzoyl)adenosine 5′-triphosphate
cAMP	Cyclic adenosine 5’monophosphate
CAPS	Cyropyrin-associated periodic syndrome
CARD	Caspase activation and recruitment domain
CASR	Calcium sensing receptor
CCL	C-C motif chemokine ligand
CD	Cluster of differentiation
cDNA	Complementary deoxyribonucleic acid
CINCA	Chronic infantile neurological cutaneous articular
CNN1	Calponin
COL	Collagen
COX	Cyclooxygenase
C_q	Quantification cycle
CXCL	C-X-C motif chemokine ligand
CYP17A1	Cytochrome P450 family 17 subfamily A member 1
CYP19A1	Cytochrome P450 family 19 subfamily A member 1
d	Distilled
DAMP	Danger-associated molecular pattern
DCN	Decorin
dd	Bidistilled
DDX4	DEAD-box helicase 4
DMEM	Dulbecco’s Modified Eagle’s Medium
DMSO	Dimethyl sulfoxide
DNA	Deoxyribonucleic acid

DNase	Deoxyribonuclease
dNTP	Deoxynucleotide triphosphate
DTT	Dithiotreitol
EC	Effective concentration
ECM	Extracellular matrix
EDTA	Ethylendiaminetetraacetic acid
ERK	Extracellular-signal regulated kinase
EtOH	Ethanol
FBS	Fetal bovine serum
FCAS	Familial cold autoinflammatory syndrome
FGFR3	Fibroblast growth factor receptor 3
GAG	Glycosaminoglycan
GDNF	Glial cell line-derived neurotrophic factor
GO	Gene ontology
GPCR	G-protein coupled receptor
GSDMD	Gasdermin D
HTPC	Human testicular peritubular cell
IAPP	Islet amyloid polypeptide
IGFBP	insulin-like growth factor-binding protein
IgG	Immunoglobulin G
IHC	Immunohistochemistry
IL	Interleukin
IP_3	Inositol triphosphate
KEGG	Kyoto Encyclopedia of Genes and Genomes
LDH	Lactate dehydrogenase
LOX	Lysyl oxidase
LPS	Lipopolysaccharide
LRR	Leucine-rich repeat
MAPK	Mitogen-activated protein kinase
mRNA	Messenger ribonucleic acid
mROS	mitochondrial reactive oxygen species
MS/MS	Tandem mass spectrometry
MWS	Muckle-Wells syndrome
MyD88	Myeloid differentiation primary response 88
NACHT	AIP, CIITA, HET-E and TP1 domain with NTPase activity
NEK7	NIMA-related kinase 7
NFκB	Nuclear factor kappa B
NLR	NOD-like receptor
NLRP3	NLR family pyrin domain containing 3
P2RX	P2X receptor
P2RY	P2Y receptor
PAGE	Polyacrylamide gel electrophoresis
PAMP	Pathogen-associated molecular pattern
PAR2	Protease activated receptor 2

PBS	Phosphate buffered saline
PIPES	Piperazine-N,N′-bis(2-ethanesulfonic acid)
PLC	Phospholipase C
PRR	Pattern recognition receptor
PTX3	Pentraxin 3
PYD	Pyrin domain
qRT-PCR	Quantitative real time polymerase chain reaction
RNA	Ribonucleic acid
RNase	Ribonuclease
ROS	Reactive oxygen species
rpm	Rounds per minute
RT-PCR	Reverse transcription polymerase chain reaction
SD	Standard deviation
SDS	Sodiumdodecylsulfate
SEM	Standard error of the mean
SLRP	Small leucine-rich proteoglycan
SPP1	Osteopontin, secreted phosphoprotein 1
SSC	Spermatogonial stem cell
T2D	Type 2 diabetes mellitus
T_a	Annealing temperature
TBE	Tris borate EDTA
TEMED	N,N,N’,N’-Tetramethylethylenediamine
TESE	Testicular sperm extraction
TGFβ	Transforming growth factor β
THBS	thrombospondin
TLR	Toll-like receptor
TNFα	Tumor necrosis factor α
TRIF	TIR-domain-containing adapter-inducing interferon β
Tris	Tris(hydroxymethyl)aminomethane
U	Unit
UDP	Uridine 5’diphosphate
UTP	Uridine 5’triphosphate
v	Volume
VEGF	Vascular endothelial growth factor
w	Weight
WB	Western Blot
WT	Wild type

List of Figures

List of Tables

Acknowledgements

First of all, I want to thank Prof. Dr. Artur Mayerhofer for giving me the opportunity to work in reproductive biology and choosing this interesting and challenging topic. I am extremely grateful for your guidance and support during my thesis. I value your opinions and input on my work, yet most of all I appreciate your enthusiasm for science and your optimism.

I want to thank PD Dr. Lars Kunz for supervising my thesis. I immensely appreciated your interest in my research projects and your critical and careful advice on how to proceed with experiments. In particular, I am grateful for your effort and scrutiny in finishing the written version of this thesis.
In this respect, I would like to thank all members of my thesis committee, especially Prof. Dr. Gisela Grupe for agreeing to be the second examiner.

Without the assistance of our collaborators, many questions that are integral parts of this thesis could not have been addressed.
I thank Prof. Dr. J. Ullrich Schwarzer and Prof. Dr. Frank-Michael Köhn for contributing patient samples that were indispensable for cellular studies and immunohistochemical stainings.
The Department of Physiology at the University of Turku developed the *AROM*$^{+}$ mice and in collaboration with them the *Bgn* knock-out crossings and analyses were performed. I want to thank Prof. Dr. Matti Poutanen and Dr. Leena Strauss for the opportunity to conduct the mouse studies in Turku and the helpful discussions regarding mouse analyses and results. Special thanks go to Hanna Heikelä for your invaluable help with lab work and analyses during my visits and for being such a wonderful and dedicated host. I further thank Dr. Marian F. Young from NIH National Institute of Dental and Craniofacial Research (Bethesda, MD, USA) for generously providing the *Bgn* knock-out mouse.
I want to thank Prof. Dr. Marc Spehr and Dr. David Fleck at the Department of Chemosensation at RWTH Aachen University for taking up interest in the electrophysiological properties of HTPCs. I greatly appreciate your contribution on purinergic receptors and signaling in HTPCs and I thank you for inviting me to some hands-on experience.
I further thank Dr. Georg J. Arnold and Dr. Thomas Fröhlich from the LAFUGA at the LMU Gene Center for performing mass spectrometric analyses of HTPC lysates and assistance with data analysis.
I am also grateful for our in-house collaboration with Prof. Dr. Axel Imhof and Dr. Shibojyoti Lahiri at the Protein Analysis Unit who introduced me to *in situ* MALDI imaging mass spectrometry and I am quite excited to finish our project.

All current and former lab members were essential in executing and completing this thesis – Daniel Aigner, Konstantin Bagnjuk, Dr. Jan Blohberger, Theresa Buck, Fangfang Chen, Kim Dietrich, Katja Eubler, Stefanie Gruschka, Theo Hack, Carola Herrmann, Dr. Andreas Huber, Verena Kast, Dr. Christine Mayer, Dr. Sabine Meinel, Karin Metzrath, Annika

Missel, Dr. Verónica Rey, Dr. Soledad Rossi, Nina Schmid, Astrid Tiefenbacher, Dr. Harald Welter and Dr. Stefanie Windschüttl.
I am indebted to our technicians for sharing their experience and always lending their helping hand during experiments. The post-docs and my fellow doctoral students are acknowledged for endless, but eventually helpful discussions on protocols and data analysis as well as their invaluable ideas on my experimental proceeding. I thank my students for contributing to this thesis and asking critical questions.
I want thank all of you for making the lab an enjoyable place to work and for providing coffee, cake, pretzels or moral support whenever needed. It was my pleasure to getting to know you and working with you. You are not merely colleagues, but the friends-that-you-work-with.

Last, but not least, I would like to thank my family, my parents Monika and Josef and my sister Hanna. You taught me to believe in myself and to find and follow my own path. I am incredibly grateful for your never-ending love and encouragement.
To my husband Constantin – I cannot thank you enough for being by my side along this journey, supporting and cherishing me. I could never wish for a more loving partner and best friend.

APPENDIX

Supporting results

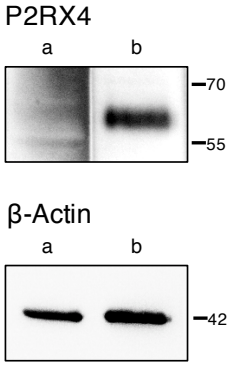

Supplementary Figure 1 Pre-adsorption control for P2RX4 expression in HTPCs.
Identity of the P2RX4 band in Western blotting (upper panel) was confirmed via pre-adsorption of the anti-P2RX4 antibody (a) versus antibody only (b). No signal was detected in the pre-adsorbed control. Detection of β-Actin (lower panel) on the same membrane served as protein loading control. Labels indicate corresponding protein weight in [kDa].

Additional projects during the thesis

α1-adrenergic signaling in HTPCs

Stress-induced catecholamines may foster an inflammatory environment in the testis, thereby contributing to testicular changes that eventually cause infertility. The catecholamine epinephrine is released during stress response of the sympathetic nervous system and non-selectively activates α and β adrenergic receptors (ADRs). Various testicular cell types express ADRs and could thus be targets of catecholamine actions. HTPCs were found to possess ADR isoforms α1(B,D), β1 and β2. Selective agonist treatment of HTPCs revealed that phenylephrine (α1-ADR agonist) mimicked epinephrine responses in HTPCs. Both molecules induced COX2 expression and elevated IL6 as well as CCL2 production and secretion in HTPCs. These effects were obliterated in the presence of the inverse α1-ADR prazosin. Hence, α1-ADR-mediated signaling in HTPCs participates in testicular inflammation[584].

My contribution to this project was the functional assessment of α1-ADR signaling. Since α1-ADR is a GPCR that activates PLC eventually leading to intracellular Ca^{2+} mobilization[585], Ca^{2+} imaging of HTPCs was employed. Exposure of HTPCs to the selective α1-ADR agonist phenylephrine uncovered robust and transient elevations of intracellular [Ca^{2+}] in two independent experiments (Supplementary Figure 2).

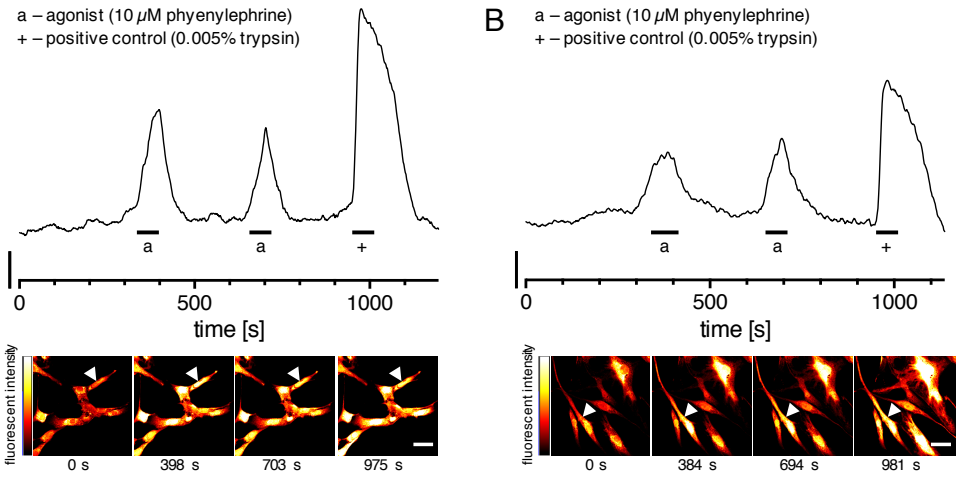

Supplementary Figure 2 Functional α1-ADR assessment in HTPCs via calcium imaging.
Top: Graphic representation of representative Ca^{2+}-dependent fluorescent signals in individual HTPCs loaded with Fluo4 or Fluoforte (5 µM) over time when exposed to different conditions. Stimulation time periods are indicated by horizontal bars. 0.005% trypsin was used as a positive control (+) in all experiments. y axis bar represents 20 a.u. fluorescent intensity. Bottom: Pseudocolor single frame images of fluorescent intensity at the beginning of the experiment (0 s) and at peak elevations during agent and positive control exposure depict the response of the measured HTPCs (arrowhead). Bars = 50 µm. **A/B.** Response to agonist exposure (a, 10 µM phenylephrine) revealed robust Ca^{2+} transients in HTPCs in two independent experiments.

Publications

Mayer C, Adam M, **Glashauser L**, Dietrich K, Schwarzer JU, Koehn FM, Strauss L, Welter H, Poutanen M, Mayerhofer A. (2016). Sterile Inflammation as a Factor in Human Male Infertility: Involvement of Toll like receptor 2, Biglycan and Peritubular Cells. *Sci Rep,* 6:37128.

Walenta L, Fleck D, Froehlich T, von Eysmondt H, Arnold GJ, Spehr J, Schwarzer JU, Koehn FM, Spehr M, Mayerhofer A. (2018). ATP-mediated Events in Peritubular Cells Contribute to Sterile Testicular Inflammation. *Sci Rep,* 8(1): 1431.

Rossi SP, **Walenta L**, Rey-Ares V, Koehn FM, Schwarzer JU, Welter H, Calandra RS, Frungieri MB, Mayerhofer A. (2018). Alpha-1 Adrenergic Receptor-mediated Inflammatory Responses in Human Testicular Peritubular Cells. *Mol Cell Endocrinol* (*in press*, doi: 10.1016/j.mce.2018.01.027)

Walenta L*, Schmid N*, Schwarzer JU, Koehn FM, Urbanski HF, Behr R, Strauss L, Poutanen M, Mayerhofer A. (2018). NLRP3 in Somatic Non-Immune Cells of Rodent and Primate Testes. *Reproduction* (*in press*, doi: 10.1530/REP-18-0111) *shared first authorship

Mayerhofer A, **Walenta L**, Mayer C, Eubler K, Welter H (2018). Human testicular peritubular cells, mast cells and testicular inflammation. *Andrologia, e13055.* (*in press*, doi: 10.1111/and.13055)

Mayer C, Adam M*, **Walenta L***, Schmid N*, Heikelä H*, Schubert K*, Flenkenthaler F*, Dietrich KG*, Gruschka S, Arnold GJ, Froehlich T, Schwarzer JU, Koehn FM, Strauss L, Welter H, Poutanen M, Mayerhofer A. (2018). Insights into the Role of Androgen Receptor in Human Testicular Peritubular Cells. *Andrology* (*in press*, doi: 10.1111/andr.12509) *shared second authorship

Scientific talks and posters

Glashauser L, Dietrich K, Tiefenbacher A, Schwarzer JU, Koehn FM, Mayerhofer A. Characterization of the Purinergic Receptor P2X7 in Human Testicular Peritubular Cells. (Poster, 6. Dachverband Reproduktionsbiologie und -medizin (DVR)-Kongress, 12/2015)

Glashauser L, Dietrich K, Tiefenbacher A, Welter H, Schwarzer JU, Koehn FM, Mayerhofer A. The Purinergic Receptor P2X7 in Human Testicular Peritubular Cells is Involved in Male Infertility. (Poster, 59. Symposium der Deutschen Gesellschaft für Endokrinologie (DACH-Tagung), 06/2016)

Glashauser L, Dietrich K, Tiefenbacher A, Schwarzer JU, Koehn FM, Mayerhofer A. Purinergic Receptors in Human Testicular Peritubular Cells – Involved in Male Infertility? (Talk, 28. Jahrestagung der Deutschen Gesellschaft für Andrologie (DGA), 09/2016)

Glashauser L, Dietrich K, Tiefenbacher A, Schwarzer JU, Koehn FM, Mayerhofer A. Purinergic Receptors in Human Testicular Peritubular Cells – Involved in Male Infertility? (Talk, Fortpflanzungstagung München, 02/2017)

Glashauser L, Fleck D, Froehlich T, Arnold GJ, Schwarzer JU, Koehn FM, Spehr M, Mayerhofer A. ATP-mediated Events in Peritubular Cells Contribute to Sterile Testicular Inflammation and Male Infertility. (Flash Talk and Poster, Society for the Study of Reproduction 50th Annual Meeting, 07/2017)

Walenta L, Schmid N, Tiefenbacher A, Schwarzer JU, Koehn FM, Strauss L, Poutanen M, Mayerhofer A. NLRP3 is expressed by Somatic Cells of the Testis. (Poster, 7. DVR-Kongress, 12/2017)

Missel A, **Walenta L**, Schwarzer JU, Koehn FM, Mayerhofer A. Inhibition of the Ectonucleotidase CD39 Reduces Inflammatory Effects of ATP in Human Testicular Peritubular Cells (Poster, 61. Deutscher Kongress für Endokrinologie, 03/2018)